

# Liquid crystalline particles prepared from dispersion and precipitation polymerization

**Citation for published version (APA):**

Liu, X. (2021). *Liquid crystalline particles prepared from dispersion and precipitation polymerization*. [Phd Thesis 1 (Research TU/e / Graduation TU/e), Chemical Engineering and Chemistry]. Eindhoven University of Technology.

**Document status and date:**

Published: 23/09/2021

**Document Version:**

Publisher's PDF, also known as Version of Record (includes final page, issue and volume numbers)

**Please check the document version of this publication:**

- A submitted manuscript is the version of the article upon submission and before peer-review. There can be important differences between the submitted version and the official published version of record. People interested in the research are advised to contact the author for the final version of the publication, or visit the DOI to the publisher's website.
- The final author version and the galley proof are versions of the publication after peer review.
- The final published version features the final layout of the paper including the volume, issue and page numbers.

[Link to publication](#)

**General rights**

Copyright and moral rights for the publications made accessible in the public portal are retained by the authors and/or other copyright owners and it is a condition of accessing publications that users recognise and abide by the legal requirements associated with these rights.

- Users may download and print one copy of any publication from the public portal for the purpose of private study or research.
- You may not further distribute the material or use it for any profit-making activity or commercial gain
- You may freely distribute the URL identifying the publication in the public portal.

If the publication is distributed under the terms of Article 25fa of the Dutch Copyright Act, indicated by the "Taverne" license above, please follow below link for the End User Agreement:

[www.tue.nl/taverne](http://www.tue.nl/taverne)

**Take down policy**

If you believe that this document breaches copyright please contact us at:

[openaccess@tue.nl](mailto:openaccess@tue.nl)

providing details and we will investigate your claim.

# **Liquid crystalline polymer particles prepared from dispersion and precipitation polymerization**

PROEFSCHRIFT

ter verkrijging van de graad van doctor aan de Technische Universiteit Eindhoven, op gezag van de rector magnificus prof.dr.ir. F.P.T. Baaijens, voor een commissie aangewezen door het College voor Promoties, in het openbaar te verdedigen op donderdag 23 september 2021 om 16:00 uur

door

Xiaohong Liu

geboren te Guangzhou, China

Dit proefschrift is goedgekeurd door de promotoren en de samenstelling van de promotiecommissie is als volgt:

voorzitter:	prof.dr. F. Gallucci
1 <sup>e</sup> promotor:	prof.dr. A.P.H.J. Schenning
copromotors:	dr. M.G. Debije
	dr.ir. J.P.A. Heuts
leden:	prof.dr. D.J. Broer
	prof.dr. K.U. Loos (University of Groningen)
	prof.dr.ir. S.A.F. Bon (University of Warwick)
	dr. C.F. van Nostrum (Utrecht University)

*Het onderzoek of ontwerp dat in dit proefschrift wordt beschreven is uitgevoerd in overeenstemming met de TU/e Gedragscode Wetenschapsbeoefening.*

读万卷书，行万里路

The research in this thesis was financially supported by The Netherlands Organization for Scientific Research (TOP-PUNT-718.016.003).

The cover image was obtained from <https://699pic.com/tupian-400118835.html> with permission and reproduced by Xiaohong Liu.

Printed by ProefschriftMaken

A catalogue record is available from the Eindhoven University of Technology Library

ISBN: 978-90-386-5359-4

Copy right © 2021 by Xiaohong Liu

## Summary

# Liquid crystalline polymer particles prepared from dispersion and precipitation polymerization

Liquid crystalline (LC) polymer particles exhibit unique functionalities over amorphous polymer particles, due to their well-defined ordered structure and have been of interest for use as absorbents, actuators, and light reflectors. Classical polymerization techniques, namely, suspension, emulsion, dispersion, and precipitation polymerizations, have been rarely applied to prepare LC particles. This thesis focuses on using dispersion and precipitation polymerization to prepare monodisperse LC polymer particles with a programmed alignment and shape.

The thesis starts with summarizing the methodologies and results in the previous literature focusing on LC polymer particles via classical polymerization techniques to present the state-of-the-art.

In the second chapter, seeded dispersion polymerization of LC monomers is introduced, based on normal dispersion polymerization. By polymerizing LC monomers in the presence of non-crosslinked polymer seeds, monodisperse, micron-sized core-shell particles can be prepared, and further converted into hollow shells by selective removal of the core seeds. The alignment of LC molecules in the shells is found to be dependent on the nature of the polymer seed. After removal of the seeds, the LC shells with radial alignment are mostly spherical with small dimples, while bipolar aligned shells have a “biconcave” shape. It is demonstrated the seeded polymerization can also be applied to prepare LC shells with various functional groups, showing the versatility of the method.

As an alternative to pure radical polymerization, base-catalyzed thiol-ene dispersion polymerization is applied to prepare monodisperse LC polymer particles with crosslinked thiol-ene networks and unreacted acrylate end groups in the third

chapter. The thiol-ene LC polymer particles are embedded in a poly(vinyl alcohol) matrix and deformed by stretching or compressing before UV polymerization of the acrylate groups. The two-step process yields LC polymer particles consisting of two networks: a spherical thiol-ene network formed in the isotropic phase, and an acrylate network that is formed in an LC phase with a deformed shape. By increasing the temperature to above the nematic-isotropic phase transition temperature, the particles undergo a physical shape change from the deformed shape to spherical. This two-step polymerization process is a novel, facile, versatile method for preparing micron-sized actuators with programmable shape changes.

Although useful for easily preparing monodisperse, micron-sized polymer particles, dispersion polymerization is sensitive to specific functional groups and crosslinkers, which limits its versatility. As a supplement to dispersion polymerization, precipitation polymerization of LC monomers is introduced to prepare monodisperse LC particles in chapter four. Monodisperse, micron-sized LC polymer network particles functionalized with carboxylic acid groups are prepared with precipitation polymerization. The original layer spacing of the monomer mixture was preserved and the LC molecules aligned radially. The polymerization conditions were varied and it was concluded that the polymerization temperature and solvent both have significant influences on the particle size. Particles dispersed in KOH solution demonstrated rapid absorption of methylene blue dye. The methylene blue could be released from the particles by adding bivalent calcium ions, while monovalent ions failed to trigger the release.

Following the introduced precipitation polymerization, a novel, disulfide-functionalized crosslinker was incorporated into the LC monomer mixture to introduce redox-responsivity to the LC polymer particles in chapter five. Flower-like polymer particles were obtained by polymerizing the LC monomer mixture and the morphology of the particles could be tuned by simply elevating the polymerization temperature, while the polymerization solvent had a pronounced impact on the final particle size. The polymerization process was monitored with time-resolved TEM

images, which revealed the morphology of the final particles formed within one hour, with further polymerization only resulting in the growth of the particles. Thermal analysis suggested the glass transition and smectic to isotropic transition temperatures are two factors determining the particle morphology. Finally, the flower-like polymer particles degraded more rapidly under reducing conditions than their spherical counterparts due to the significantly higher surface-to-volume ratio.

In conclusion, this thesis highlights the preparation of LC polymer particles through dispersion and precipitation polymerizations. Monodisperse LC particles with programmed alignment and shape can be easily prepared while showing responsivity to temperature, ionic content, and reductive environments. These LC polymer particles are promising candidates for use as drug carriers, reusable absorbents, actuators, and beyond.



# Contents

<b>Chapter 1</b>	Introduction	<b>1</b>
<b>Chapter 2</b>	Monodisperse liquid crystalline polymer shells with programmable alignment and shape prepared by seeded dispersion polymerization	<b>25</b>
<b>Chapter 3</b>	Programmable liquid crystalline polymer particles as microactuators prepared via thiol-ene dispersion polymerization	<b>49</b>
<b>Chapter 4</b>	Monodisperse liquid crystalline polymer particles synthesized via precipitation polymerization	<b>63</b>
<b>Chapter 5</b>	Flower-like colloidal particles through precipitation polymerization of redox responsive liquid crystals	<b>80</b>
<b>Chapter 6</b>	Technology assessment	<b>100</b>
	<b>Curriculum Vitae</b>	<b>113</b>
	<b>List of publications</b>	<b>114</b>
	<b>Acknowledgement</b>	<b>115</b>

## Chapter 1

# Introduction

### Abstract

Liquid crystalline polymer particles prepared by classical polymerization techniques are receiving increased attention as promising candidates for use in a variety of applications including micro-actuators, structurally colored objects, and absorbents. These particles have anisotropic molecular order and liquid crystalline phases that distinguish them from conventional polymer particles. In this chapter, the preparation of liquid crystalline polymer particles from classical suspension, (mini-)emulsion, and dispersion polymerization reactions are discussed. The particle sizes, molecular orientations, and liquid crystalline phases produced by each technique are summarized and compared. We conclude with a discussion of the challenges and prospects of the preparation of liquid crystalline polymer particles by classical polymerization techniques.

This chapter is partially reproduced from X. Liu, M. Debije, H. Heuts, A. P. H. J. Schenning, *Chem. – A Eur. J.* **2021**, Accepted Author Manuscript. <https://doi.org/10.1002/chem.202102224>

## 1. General Introduction

Liquid crystals (LCs) have unique properties which makes them attractive for the preparation of polymer particles. The liquid crystalline state is a phase between solid crystals and isotropic liquids in which molecules preserve some degree of the molecular order of a crystal but flow like a liquid. Molecules that show an LC state in a specific temperature range are called thermotropic LCs, and these molecules usually are geometrically anisotropic, often rod-like.<sup>1,2</sup> LC phases can be further categorized based on the organization of the individual molecules (Figure 1).<sup>3,4</sup> For instance, LC molecules in the nematic phase have no positional order but directional order described by the “molecular director”, while LC molecules in the smectic phase have both positional and orientational order and form layers. Chiral nematic (or cholesteric) LC molecules are rotated along the axis perpendicular to the molecular director, and the distance for the molecular director to rotate over  $360^\circ$  is defined as the pitch.

The self-assembly of the LC can be controlled by aligning LC molecules with surface alignment layers,<sup>5</sup> mechanical forces,<sup>6</sup> or external electric fields,<sup>7</sup> and by doing so bulk LC materials with macroscopic anisotropy can be obtained.<sup>8-10</sup> When liquid crystalline molecules are equipped with polymerizable units, the liquid crystalline phase can be fixed by polymerization allowing a wide variety of polymer films, fibers, and particles with different alignments and molecular organization.

LC polymer particles are a class of microscopic LC materials with a typical diameter less than 1 mm that exhibit anisotropic functionalities not found in amorphous polymer particles and have been suggested for use as micropumps,<sup>11</sup> actuators,<sup>12,13</sup> and light reflectors.<sup>14</sup> A widely applied method to prepare LC polymer particles is microfluidics, as highly monodisperse, monodomain, multi-structured particles with typical dimensions between  $100\ \mu\text{m}$  - 1 mm and a variety of morphologies can be prepared.<sup>15-19</sup> Nevertheless, the preparation of smaller LC polymer particles ( $d < 10\ \mu\text{m}$ ) via microfluidics becomes increasingly challenging

when attempting to further reduce the particle size and has not been reported, since the narrower micro-channels can be easily clogged by the monomer droplets and polymerized particles during preparation.<sup>20</sup>

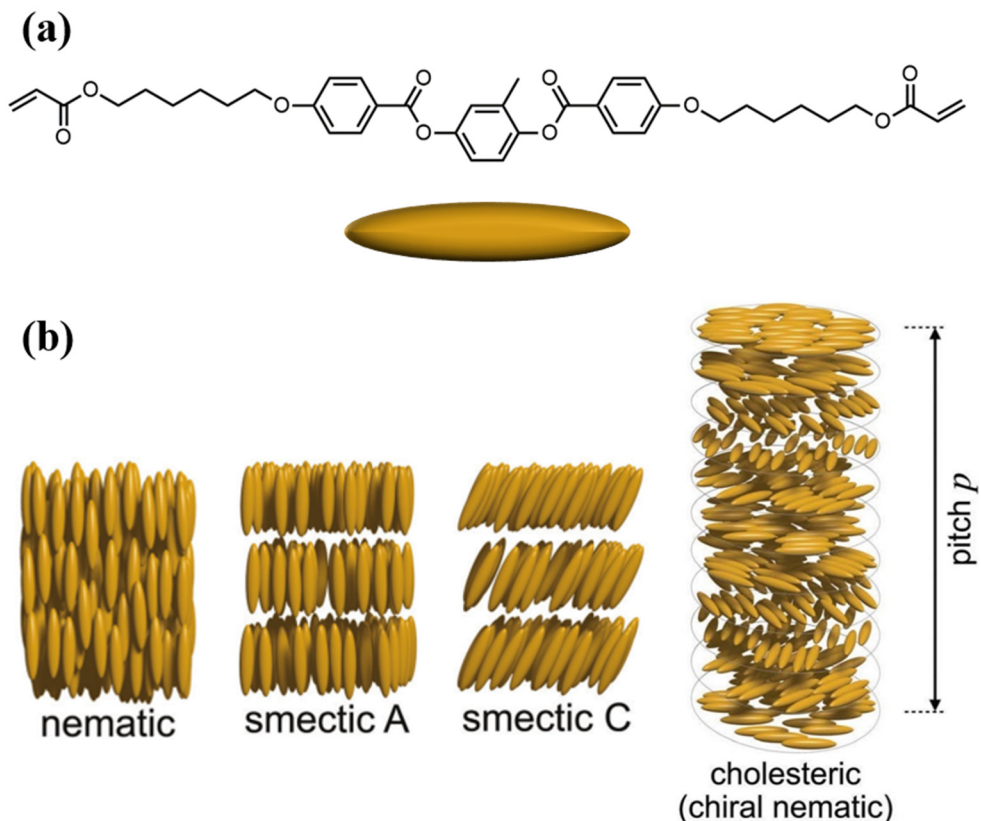


Figure 1. (a) An example of the chemical structure of a rod-like LC molecule. (b) Schematic representation of molecular alignment in various LC phases. Reprinted (adapted) with permission from Ref. 4.

On the other hand, classical polymerization techniques can be readily applied for the preparation of smaller particles. Classical polymerization techniques, including suspension, mini-emulsion, and dispersion polymerizations, are more suitable for preparing smaller LC polymer particles (Figure 2a).<sup>21</sup> Suspension polymerization has been widely applied to prepare LC polymer particles with an average diameter  $> 1 \mu\text{m}$ . LC polymer particles with various LC phases and

alignments have been successfully prepared, with both the phase and alignment having profound influences on the properties of the LC polymer particles. In mini-emulsion polymerization, the average diameter is reduced to  $< 1 \mu\text{m}$ : due to the resolution of polarized optical microscopy (POM), the specific alignment usually remains unidentified. Dispersion polymerizations start as homogeneous systems, with monomers dissolved in a solvent. During polymerization, propagating chains precipitate from the solvent and form preliminary particles that grow into final particles. The alignment can be controlled with the solvent/surfactant mixture in dispersion polymerization.

This chapter focuses on the preparation of LC polymer particles with a diameter  $< 10 \mu\text{m}$  via these classical polymerization techniques. Previous publications on LC polymer particles with a wide range of particle sizes, chemical structures, and LC phases are summarized in Table 1 and the control of the alignment of LC molecules is discussed.

Table 1. Summary of classical polymerization techniques.

Process	Suspension	Mini-emulsion	Dispersion
Component	Solvent (immiscible with monomers), initiator, LC monomers, stabilizer (optional)	Solvent (immiscible with monomers), initiator, LC monomers, stabilizer	Solvent (miscible with monomers), initiator, LC monomers, stabilizer
Particle size/distribution	$d > 1 \mu\text{m}$ / polydisperse	$d < 1 \mu\text{m}$ / narrowly dispersed	$d \sim 1$ to $10 \mu\text{m}$ / monodisperse

Alignment	Bipolar, radial, non-uniform, cholesteric	Onion-like layers, straight layers	Bipolar, radial
LC phase	Nematic, smectic, cholesteric	Nematic, smectic	Nematic, smectic
Drawbacks	Broad size distribution	Alignment is largely unrevealed	Sensitive to the monomer composition

## 2. Suspension polymerization

Suspension polymerization starts with adding LC monomers and initiators to an immiscible solvent and then agitating to form a micron-size droplets suspension. The temperature is then adjusted so the molecules are in the LC phase, and the monomer droplets are then polymerized to yield the LC polymer particles. It is noteworthy that photoinitiators are commonly used to start the polymerization rather than thermal initiators so the polymerization can be conducted at any temperature and so fix the particles in different liquid crystal phases and alignments.

The first preparation of LC polymer particles by suspension photopolymerization involved an LC monomer, RM257 (Figure 3a, **1**), and a photoinitiator in glycerol at 90 °C (in the nematic phase).<sup>22,23</sup> Although no average diameter was reported, scanning electron microscopy (SEM) and POM images showed that at least some of the polymer particles were larger than 5 μm in diameter. The LC molecules in the monomer droplets showed a bipolar alignment (Figure 2b) which was preserved in the final LC polymer particles that were stable over a wide temperature range. This bipolar alignment resulted in a net dipole moment that interacted with an applied in-plane electric field which was used to rotate the particles (Figure 3b), and this rotation was monitored by changes in the birefringence pattern under POM.

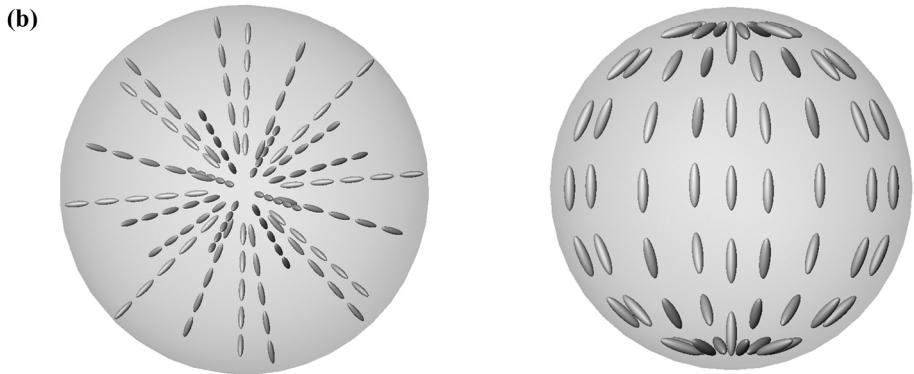
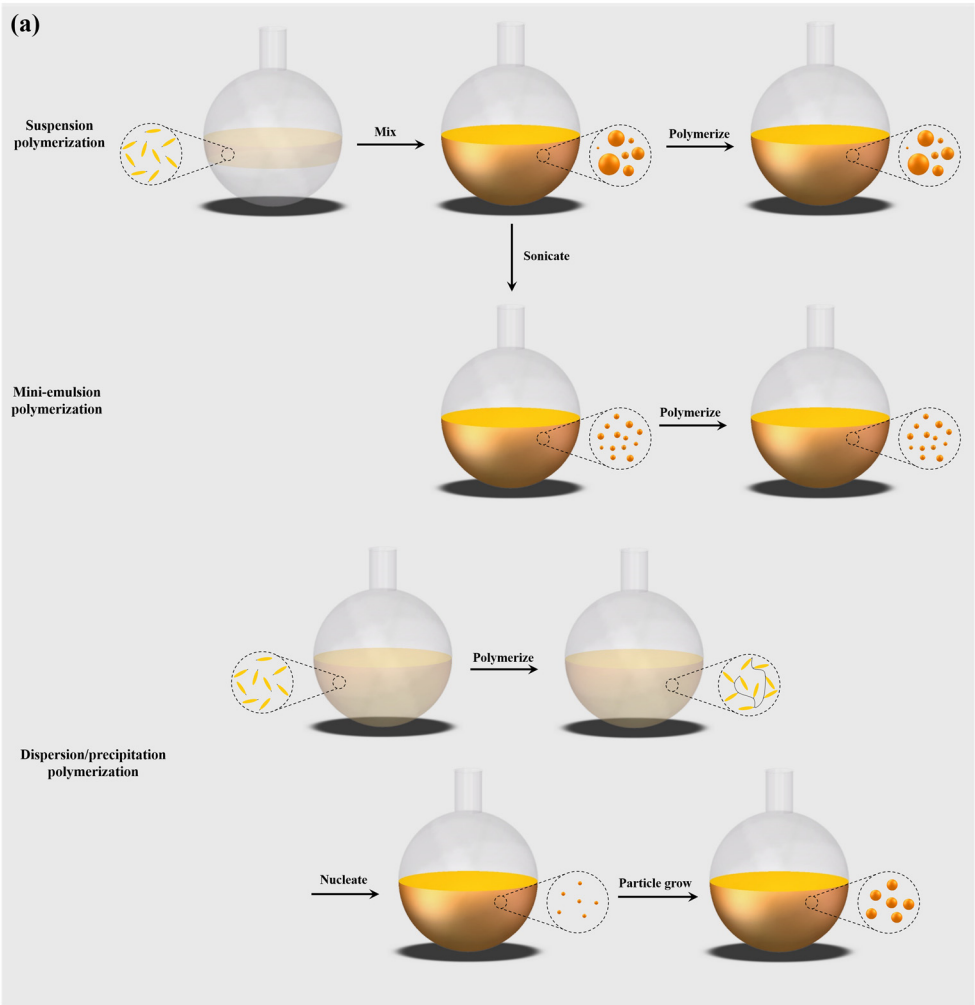


Figure 2. (a) Schematic representation of classical polymerization techniques. (b)

Schematic representation of radial (left) and bipolar (right) alignment.

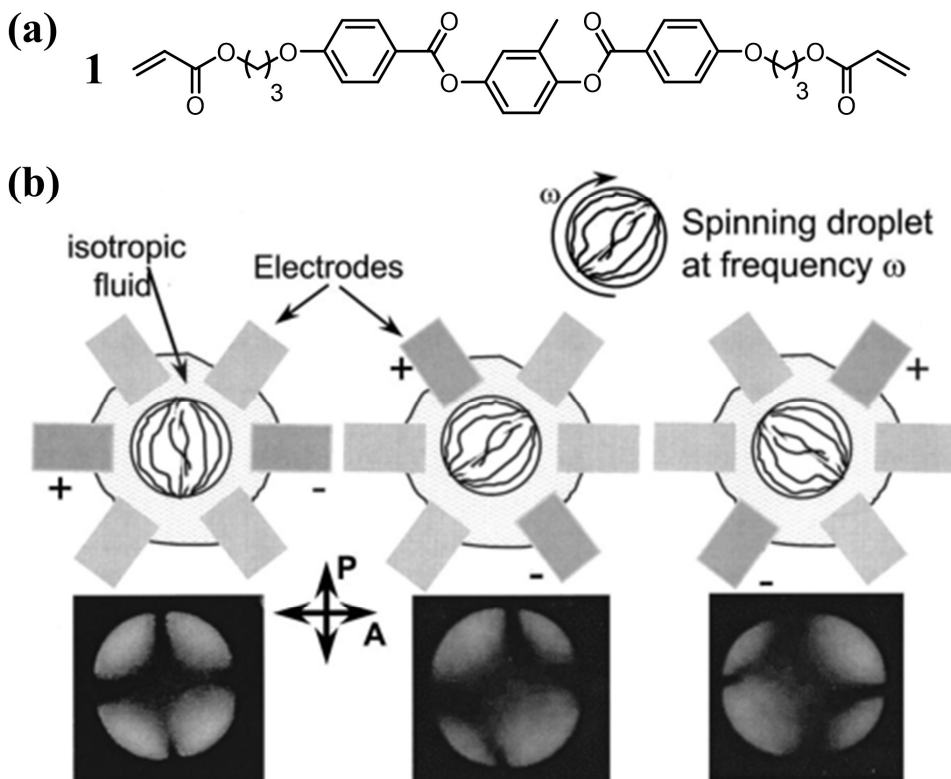


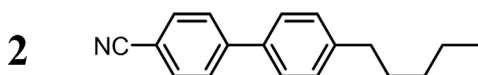
Figure 3. (a) The chemical structure of RM257 (1). (b) Schematic representation of the rotation of an LC polymer particle with an applied electric field and the corresponding change in birefringence pattern. Reprinted (adapted) with permission from Ref. 23.

LC polymer particles with internal free volume that shrank anisotropically were prepared by adding a non-polymerizable LC molecule, 5CB (Figure 4, 2), to the same LC monomer mixture and subsequently removing it by washing with solvent after polymerization.<sup>24</sup> The LC monomer mixture (RM257:5CB = 20:80, w/w) was first suspended in a water/glycerol mixture (90% v/v) in the presence of fluorescence-labeled polystyrene (PS) particles and photopolymerized. POM images



showed bipolar alignment of the LC polymer particles. By extracting 5CB with ethanol, the polymer particles shrank anisotropically, resulting in an ellipsoidal shape. The particles appeared bright when tilted with respect to the crossed polarizers, and dark when parallel, indicating the bipolar alignment was maintained after the 5CB extraction, shrinkage occurring in the direction perpendicular to the line joining the two defects (Figure 2b). Fluorescence microscopy images revealed the PS particles did not randomly distribute on the surface of the LC particles but were directed to the point defects. The direction of the PS particles was attributed to the anisotropic van der Waals interaction between PS and bipolar LC polymer particles originating from the LC alignment.<sup>25</sup> A further systematic investigation of RM257/5CB LC polymer particles with different cross-linking densities, alignments, and morphologies after the removal of the small molecules (Figure 4b) demonstrated

(a)



(b)

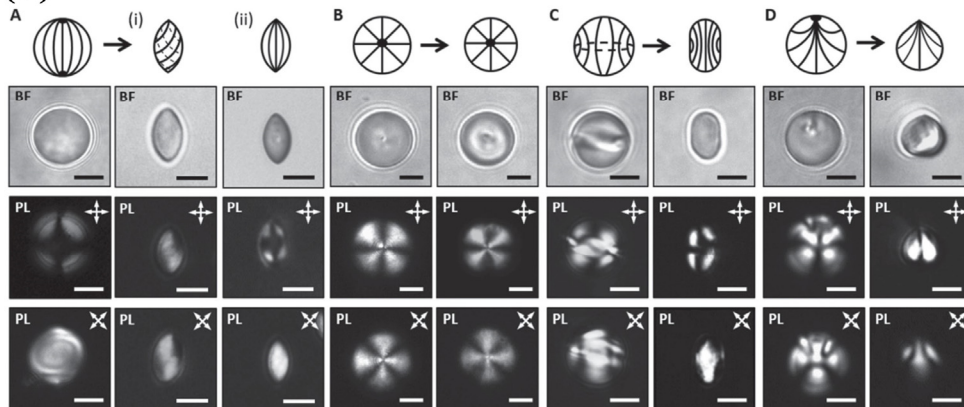


Figure 4. (a) The chemical structure of 5CB (2). (b) Schematic representation and POM images of LC polymer particle with bipolar (A), radial (B), axial (C), and preradial (D) alignment. The left and right columns are the particles before and after extraction of 5CB. Reprinted (adapted) with permission from Ref. 26.

that by adjusting the solvent environment and adding surfactant or colloids, the alignment of the LC polymer particles can be readily manipulated to be bipolar, radial, axial, or preradial.<sup>20,26</sup> After the extraction of 5CB, the directional shrinkage can be programmed with the alignment, as the radial LC polymer particles showed no significant shrinkage but formed porous structures, while the LC polymer particles with other alignments shrank anisotropically, that is, perpendicular to the local director.

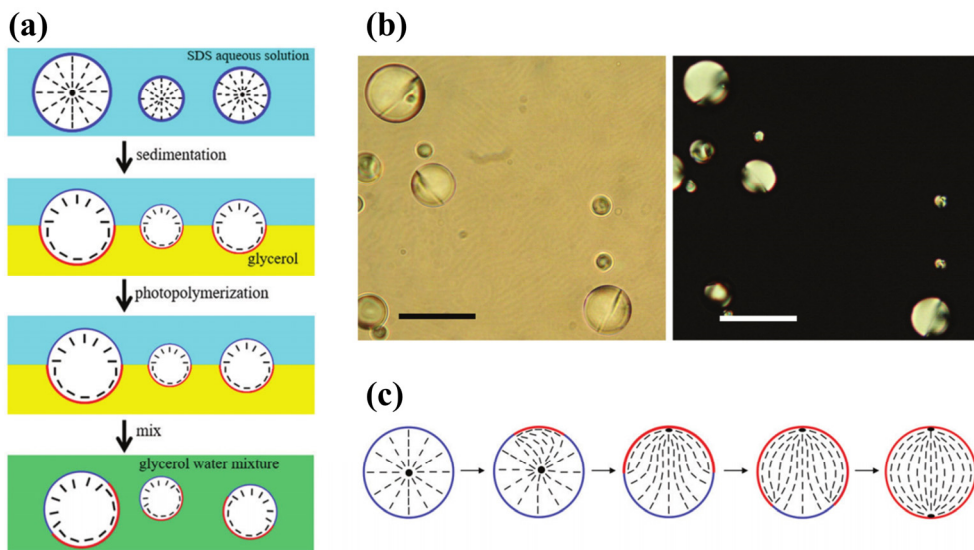


Figure 5. (a) Schematic representation of the preparation of Janus LC polymer particles with coexisting radial and bipolar alignment. (b) POM images of the Janus LC polymer particles without (left) and with (right) cross polarizers. (c) Schematic representation of the transformation of the LC alignment in an LC monomer droplet. Reprinted (adapted) with permission from Ref. 27.

Since the alignment in the LC polymer particles can be manipulated by the solvent,<sup>27</sup> RM257/5CB (1/2) monomer droplets were polymerized at the interface of an aqueous sodium dodecyl sulfate (SDS) solution and glycerol (the former induces radial and the latter bipolar alignments (Figure 5) to create “Janus-like” LC polymer particles with non-uniform, controlled alignments. The LC monomers were first

suspended in an SDS solution and aligned radially; this suspension was dropped on top of glycerol, and the monomer droplets sedimented towards the glycerol phase underneath. The mutual diffusion of water and glycerol generated a gradient in the composition of the local solvent mixture, with higher glycerol content as the LC monomer droplets sedimented. The LC molecules at the bottom of the droplets realigned in a bipolar alignment, while at the top the molecules retained radial alignment. Photopolymerization was performed to fix the non-uniform alignments in the LC monomer droplets and yield the Janus LC polymer particles, with both radial and bipolar alignments coexisting in the same LC polymer particles.

Suspension polymerization has also been used to prepare smectic LC polymer particles, in which LC molecules not only preserve directional order but also form smectic layers.<sup>28</sup> The general procedure is similar to the preparation of nematic LC polymer particles, except that the LC monomer mixture (Figure 6a) was first suspended in the low viscosity nematic phase, and further cooled to the smectic C phase for polymerization. The LC monomers showed a bipolar alignment in the nematic phase (Figure 6b, top row), which rearranged into a radial alignment upon cooling to the smectic C phase (Figure 6b, bottom row). After polymerization, the average diameter of the LC polymer particles was 1.4  $\mu\text{m}$ , and the layer structure was confirmed with X-ray diffraction (XRD), showing a layer spacing of 3.2 nm. Upon treating with KOH solution and deprotonating the carboxylic acid groups, the LC polymer particles showed rapid absorption kinetics and high absorption capacity to a cationic dye, methylene blue, while rejecting an anionic dye, methyl orange, making them promising candidates for separation and purification.

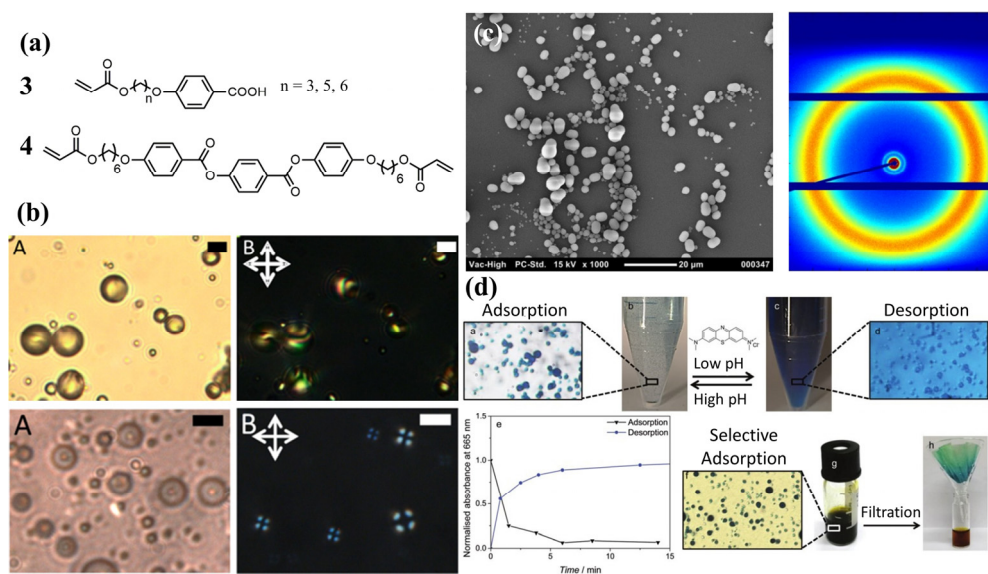


Figure 6. (a) The chemical structure of the LC monomers. **3** is a mixture of 3 monomers in a weight ratio = 1:1:1, and the weight ratio of **3**:**4** = 9:1. (b) POM images of the LC monomer droplets in nematic (top row, scale bar = 10  $\mu$ m) and smectic (bottom row, scale bar = 5  $\mu$ m) phases. (c) SEM image (left) and XRD profile (right) of the LC polymer particles. (d) Adsorption and release study of cationic/anionic dyes by the LC polymer particles. Reprinted (adapted) with permission from Ref. 28.

Cholesteric LC polymer particles in which the director of LC molecules rotates periodically through the layer depth and forms a helical structure have also been prepared by suspension polymerization. The helical structure enables the cholesteric LC polymer particles to optomechanically and optically interact with light, such as generating torque and force<sup>29–33</sup> and reflecting light with specific wavelengths.<sup>34–37</sup> The monomer mixture typically consists of LC monomers with chiral molecules that induce rotation of the LC director (Figure 7a, **5** and **6**). Similar to nematic LC polymer particles, cholesteric LC polymer particles are prepared by first suspending cholesteric LC monomers in an immiscible solvent and irradiating with UV light to photopolymerize the cholesteric phase. A detailed investigation revealed that the chirality, particle size, and solvent-LC interfacial properties

determined the alignment of the LC molecules and their helical structure (Figure 7b),<sup>38,39</sup> which have a profound influence on the properties of the particles. For instance, homeotropic alignment of the LC molecules and an anisotropic helical structure led to edge-reflection (Figure 7c and d),<sup>35</sup> while planar alignment of the LC molecules and a concentric helical structure were found in particles with center-reflection (Figure 7e and f).<sup>34</sup> An interesting application of these cholesteric LC polymer particles is to produce reflective coatings by mixing the particles with a matrix with a matching refractive index (Figure 7g).<sup>34,36,37</sup> Distinctive from cholesteric LC films, the particulate coating showed no viewing angle dependence, due to the spherical geometry of the LC polymer particles, and the color can be readily controlled with the concentration of the chiral molecules, making them an interesting and versatile multi-wavelength reflecting system.

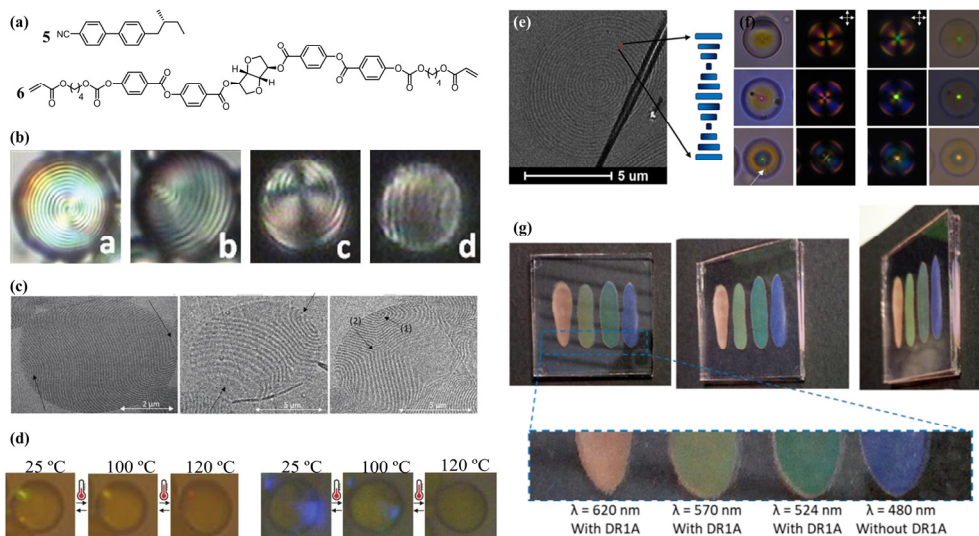


Figure 7. (a) Example of a non-polymerizable (**5**) and polymerizable (**6**) chiral molecules used to induce the cholesteric phase. (b) Possible LC alignments in cholesteric LC polymer particles. Image b and c are the same particles observed at different viewing angles. Reprinted (adapted) with permission from Ref. 39. Transmission electron microscopy (TEM) (c), and POM (d) images of cholesteric LC polymer particles with homeotropic alignment of the LC molecules and anisotropic helical structure. Reprinted (adapted) with permission from Ref. 35. TEM (e) and

POM (f) images of cholesteric LC polymer particles with planar alignment of the LC molecules and concentric helical structure. (g) Reflective coatings prepared with cholesteric LC polymer particles with different reflection wavelengths viewed at different angles. Reprinted (adapted) with permission from Ref. 34.

### 3. Mini-emulsion polymerization

Mini-emulsion is the only emulsion polymerization technique that has been applied to prepare LC polymer particles. Generally, the LC monomers are first added to water in the presence of a surfactant to form a suspension, followed by sonication or strong stirring to form sub-micron droplets before polymerization. The average diameter of the LC polymer particles prepared via mini-emulsion polymerization is generally  $< 1 \mu\text{m}$ .<sup>40</sup>

A polymerizable surfactant, AC10COONa (Figure 8a, **7**), which consists of an acrylate and a sodium carboxylate group, was used for the emulsion polymerization of LC monomers.<sup>41</sup> The LC monomer mixtures were first dissolved (Figure 8a, **8** and **9**) in chloroform and then added to an aqueous solution of AC10COONa and ultrasonicated to produce the mini-emulsion. The emulsion was then heated to evaporate the chloroform and polymerize the monomers, yielding LC polymer particles with an average diameter of approximately 210 nm. The electrostatic stabilization of the surfactant was critical in preventing coalescence upon drying, while steric stabilizers such as polyvinyl alcohol failed to provide stabilization, and the particles aggregated. With this surfactant, tuning both the stiffness and morphology of the LC polymer particles have been explored,<sup>42</sup> and the LC polymer particles have been suggested as drug delivery materials,<sup>43-48</sup> hosts for adjustable fluorescent dyes,<sup>49,50</sup> and photo-actuators.<sup>51</sup> For instance, fluorescent LC polymer particles were prepared with LC monomer **9** and a fluorescent dye **10**, of which the fluorescent emission redshifts upon aggregation into dimers, trimers, etc (Figure 8c).<sup>50</sup> The LC molecules prevented the aggregation of the fluorescent dye

and as a result, enabled the tuning of the emission spectrum by the concentration of the dye (Figure 8d).

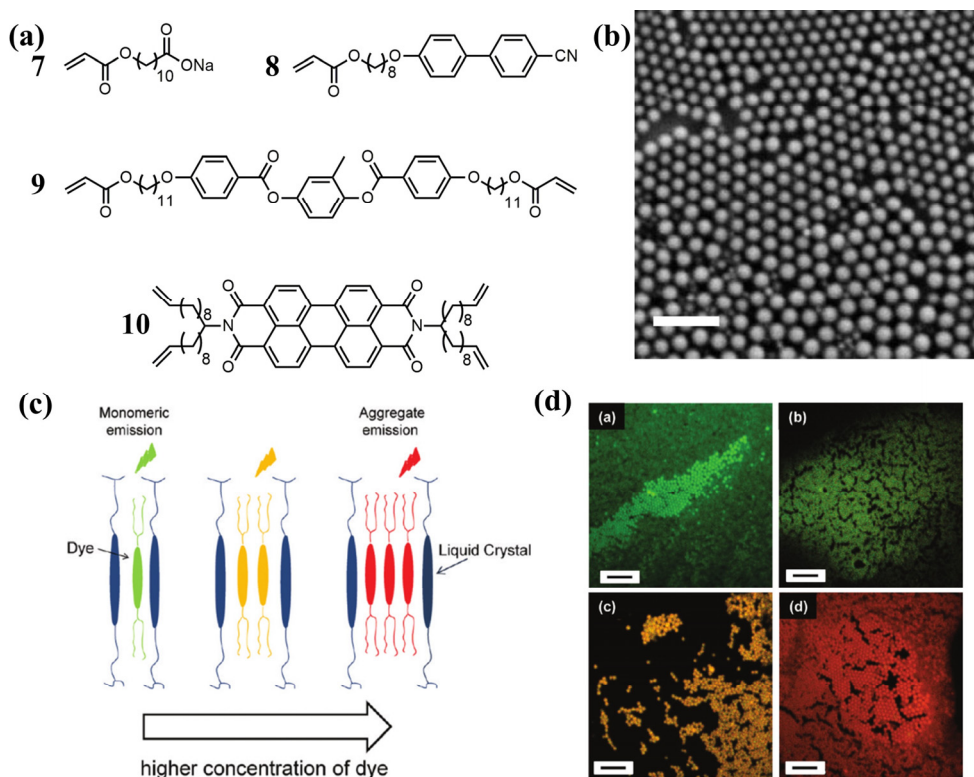


Figure 8. (a) The chemical structure of AC10COONa (**7**), the LC monomers (**8** and **9**), and a fluorescence dye (**10**). (b) LC polymer particles prepared with **7**, **8**, and **9**. Scale bar = 1  $\mu\text{m}$ . Reprinted (adapted) with permission from Ref. 41. (c) Schematic representation of the interaction between dyes and LC molecules. (d) Confocal images of fluorescent LC polymer particles with increasing dye concentration deposited on a substrate. Scale bar = 2  $\mu\text{m}$ . Reprinted (adapted) with permission from Ref. 50.

The main drawback of the mini-emulsion technique is that it is usually difficult to use POM to determine the LC alignment in the particles since the typical average diameter of the LC polymer particles prepared via mini-emulsion polymerization is  $< 1 \mu\text{m}$ . In the only publication in which the LC alignment of such small LC polymer particles was successfully determined, TEM showed well-defined





BPO was added to initiate the polymerization which was carried out for 24 hours to yield the LC polymer particles. The concentrations of both HPC and BPO were varied but neither showed influence on the particle size, while the solvent mixture showed a large influence. POM images reveal a “uniform director orientation” of the LC polymer particles, although the direction is not stated. A subsequent, systematic investigation in which LC polymer particles were prepared from various LC monomers and solvent mixtures via dispersion polymerization demonstrated that the dispersion polymerization method was universally applicable in preparing micron-sized LC polymer particles with a narrow size distribution from LC monomers (Figure 10a).<sup>54</sup> It is noteworthy that the solvent mixture needed to be carefully selected since generally larger diameters and more polydisperse particle size distributions were obtained with increasing fraction of 2-methoxyethanol, which is a good solvent for the LC monomers and polymers. Most particles showed bipolar alignment, enabling the LC polymer particles to be trapped with optical tweezers and rotated with circularly polarized light. The LC alignment can be further controlled from planar (bipolar) to homeotropic (axial or radial) by selecting the solvent/surfactant mixture.<sup>55</sup>

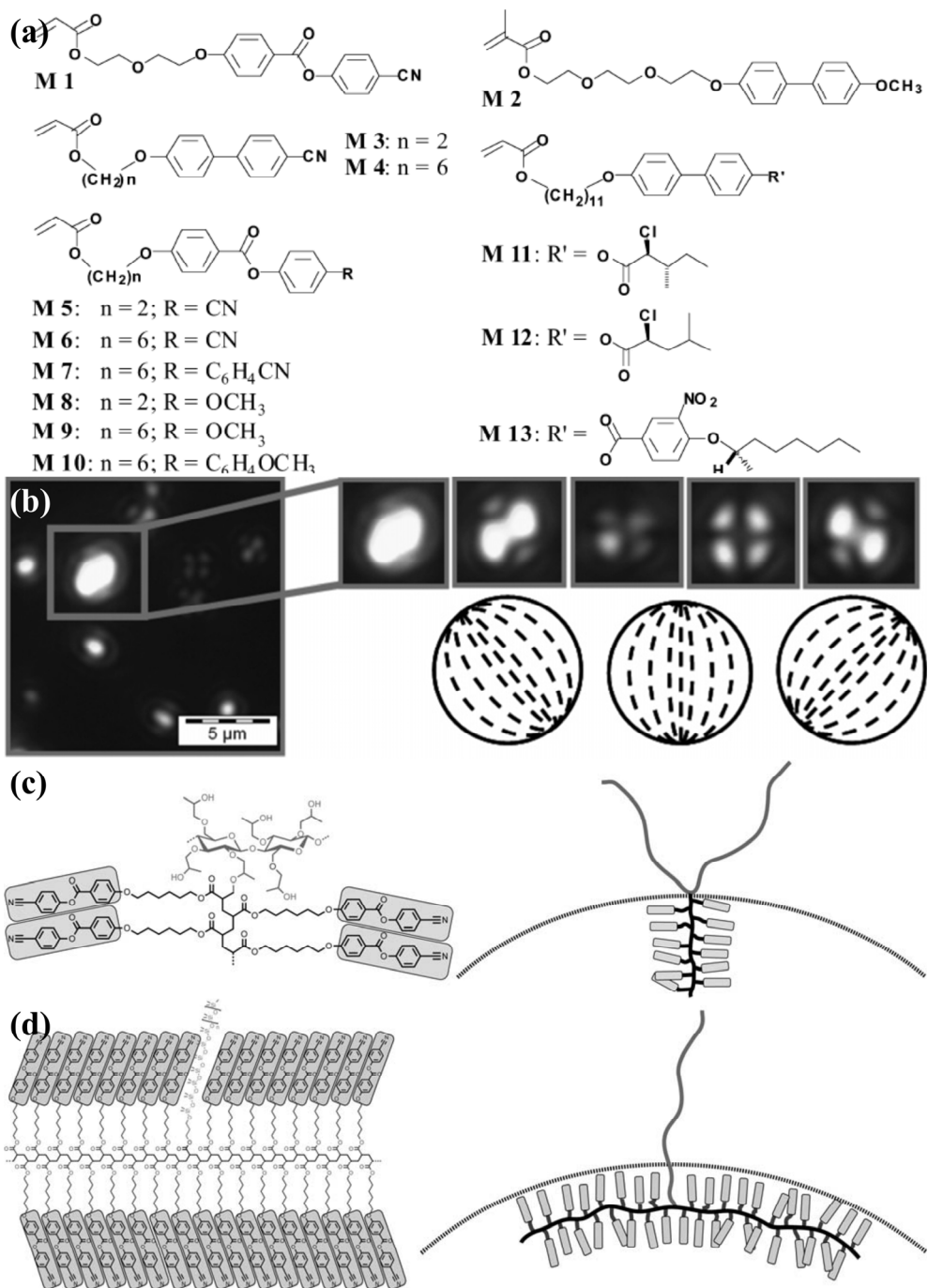


Figure 10. (a) The chemical structures of the LC monomers used to prepare LC polymer particles via dispersion polymerization. (b) POM images of LC polymer

particles prepared from M6. The cross polarizers were rotated to record the images in the inset. Reprinted (adapted) with permission from Ref. 54. The proposed mechanism of the formation of the bipolar (c) and radial (d) LC polymer particles. Reprinted (adapted) with permission from Ref. 55.

## 5. Aim and outline of the thesis

As can be concluded from this chapter, LC polymer particles with various sizes, LC phases, and molecular alignments via classical polymerization techniques, including suspension, mini-emulsion, and dispersion polymerizations, can be synthesized. These LC polymer particles have found applications as light-<sup>33</sup> and electricity-driven rotors,<sup>56</sup> absorbents,<sup>28</sup> cell scaffolds,<sup>57,58</sup> reflectors,<sup>34</sup> actuators,<sup>35</sup> and drug carriers.<sup>48</sup> However, most works focused on the preparation of LC polymer particles with suspension or mini-emulsion polymerization, and while dispersion and precipitation polymerizations both offer excellent control of the particle size, distribution, LC alignment, and structure, they are less explored processes for making such particles. Hence, this thesis aims to prepare LC polymer particles with a variety of architectures, morphologies, alignments, and responsivities with dispersion and precipitation polymerization.

In chapter 2, seeded dispersion polymerization of LC monomers is applied to prepare core-shell LC polymer particles. Upon removal of the seeds, hollow LC polymer shells are obtained. The alignment of LC molecules and the morphology of the shells are found to be dependent on the nature of the polymer seed. Finally, LC shells functionalized with carboxylic acid groups are applied to prepare LC shells, showing the versatility of the method.

In chapter 3, a base-catalyzed thiol-ene dispersion polymerization is applied to prepare monodisperse LC polymer particles. By mechanically deforming the particles and subsequent photopolymerization of the remaining acrylate groups, the resultant LC polymer particles show reversible shape changes from the programmed shape to spherical upon heated above the nematic-isotropic transition temperature.

This two-step polymerization process is a novel, facile, versatile method for preparing micron-sized actuators with programmable shape changes.

In chapter 4, precipitation polymerization was applied to prepare carboxylic acid-functionalized LC polymer particles. The particle size is dependent on the solvent and polymerization temperature, while the LC molecules always align radially, preserving the smectic alignment of the layer. The LC polymer particles can rapidly absorb the cationic dye methylene blue, and release in the presence of  $\text{Ca}^{2+}$ .

In chapter 5, a newly synthesized disulfide-functionalized crosslinker is incorporated into an LC monomer mixture for precipitation polymerization. Flower-like polymer particles are obtained by polymerizing the LC monomer mixture; the morphology of the particles can be tuned by simply elevating the polymerization temperature, while the polymerization solvent had a pronounced impact on the final particle size. Time-resolved TEM reveals that the morphology forms within one hour. A mechanism is proposed based on thermal analysis. Finally, the flower-like particles can be degraded more rapidly under reducing conditions than their spherical counterparts due to the significantly higher surface-to-volume ratio.

In chapter 6, the classical polymerization techniques are compared to microfluidics. Further possible applications of these LC polymer particles as micro-actuators and as absorption and release systems are also discussed.

## 6. References

- [1] P. Zugenmaier, *Int. J. Mol. Sci.* **2011**, *12*, 7360–7400.
- [2] M. Funahashi, T. Kato, *Liq. Cryst.* **2015**, *42*, 909–917.
- [3] T. Kato, Y. Hirai, S. Nakaso, M. Moriyama, *Chem. Soc. Rev.* **2007**, *36*, 1857–1867.
- [4] A. G. Dumanli, T. Savin, *Chem. Soc. Rev.* **2016**, *45*, 6698–6724.
- [5] A. J. J. Kragt, D. C. Hoekstra, S. Stallinga, D. J. Broer, A. P. H. J. Schenning, *Adv. Mater.* **2019**, *31*, 1–7.

- [6] P. Zhang, G. Zhou, L. T. de Haan, A. P. H. J. Schenning, *Adv. Funct. Mater.* **2021**, *31*, 1–9.
- [7] H. Shimura, M. Yoshio, A. Hamasaki, T. Mukai, H. Ohno, T. Kato, *Adv. Mater.* **2009**, *21*, 1591–1594.
- [8] D. Mistry, H. F. Gleeson, *J. Polym. Sci. Part B Polym. Phys.* **2019**, *57*, 1367–1377.
- [9] T. Liang, H. P. C. Van Kuringen, D. J. Mulder, S. Tan, Y. Wu, Z. Borneman, K. Nijmeijer, A. P. H. J. Schenning, *ACS Appl. Mater. Interfaces* **2017**, *9*, 35218–35225.
- [10] N. Herzer, H. Guneyusu, D. J. D. Davies, D. Yildirim, A. R. Vaccaro, D. J. Broer, C. W. M. Bastiaansen, A. P. H. J. Schenning, *J. Am. Chem. Soc.* **2012**, *134*, 7608–7611.
- [11] E. K. Fleischmann, H. L. Liang, N. Kapernaum, F. Giesselmann, J. Lagerwall, R. Zentel, *Nat. Commun.* **2012**, *3*, 1178.
- [12] J. E. Marshall, S. Gallagher, E. M. Terentjev, S. K. Smoukov, *J. Am. Chem. Soc.* **2014**, *136*, 474–479.
- [13] C. Ohm, E. K. Fleischmann, I. Kraus, C. Serra, R. Zentel, *Adv. Funct. Mater.* **2010**, *20*, 4314–4322.
- [14] S. S. Lee, H. J. Seo, Y. H. Kim, S. H. Kim, *Adv. Mater.* **2017**, *29*, 1–8.
- [15] C. Ohm, C. Serra, R. Zentel, *Adv. Mater.* **2009**, *21*, 4859–4862.
- [16] H.-Q. Q. Chen, X.-Y. Y. Wang, H. K. Bisoyi, L.-J. J. Chen, Q. Li, *Langmuir* **2021**, *37*, 3789–3807.
- [17] T. Hessberger, L. B. Braun, F. Henrich, C. Müller, F. Gießelmann, C. Serra, R. Zentel, *J. Mater. Chem. C* **2016**, *4*, 8778–8786.
- [18] V. S. R. Jampani, D. J. Mulder, K. R. De Sousa, A. H. Gélébart, J. P. F. Lagerwall, A. P. H. J. Schenning, *Adv. Funct. Mater.* **2018**, *28*, 1801209.
- [19] C. Ohm, N. Kapernaum, D. Nonnenmacher, F. Giesselmann, C. Serra, R. Zentel, *J. Am. Chem. Soc.* **2011**, *133*, 5305–5311.
- [20] X. Wang, E. Bukusoglu, N. L. Abbott, *Chem. Mater.* **2017**, *29*, 53–61.
- [21] R. Arshady, *Colloid Polym. Sci.* **1992**, *270*, 717–732.
- [22] D. R. Cairns, N. S. Eichenlaub, G. P. Crawford, *Mol. Cryst. Liq. Cryst. Sci. Technol. Sect. A Mol. Cryst. Liq. Cryst.* **2001**, *352*, 275–282.
- [23] D. R. Cairns, M. Sibulkin, G. P. Crawford, *Appl. Phys. Lett.* **2001**, *78*, 2643–2645.

- [24] F. Mondiot, X. Wang, J. J. De Pablo, N. L. Abbott, *J. Am. Chem. Soc.* **2013**, *135*, 9972–9975.
- [25] H. A. Fuster, X. Wang, X. Wang, E. Bukusoglu, S. E. Spagnolie, N. L. Abbott, *Sci. Adv.* **2020**, *6*, eabb1327.
- [26] X. Wang, E. Bukusoglu, D. S. Miller, M. A. Bedolla Pantoja, J. Xiang, O. D. Lavrentovich, N. L. Abbott, *Adv. Funct. Mater.* **2016**, *26*, 7343–7351.
- [27] X. Wang, Y. Zhou, Y. K. Kim, D. S. Miller, R. Zhang, J. A. Martinez-Gonzalez, E. Bukusoglu, B. Zhang, T. M. Brown, J. J. De Pablo, N. L. Abbott, *Soft Matter* **2017**, *13*, 5714–5723.
- [28] H. P. C. Van Kuringen, D. J. Mulder, E. Beltran, D. J. Broer, A. P. H. J. Schenning, *Polym. Chem.* **2016**, *7*, 4712–4716.
- [29] O. Brzobohatý, R. J. Hernández, S. Simpson, A. Mazzulla, G. Cipparrone, P. Zemánek, *Opt. Express* **2016**, *24*, 26382.
- [30] R. J. Hernández, A. Mazzulla, A. Pane, K. Volke-Sepúlveda, G. Cipparrone, *Lab Chip* **2013**, *13*, 459–467.
- [31] A. Mazzulla, G. Cipparrone, R. J. Hernandez, A. Pane, R. Bartolino, *Mol. Cryst. Liq. Cryst.* **2013**, *576*, 15–22.
- [32] M. G. Donato, A. Mazzulla, P. Pagliusi, A. Magazzù, R. J. Hernandez, C. Provenzano, P. G. Gucciardi, O. M. Maragò, G. Cipparrone, *Sci. Rep.* **2016**, *6*, 1–7.
- [33] M. G. Donato, J. Hernandez, A. Mazzulla, C. Provenzano, R. Saija, R. Sayed, S. Vasi, A. Magazzù, P. Pagliusi, R. Bartolino, P. G. Gucciardi, O. M. Maragò, G. Cipparrone, *Nat. Commun.* **2014**, *5*, 1–7.
- [34] A. Belmonte, T. Bus, D. J. Broer, A. P. H. J. Schenning, *ACS Appl. Mater. Interfaces* **2019**, *11*, 14376–14382.
- [35] A. Belmonte, Y. Y. Ussembayev, T. Bus, I. Nys, K. Neyts, A. P. H. J. Schenning, *Small* **2020**, *16*, 1905219.
- [36] A. Belmonte, M. Pilz da Cunha, K. Nickmans, A. P. H. J. Schenning, *Adv. Opt. Mater.* **2020**, *8*, 2000054.
- [37] E. Beltran-Gracia, O. L. Parri, *J. Mater. Chem. C* **2015**, *3*, 11335–11340.
- [38] C. Provenzano, A. Mazzulla, P. Pagliusi, M. P. De Santo, G. Desiderio, I. Perrotta, G. Cipparrone, *APL Mater.* **2014**, *2*, 0–7.
- [39] G. Cipparrone, A. Mazzulla, A. Pane, R. J. Hernandez, R. Bartolino, *Adv. Mater.* **2011**, *23*, 5773–5778.

- [40] R. Arshady, *Colloid Polym. Sci.* **1992**, *270*, 717–732.
- [41] C. M. Spillmann, J. Naciri, K. J. Wahl, Y. H. Garner, M. S. Chen, B. R. Ratna, *Langmuir* **2009**, *25*, 2419–2426.
- [42] J. C. Zhou, S. Tsoi, C. M. Spillmann, J. Naciri, B. Ratna, *J. Colloid Interface Sci.* **2012**, *368*, 152–157.
- [43] O. K. Nag, J. Naciri, E. Oh, C. M. Spillmann, J. B. Delehanty, *Bioconjug. Chem.* **2016**, *27*, 982–993.
- [44] O. K. Nag, J. Naciri, J. S. Erickson, E. Oh, J. B. Delehanty, *Bioconjug. Chem.* **2018**, *29*, 2701–2714.
- [45] O. K. Nag, J. B. Delehanty, J. Naciri, in *Colloid. Nanoparticles Biomed. Appl. XIII* (Eds.: X.-J. Liang, W.J. Parak, M. Osiński), SPIE, **2018**, p. 36.
- [46] O. K. Nag, J. Naciri, E. Oh, C. M. Spillmann, J. B. Delehanty, *J. Vis. Exp.* **2017**, *2017*, 1–8.
- [47] O. K. Nag, J. Naciri, C. M. Spillmann, J. B. Delehanty, *Colloid. Nanoparticles Biomed. Appl. XI* **2016**, 9722, 972215.
- [48] C. M. Spillmann, J. Naciri, W. R. Algar, I. L. Medintz, J. B. Delehanty, *ACS Nano* **2014**, *8*, 6986–6997.
- [49] J. Li, M. Tian, H. Xu, X. Ding, J. Guo, *Part. Part. Syst. Charact.* **2019**, *36*, 1–8.
- [50] C. M. Spillmann, J. Naciri, G. P. Anderson, M. S. Chen, B. R. Ratna, *ACS Nano* **2009**, *3*, 3214–3220.
- [51] S. Tsoi, J. Zhou, C. Spillmann, J. Naciri, T. Ikeda, B. Ratna, *Macromol. Chem. Phys.* **2013**, *214*, 734–741.
- [52] M. Vennes, R. Zentel, M. Rössle, M. Stepputat, U. Kolb, *Adv. Mater.* **2005**, *17*, 2123–2127.
- [53] M. Vennes, R. Zentel, *Macromol. Chem. Phys.* **2004**, *205*, 2303–2311.
- [54] M. Vennes, S. Martin, T. Gisler, R. Zentel, *Macromolecules* **2006**, *39*, 8326–8333.
- [55] S. Haseloh, P. Van Der Schoot, R. Zentel, *Soft Matter* **2010**, *6*, 4112–4119.
- [56] S. Haseloh, R. Zentel, *Macromol. Chem. Phys.* **2009**, *210*, 1394–1401.
- [57] T. Bera, C. Malcuit, R. J. Clements, E. Hegmann, *Front. Mater.* **2016**, *3*, 1–8.

- [58] T. Bera, E. J. Freeman, J. A. McDonough, R. J. Clements, A. Aladlaan, D. W. Miller, C. Malcuit, T. Hegmann, E. Hegmann, *ACS Appl. Mater. Interfaces* **2015**, *7*, 14528–14535.





## Chapter 2

# Monodisperse liquid crystalline polymer shells with programmable alignment and shape prepared by seeded dispersion polymerization

### Abstract

Monodisperse, micron-sized LC shells are prepared by seeded dispersion polymerization. After polymerizing LC monomer mixtures in the presence of non-crosslinked polymer seeds, hollow LC polymer shells with programmable alignment and shape are prepared by removing the seeds. The LC alignment in the LC polymer shells can be easily manipulated by the polymer seeds, as a radial alignment is observed with amorphous poly(phenyl methacrylate) seeds and a bipolar alignment is observed with bipolar LC polymer seeds. After removal of the seeds, the radially aligned samples give radially aligned shells with small dimples. The resulting bipolar LC polymer shells collapse into a biconcave shape. POM and TEM indicate that the collapse occurs at the defect points in the shell. In the case of a lower crosslink density, LC polymer hollow shells with larger dimples are obtained, resulting in cup-shaped polymer particles. Biconcave LC polymer shells based on other LC mixtures have also been prepared, showing the versatility of the seeded dispersion polymerization method.

This chapter is partially reproduced from X. Liu, M.-A. Moradi, T. Bus, J. P. A. Heuts, M. G. Debije, A. P. H. J. Schenning, *Macromolecules* **2021**, *54*, 6052–6060.

## 1. Introduction

Polymer shells are of interest for use in drug delivery,<sup>1-3</sup> in separation of chiral mixtures,<sup>4-7</sup> and as a host for catalysts.<sup>8-10</sup> Among hollow particles, LC polymer shells are particularly interesting, as the alignment of LC molecules gives rise to novel anisotropic functional properties.<sup>11-14</sup> Monodisperse LC polymer shells have been prepared using microfluidics;<sup>11-14</sup> however, preparing well-defined LC polymer shells with tunable alignment with dimensions smaller than 10  $\mu\text{m}$  remains a challenge.

Requiring only temperature control and mild agitation, dispersion polymerizations have emerged as promising alternatives for preparing monodisperse LC polymer particles with average diameters ranging from a few microns to less than 1  $\mu\text{m}$ .<sup>15-17</sup> Based on these polymerization methods, seeded dispersion polymerization has been developed for amorphous polymers.<sup>18,19</sup> In this process, polymerization commences in the presence of preexisting seeds with the newly-formed polymer chains adsorbing onto the surface of the seeds, resulting in a distinctive core-shell structure. The technique offers great versatility in chemical composition, and by selectively removing the inner core, hollow polymer particles can be prepared. This method has been widely used to prepare amorphous particles, but to the best of our knowledge, ordered LC polymer shells prepared by seeded dispersion polymerization have never been reported.

Herein, we report the facile preparation of monodisperse micron-sized LC polymer shells with programmed alignment and shape via seeded dispersion polymerization. Since the outer surface of the seed functions as an alignment layer for the LC molecules making up the shell, we expected differing alignments in the shell dependent on whether amorphous poly(phenyl methacrylate) (PPhMA) or LC bipolar polymer particles were used as seeds. In what follows, we show that the nature of the seed indeed determines the alignment and shape of the monodisperse,

micron-sized shell, which consists of a combination of the acrylic LC monomers as shown in Figure 1.

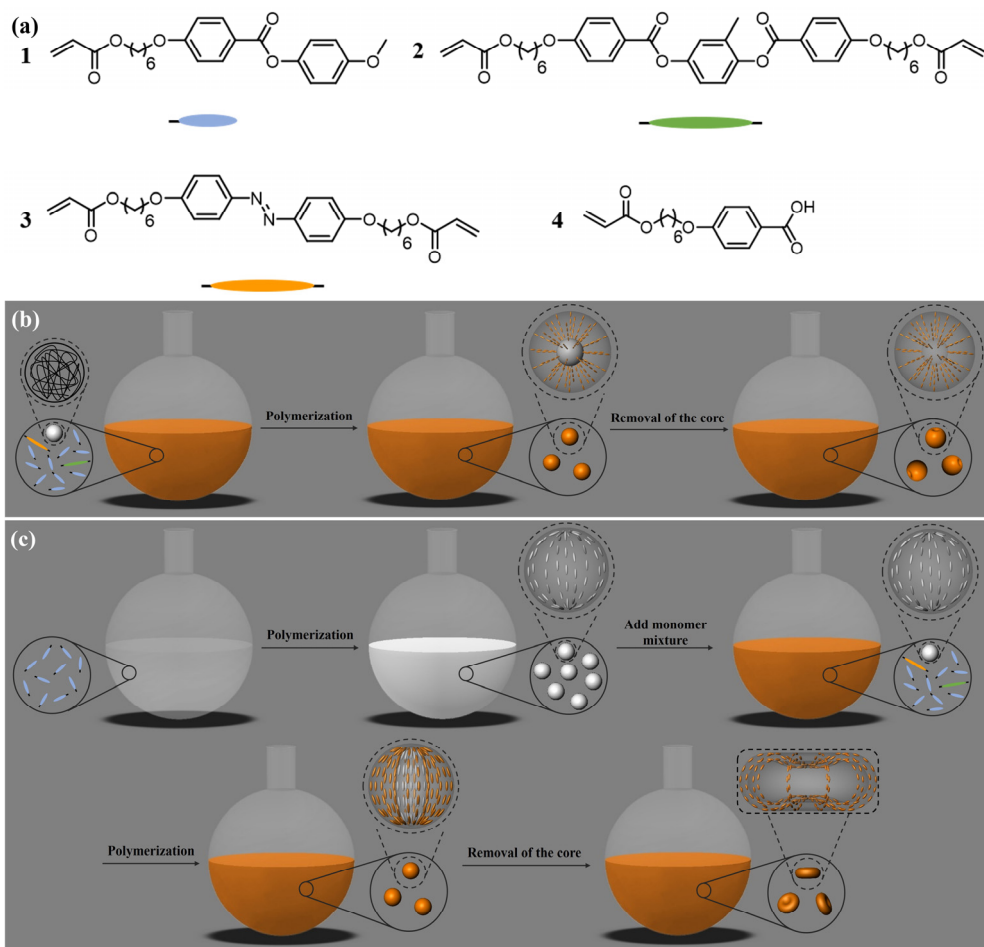


Figure 1. (a) Monomers employed to prepare the LC polymer shells. (b) Schematic representation of the synthesis of LC shells with radial alignment using amorphous PPhMA seeds. (c) Schematic representation of the synthesis of LC shells with bipolar alignment using bipolar LC seeds.

## 2. Experimental

### 2.1. Materials

4-Methoxyphenyl 4-((6-(acryloyloxy)hexyl)oxy)benzoate (**1**), 2-methyl-1,4-phenylene bis(4-((6-(acryloyloxy)hexyl)oxy)benzoate) (**2**), 4,4'-bis(6-acryloyloxyhexyloxy) azobenzene (**3**), and 4-(6-acryloyloxyhexyl-1-oxy)benzoic acid (**4**) (see Figure 1) were purchased from Synthron Chemicals, Germany. Phenyl methacrylate (PhMA, 97%) was purchased from TCI Europe. Polyvinyl pyrrolidone (PVP K30), 2,2'-azobis(2-methylpropionitrile) (AIBN, 98%), and chloroform-d (99.8% atom % D) were purchased from Sigma-Aldrich. All solvents were purchased from Biosolve.

## **2.2. Preparation of LC shells via seeded dispersion polymerization**

### **2.2.1. Synthesis of core-shell LC particles with amorphous PPhMA seeds**

PPhMA seeds were prepared by dispersion polymerization. To this end, 100 mg of PVP and 10 mg of AIBN were added to a 50 mL round-bottom flask, which was then evacuated and backfilled with nitrogen 3 times. Subsequently, 1 mL of PhMA dissolved in 9 mL of ethanol was added to the flask, after which the flask was put into an oil bath preheated to 70 °C and stirred at 200 rpm under N<sub>2</sub> overnight. After the polymerization, the PPhMA particles were centrifuged and washed with ethanol three times. Yield = 77%.

The PPhMA seed particles were then used to prepare core-shell LC particles. To a 50 mL round-bottom flask, 90 mg of monomer **1**, 5 mg of monomer **2**, 5 mg of monomer **3**, 20 mg of PVP, and 2 mg of AIBN were added, after which the round-bottom flask was then pumped and backfilled with nitrogen 3 times. Subsequently, 5 mL of ethanol was added and the round-bottom flask was put into an oil bath preheated to 70 °C. Upon complete dissolution of the monomers, 100 mg of PPhMA particles were dispersed in 5 mL of ethanol and added. The polymerization was carried out at 70 °C and stirred at 200 rpm under N<sub>2</sub> overnight. After polymerization, the dispersion was centrifuged and washed with ethanol to obtain the particles. The particles were stored in 5 mL of ethanol prior to use, and the solid content was

accurately measured by drying 50  $\mu$ L of suspension in a differential scanning calorimetry (DSC) pan. Yield = 88%, where yield is defined as the weight of the core-shell LC particles after seeded dispersion polymerization divided by the total weight of LC monomers and PPhMA seeds.

### **2.2.2. Synthesis of core-shell LC particles with LC seeds**

First, the LC seed particles were synthesized via dispersion polymerization. To a 50 mL round-bottom flask 100 mg of monomer **1**, 10 mg of PVP, and 2 mg of AIBN were added, after which the flask was pumped and backfilled with nitrogen 3 times. Subsequently, 5 mL of ethanol was added to the flask, which was then put into an oil bath preheated to 70  $^{\circ}$ C and stirred at 200 rpm under  $N_2$  for 2 h. Without isolating the seed particles, 60 mg of monomer **1**, 5 mg of monomer **2**, 5 mg of monomer **3**, and 10 mg of PVP were dissolved in 5 mL of hot ethanol and added to the reaction mixture in the flask. The polymerization was carried out overnight. After polymerization, the dispersion was centrifuged and washed with ethanol to obtain the particles. The particles were stored in 5 mL of ethanol prior to use, and the solid content was accurately measured by drying 50  $\mu$ L of suspension in a DSC pan. Yield = 73%, where yield is defined as the weight of the core-shell particles after seeded dispersion polymerization divided by the total weight of LC monomers.

### **2.2.3. Synthesis of carboxylic acid functionalized core-shell LC particles with LC seeds**

Carboxylic acid-functionalized core-shell LC particles were prepared in a similar manner as described in 2.2.2. First, the LC seed was prepared by adding 100 mg of monomer **1**, 10 mg of PVP, and 2 mg of AIBN to a 50 mL round-bottom flask, pumping and backfilling the flask with nitrogen 3 times, adding 5 mL of ethanol to the flask and reacting it for 2 h under  $N_2$ , and continuous stirring at 200 rpm at 70 $^{\circ}$ C in an oil bath. Again, without isolating the seeds, 35 mg of monomer **1**, 15 mg of

monomer **2**, 20 mg of carboxylic acid monomer **4**, and 40 mg of PVP were dissolved in 5 mL of hot ethanol and added to the flask. The polymerization was carried out for another 4 h. After polymerization, the dispersion was centrifuged and washed with ethanol to obtain the particles. The core-shell particles were stored in 5 mL of ethanol prior to use, and the solid content was accurately measured by drying 50  $\mu$ L of suspension in a DSC pan. Yield = 61%, where yield is defined as the weight of the core-shell particles after seeded dispersion polymerization divided by the total weight of LC monomers.

### **2.3. Removal of the seeds**

The particle suspension (1 mL) of predetermined solid content was added to 9 mL of tetrahydrofuran (THF), and the particles were allowed to sediment. The solvent was then poured out, and fresh THF was added. This process was repeated 3 times in total. Then, 10 mL of ethanol was added dropwise with agitation and the particles were allowed to sediment. The solvent was poured out, and 10 mL of fresh ethanol was added dropwise with agitation. This process was repeated 3 times in total. The LC polymer shells were stored in 5 mL of ethanol prior to use, and the solid content was accurately measured by drying 50  $\mu$ L of suspension in a DSC pan. Weight loss = 52% (entry 1), 63% (entry 3), and 36% (entry 5), where weight loss =  $1 - (\text{weight of THF-treated particles} / \text{weight of initial particles})$ ; the weights were calculated from the solid content and the volume of the corresponding suspensions.

### **2.4. Photoresponsiveness of the bipolar LC polymer shell**

LC polymer shells in chlorobenzene (0.3 mg/mL) were added in a quartz cuvette. The suspension was immediately subjected to UV-vis measurement, denoted as “measurement 0.” Then, the suspension was irradiated with 365 nm light for 1 min, and the suspension was subjected to another UV-vis measurement, denoted as “measurement 1.” The suspension was irradiated with 455 nm light for 1

min, and the suspension was subjected to another UV-vis measurement, denoted as “measurement 2.” Five cycles of alternative irradiation were performed, and the UV-vis spectra were measured.

## **2.5. Characterization**

POM images were taken with a Leica CTR6000 polarized optical microscope and a Leica DFC 420C camera. POM images were taken by drying the particle suspensions on clean glass slides unless otherwise stated.  $^1\text{H}$  nuclear magnetic resonance (NMR) spectra were recorded on a 400 MHz Bruker Avance III HD spectrometer in deuterated chloroform with tetramethyl silane used as an internal standard. SEM images were taken with a JEOL TM 220 A. The average size and coefficient of variation of the particle size distribution ( $C_v = \frac{\bar{d}}{SD}$ ) were measured using ImageJ. The polymer particles and their cross sections were investigated via TEM using a Tecnai 20 (type Sphera) by FEI operating with a LaB 6 filament at 200 kV under slight under-focus conditions. For the cross-section, particles were embedded in an EPOFIX epoxy medium. Cross sections were cut at room temperature using an ultra- microtome (Reichert-Jung Ultracut E) with a setting thickness of 60 nm. The obtained cross sections were transferred to a carbon film-covered grid (Electron Microscopy Sciences, CF200-CU). UV-vis spectra were measured with a Shimadzu UV-3102 PC. Thorlabs light emitting diode lamps with collimation adapters were used to provide 365 and 455 nm lights. The distance between the lamps and the cuvette was about 30 cm. The light intensities were about 120 mW/cm<sup>2</sup> (365 nm) and 45 mW/cm<sup>2</sup> (455 nm).

## **3. Result and discussion**

### **3.1. Synthesis of LC shells via seeded dispersion polymerization with PPhMA seeds**



Table 1. LC polymer core-shell particles and hollow shells prepared by seeded dispersion polymerization.

entry	monomer mixture	type/diameter of the seeds	diameter of the core-shell particles	diameter/shape of the LC shells	alignment of the LC shells
1	<b>1, 2, 3</b>	PPhMA/1.50 $\mu\text{m}$	1.69 $\mu\text{m}$	1.46 $\mu\text{m}$ /spheres with small dimples	radial
2	<b>1, 3</b>	PPhMA/1.50 $\mu\text{m}$	1.86 $\mu\text{m}$	<i>N.A.</i> <sup>b</sup> /cup-shape	radial
3	<b>1, 2, 3</b>	bipolar LC polymer seeds <sup>a</sup>	1.63 $\mu\text{m}$	1.59 $\mu\text{m} \times 0.61 \mu\text{m}$ /biconcave	bipolar
4	<b>1, 3</b>	bipolar LC polymer seeds <sup>a</sup>	1.82 $\mu\text{m}$	<i>N.A.</i> <sup>b</sup> /cup-shape	radial
5	<b>1, 2, 4</b>	bipolar LC polymer seeds <sup>a</sup>	1.38 $\mu\text{m}$	1.32 $\mu\text{m} \times 0.68 \mu\text{m}$ /biconcave	bipolar

<sup>a</sup>No diameters were measured because the seeds were not isolated; <sup>b</sup>The diameter of the LC shells cannot be measured accurately due to the extensive deformations.

Monodisperse PPhMA particle seeds were first prepared by dispersion polymerization at 70 °C in ethanol, with PVP as the stabilizer and AIBN as the thermal initiator. SEM images revealed an average diameter of 1.50  $\mu\text{m}$  and a coefficient of variation of 3.7% (Figure 2a). The PPhMA particle seeds were redispersed in ethanol, and then added to an ethanol solution containing LC monoacrylate **1**, LC diacrylate **2**, and azobenzene diacrylate **3** (Table 1, entry 1,

Figure 2b), PVP, and AIBN. The suspension was heated to 70 °C and polymerized overnight, yielding spherical core-shell particles with an average diameter of 1.69  $\mu\text{m}$  and a coefficient of variation of 3.8% (Figure 2b). This indicates a thickness of approximately 100 nm for the cross-linked shell. To remove the PPhMA core (which consists of linear PPhMA chains), the particles were treated with THF repeatedly, prior to transferring and storing in ethanol. The treatment with THF resulted in a weight reduction of 52%, which suggests a near complete removal of the PPhMA core; the original composition of the core-shell particles was 56 wt % core and 44 wt % shell. SEM images of the LC shells (Figure 2c) show dimpled particles with an average diameter of about 1.46  $\mu\text{m}$ . The Hansen solubility parameter (HSP) of the LC polymer shells was estimated with a group contribution method,<sup>20</sup> and the solubility distance ( $R_a$ ) to ethanol and THF was calculated (Tables S1 to S3). The lower number of  $R_a$  to THF suggests that THF has a higher compatibility than ethanol with the LC and hence, it is conceivable that THF diffusion out of the shell is faster than ethanol diffusion into the shells, resulting in an osmotic pressure that could locally compress the shell. The TEM images of a cross-section of the shells (Figure 2d) confirm a thickness of about 100 nm for the LC shells, which can be seen as the dark rings with dimples; this result is consistent with the increase of the particle diameter after the seeded dispersion polymerization (Figure 2a,b).

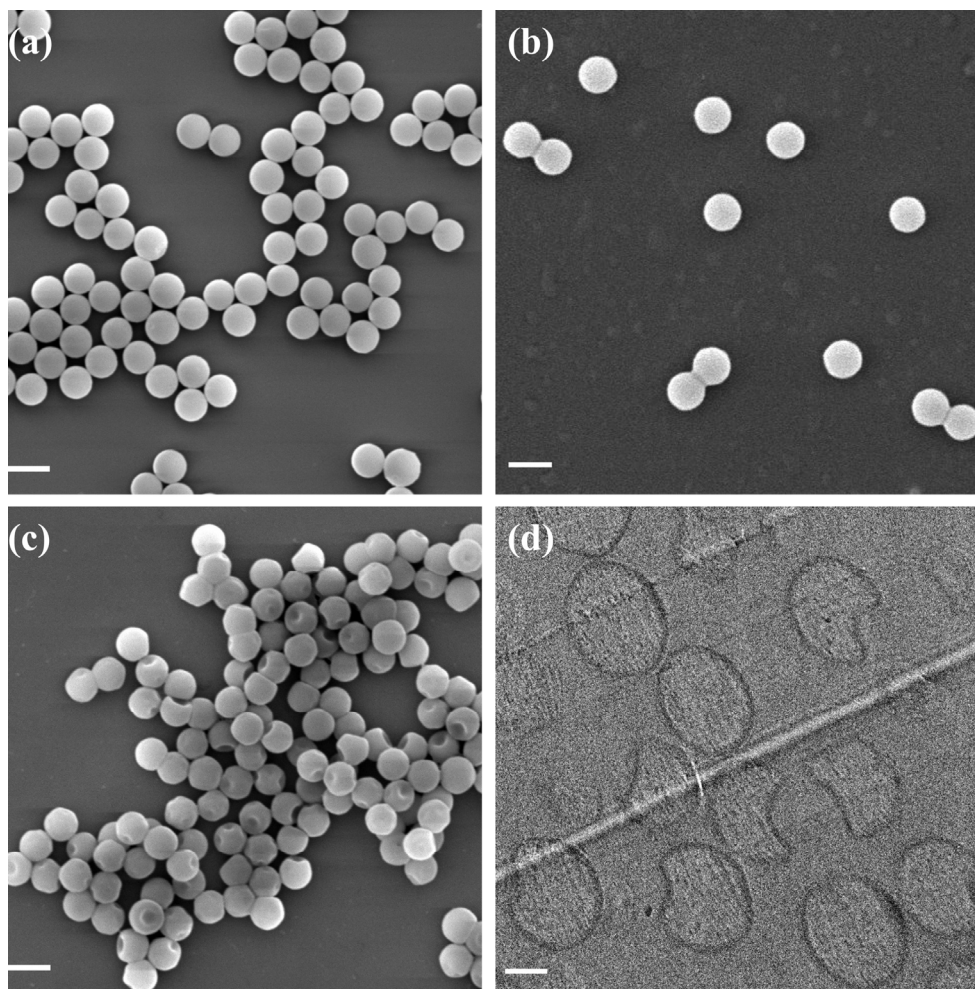


Figure 2. SEM images of (a) PPhMA seeds, (b) core-shell particles after seeded dispersion polymerization, and (c) LC shells after THF treatment (scale bar (a – c) = 2  $\mu\text{m}$ ); (d) TEM images of the cross section of the LC shells (scale bar = 0.5  $\mu\text{m}$ ).

To study the LC alignment, the LC shells were dispersed in ethanol and dried on a glass slide for POM. The POM image in Figure 3a without crossed polarizers shows monodisperse, micron-sized, almost spherical shells with occasional dimples consistent with the SEM image in Figure 2c. The POM images obtained with crossed polarizers are shown in Figures 3b,c. Maltese crosses were always observed whose direction was always parallel to the orientation of one of the crossed polarizers,

indicating that the LC molecules in the polymer shells aligned radially, that is, perpendicular to the shell surface, as schematically shown in Figure 3d.

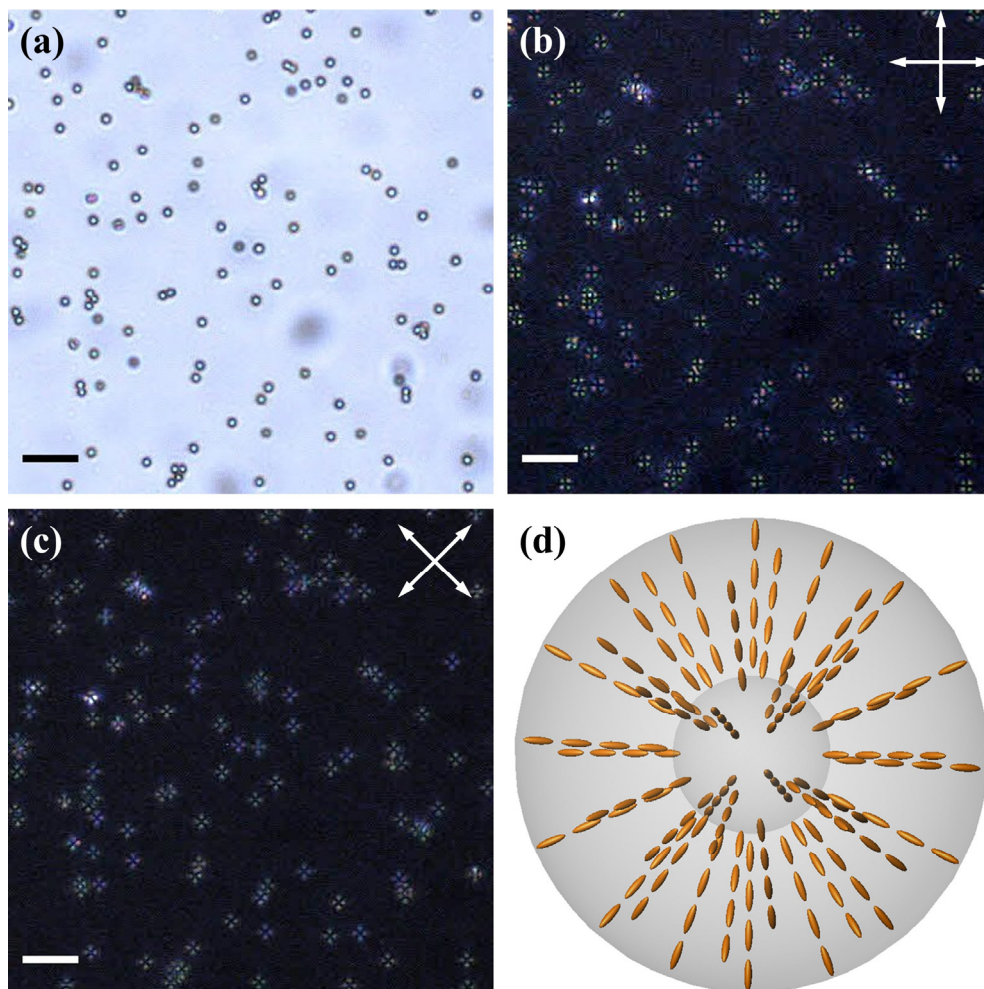


Figure 3. POM images of LC shells (a) without and (b, c) with crossed polarizers (scale bar = 10  $\mu\text{m}$ ) prepared by using PPhMA seeds. The orientation of the crossed polarizers is indicated by the arrows. (d) Schematic representation of the LC alignment in the LC shells using PPhMA seeds.

Seeded dispersion polymerization of an LC monomer mixture consisting of monomers **1** and **3** was also performed (Table 1, entry 2, and Figure 4). Since there

are relatively more monoacrylates in the forming shells than in entry 1, final crosslink density in the polymerized shells is likely lower, resulting in the hollow shells capable of collapsing and forming larger dimples and cup-shaped polymer particles. Maltese crosses were observed in the POM images, again indicating radial alignment of the LCs in the polymer shells.

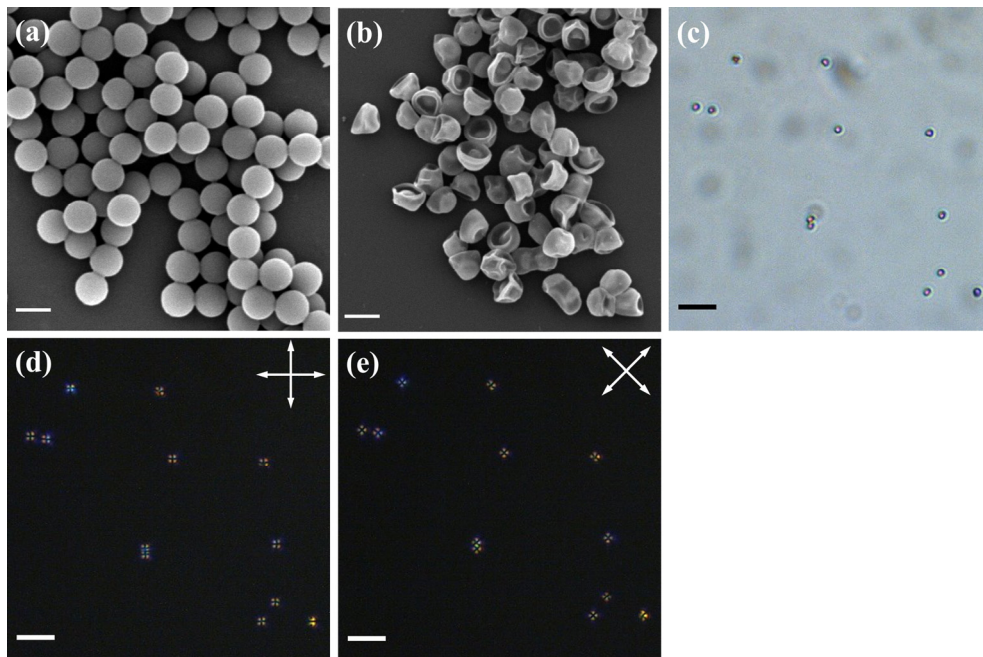


Figure 4. SEM images of core-shell particles (a) and LC shells (b) (scale bar = 2  $\mu\text{m}$ ). POM images of LC shells without (c) and with (d and e) cross polarizers (scale bar = 10  $\mu\text{m}$ ). The orientation of the cross polarizers is indicated by the arrows.

### 3.2. Synthesis of LC shells via seeded dispersion polymerization with bipolar LC seeds

To induce noncentral symmetric alignment in the LC shells, dispersion polymerization of LC monomer **1** developed by Zentel *et al.* was adopted<sup>15,21</sup> to produce non-crosslinked bipolar LC polymer seeds, which were then used as seeds. Upon forming the bipolar LC polymer seeds, the monomer mixture for the LC polymer shell was added to the dispersion without separation of the seeds, and the

polymerization was continued to form the core-shell particles. LC monomer **1**, PVP, and AIBN were dissolved in ethanol and polymerized at 70 °C for 2 h to form the non-crosslinked bipolar LC seeds *in situ* (Figure 5a). A small volume of suspension was withdrawn from the mixture and subjected to POM and <sup>1</sup>H NMR to determine the alignment of these LC particles and the conversion, respectively. The LC particle seeds showed bright spots under crossed polarizers, indicating that the LC molecules in the particles aligned in a bipolar manner, similar to that reported before<sup>15</sup>. The integration of remaining acrylate peaks at 5.5 to 6.5 ppm in the <sup>1</sup>H NMR spectrum indicated that around 30% of monomer **1** remained unreacted at this point (Figure S1). Therefore, the amount of monomer **1** added in the second stage was correspondingly reduced to maintain the composition of the shells identical to the shells made using the PPhMA seeds; the LC monomer mixture was added in the flask without separation and purification of the LC seeds. Seeded dispersion polymerization was continued overnight, yielding core-shell particles with an average diameter of 1.63 μm and a coefficient of variation of 4.3% (Table 1, entry 3, and Figure 5b). The non-crosslinked LC seeds were removed by THF, similar to the removal of the PPhMA seeds. The weight of the LC shells was reduced by 63%, suggesting successful seed removal, as the core and shell initially made up 57 and 43% of the core-shell particle. SEM images revealed that the remaining hollow shells collapsed into a biconcave shape with two dimples distributed symmetrically at opposite faces of the hollow shells (Figure 5c). While the average diameter of the shells remained almost unchanged as 1.59 μm, the height of the shell decreased significantly to 0.61 μm. TEM images further confirmed the size and shape of the LC shells, and the symmetrically distributed dimples were observed as a relatively brighter center upon tilting the sample (Figure 5d to f).

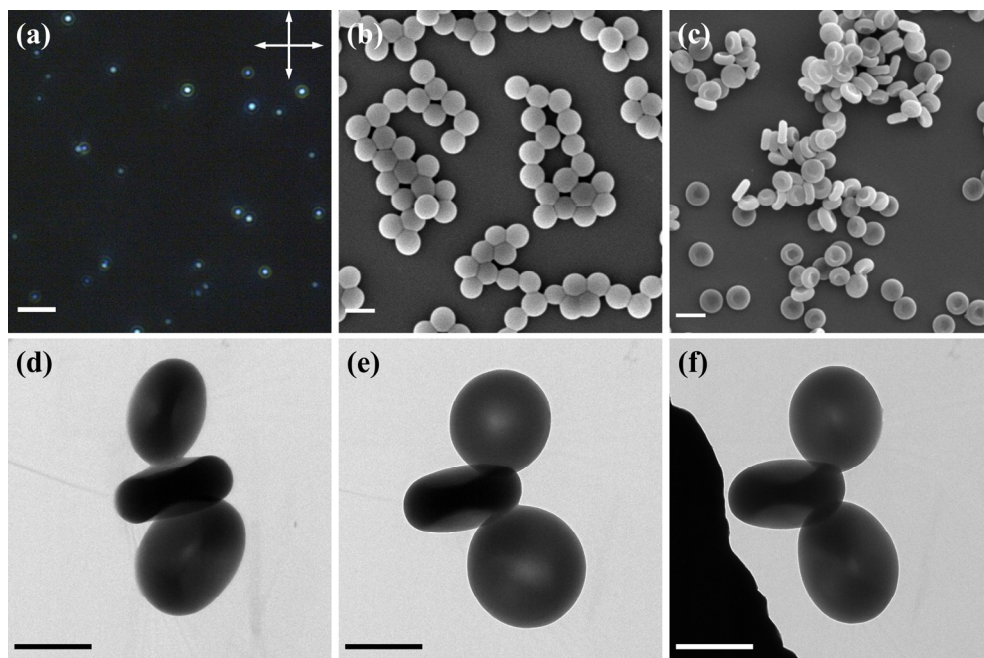


Figure 5. (a) POM images of non-crosslinked LC seeds prepared with monomer **1** with polarizers (scale bar = 10  $\mu\text{m}$ ); SEM images of (b) core-shell particles after seeded dispersion polymerization and (c) hollow LC shells after removing the polymer seeds (scale bar = 2  $\mu\text{m}$ ); (d) to (f): tilt series TEM image of LC shells from different angles (scale bar = 1  $\mu\text{m}$ ).

Maltese crosses were observed parallel to the directions of the cross polarizers after drying the shells on a glass slide (Figure 6a to c). However, since the biconcave shells uniformly “lie down” on the glass slide, meaning that the radii of the spheroids are coplanar with the glass slide surface, in order to investigate the birefringence from different angles, the shells were suspended in glycerol and filled in a glass cell for POM (Figure 6d to f). Static POM images were taken when the shells stopped moving, and some shells showed dark lines parallel to the direction of the collapse rather than the Maltese cross. From the POM images, it was concluded that the LC shells had a bipolar alignment, and the collapse occurred at the defects,

which is probably because the unaligned defects have lower modulus than the aligned regions (Figure 6g).

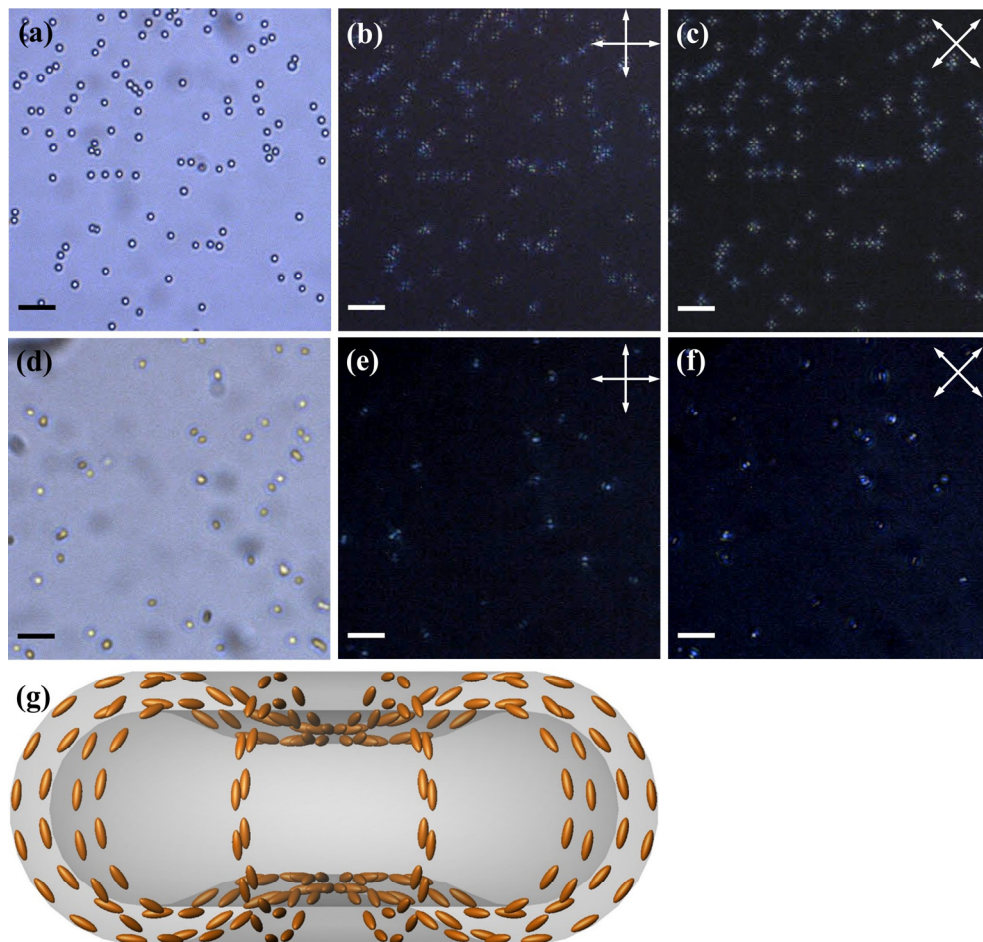


Figure 6. POM images of the LC shells (a) without and (b and c) with crossed polarizers (scale bar = 10  $\mu\text{m}$ ) prepared by using bipolar LC seeds. POM images of the LC shells suspended in glycerol (d) without and (e and f) with crossed polarizers (scale bar = 10  $\mu\text{m}$ ). The orientation of the crossed polarizers is indicated by the arrows. (g) Schematic representation of the structure and LC alignment of the LC shells.

LC shells prepared with bipolar LC seeds and an LC monomer mixture with a lower crosslink density (Table 1, entry 4, Figure 7) showed cup-shaped particles



with large dimples, similar to the shells prepared with PPhMA seeds using the same LC mixture (Table 1, entry 2, Figure 4). Moreover, Maltese crosses were observed in POM images, indicating that the LC molecules aligned radially in the shells, even with bipolar LC seeds. This result suggests that an appropriate crosslink density is necessary to obtain the bipolar alignment in the shells.

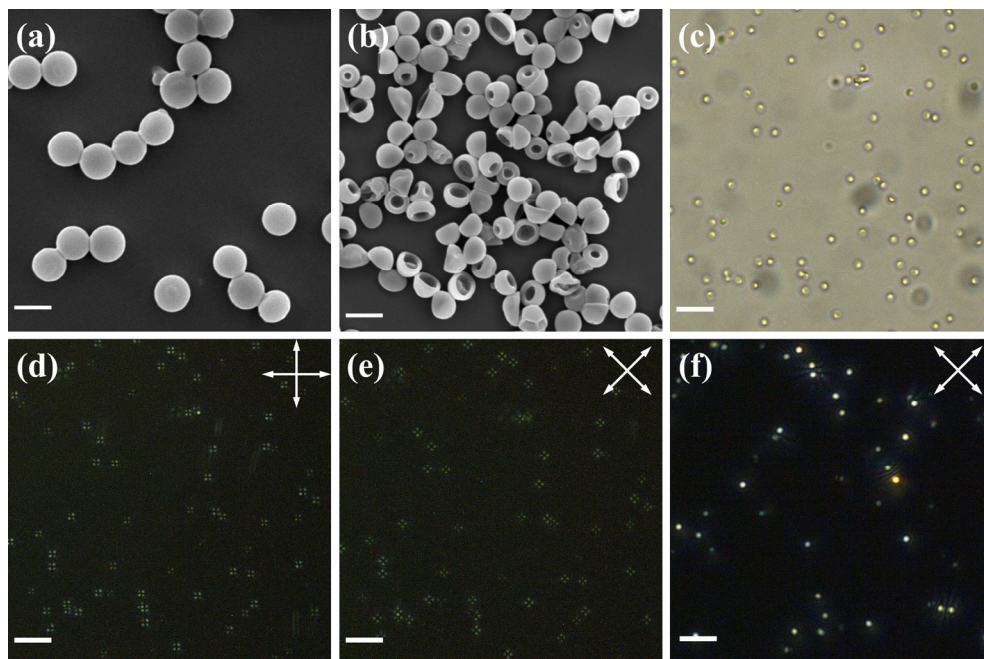


Figure 7. SEM images of (a) core-shell particles and (b) LC shells (scale bar = 2  $\mu\text{m}$ ). POM images of LC shells (c) without and (d and e) with cross polarizers (scale bar = 10  $\mu\text{m}$ ). The orientation of the cross polarizers is indicated by the arrows.

### 3.3. Seeded dispersion polymerization of other LC mixtures

Seeded dispersion polymerization was also performed using a nematic LC mixture containing monomers **1**, **2**, and **4** (weight ratio = 65/15/20, Table 1, entry 5). Monomer **4** (Figure 1a) is chosen to investigate the versatility of this seeded dispersion polymerization approach since carboxylic acid-functionalized monomers have been known to significantly undermine the colloidal stability and make dispersion polymerization challenging.<sup>22</sup> The *in situ* preparation of the bipolar LC

seeds of monomer **1** was performed as previously described, but since carboxylic acid groups significantly undermine the colloidal stability and are known to make dispersion polymerization challenging,<sup>22</sup> the second stage of the seeded dispersion polymerization was modified, with the amount of PVP increased and the polymerization time reduced to 4 h. SEM images showed that the average diameter of the resulting core-shell particles was 1.38  $\mu\text{m}$  and the coefficient of variation was 8.1% (Figure 8a), indicating that stable dispersion and particles with low polydispersity were obtained, even in the presence of the carboxylic acid-functionalized LC monomers. The core-shell particles were smaller than the previous core-shell particles (Table 1, entry 3), probably because the yield is lower as the polymerization time is shortened. After THF treatment, a weight loss of 36% was observed, while the core and shell initially made up 68 and 32% of the core-shell particle. This indicates that the removal of the seeds is not complete, probably because the diffusion of the polymer chains out of the particles was slowed by the dense LC shell, and harsher conditions are needed to remove the LC seeds more completely. Similar birefringence patterns to those seen in the previous bipolar shells were observed with POM (Figure 8c to h), confirming bipolar alignment in these LC shells, and that effective control on the LC alignment is feasible with the seeded dispersion polymerization method even with more challenging LC monomers.

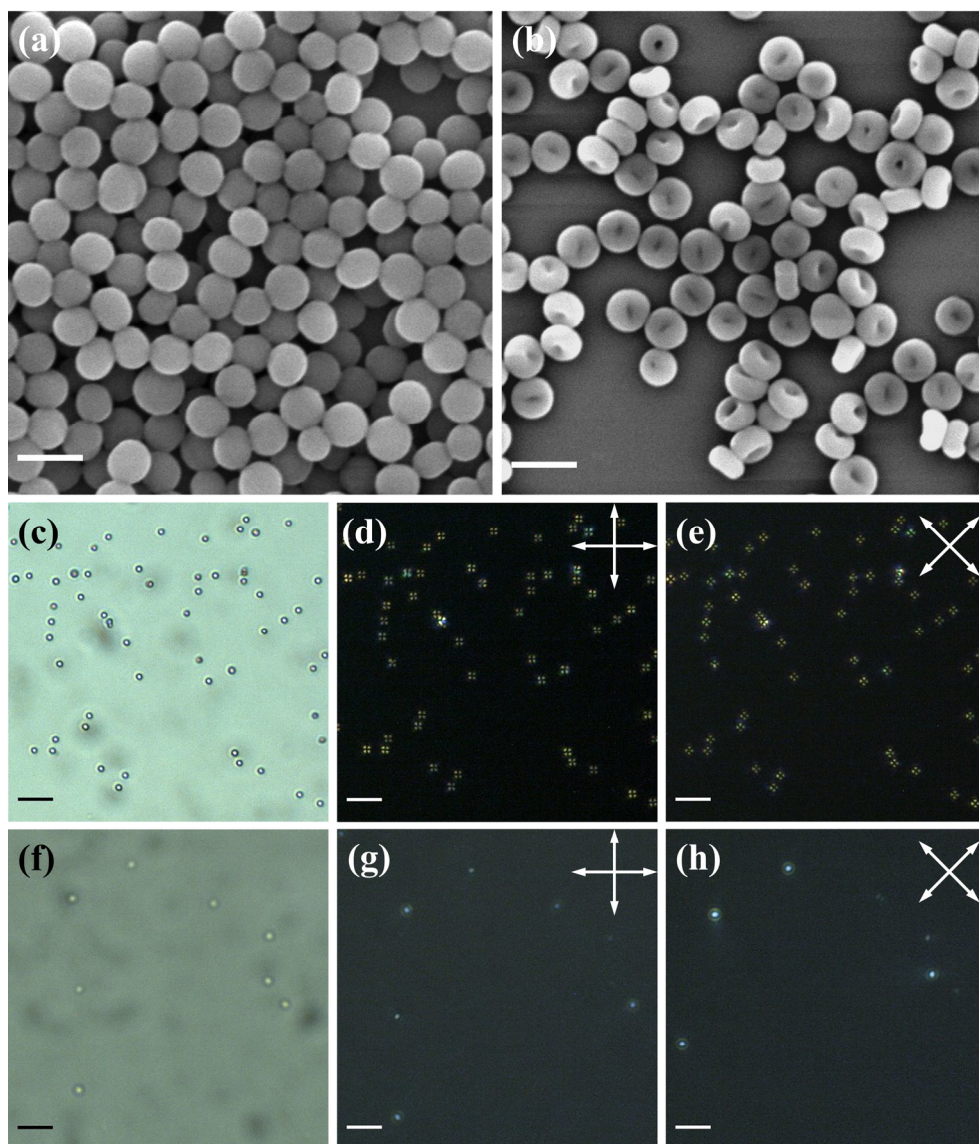


Figure 8. SEM images of the (a) core-shell particles and the (b) shells prepared from the monomers **1**, **2**, and **4** (weight ratio = 20/65/15) (scale bar = 2  $\mu\text{m}$ ). POM images of the shells (c) without and (d and e) with crossed polarizers (scale bar = 10  $\mu\text{m}$ ); POM images of the shells suspended in glycerol (f) without and (g and h) with crossed polarizers (scale bar = 10  $\mu\text{m}$ ). The orientation of the crossed polarizers is indicated by the arrows.

## 4. Conclusion

We report the successful preparation of monodisperse, micron-sized LC polymer shells via seeded dispersion polymerization. Investigation of the chemical structure of the seeds revealed that with non-LC (PPhMA) seeds, the molecules in the LC polymer shells aligned radially, and shells with small dimples are formed. By polymerizing a monomer mixture with an appropriate crosslinking density in the presence of bipolar LC seeds, hollow bipolar LC polymer shells can be prepared which collapsed in a biconcave shape. For lower crosslink density LC polymers cup-shaped polymer shells are formed. LC polymer shells with other functional groups can also be prepared with this method, revealing the versatility of the seeded dispersion polymerization method.

Our findings disclose a new method to fabricate monodisperse LC polymer shells with programmable alignments and shapes. Preliminary results reveal that the azobenzene moieties in the shells can be photoswitched by alternative irradiation of 365 and 455 nm light (Figure S2) which might be interesting for drug delivery and soft actuator applications.

## 5. References

- [1] W. Yu, Y. Chen, Z. Mao, *J. Nanosci. Nanotechnol.* **2016**, *16*, 5435–5446.
- [2] T. Liu, J. Hu, X. Ma, B. Kong, J. Wang, Z. Zhang, D. S. Guo, X. Yang, *J. Mater. Chem. B* **2017**, *5*, 7519–7528.
- [3] A. K. Yamala, V. Nadella, Y. Mastai, H. Prakash, P. Paik, *Nanoscale* **2017**, *9*, 14006–14014.
- [4] X. Yong, Y. Wu, J. Deng, *Polym. Chem.* **2019**, *10*, 4441–4448.
- [5] S. Raza, X. Yong, J. Deng, *Ind. Eng. Chem. Res.* **2019**, *58*, 4090–4098.
- [6] K. Zhou, L. Tong, J. Deng, W. Yang, *J. Mater. Chem.* **2010**, *20*, 781–789.
- [7] Y. Qin, L. Wang, C. Zhao, D. Chen, Y. Ma, W. Yang, *ACS Appl. Mater. Interfaces* **2016**, *8*, 16690–16698.
- [8] X. Wang, H. Ji, X. Zhang, H. Zhang, X. Yang, *J. Mater. Sci.* **2010**, *45*, 3981–3989.

- [9] Q. Tian, X. Yu, L. Zhang, D. Yu, *J. Colloid Interface Sci.* **2017**, *491*, 294–304.
- [10] X. Li, T. Cai, E. T. Kang, *Macromolecules* **2016**, *49*, 5649–5659.
- [11] E.-K. Fleischmann, H.-L. Liang, N. Kapernaum, F. Giesselmann, J. Lagerwall, R. Zentel, *Nat. Commun.* **2012**, *3*, 1178.
- [12] E.-K. Fleischmann, H.-L. Liang, J. Lagerwall, R. Zentel, in *Emerg. Liq. Cryst. Technol. VII* (Ed.: L.-C. Chien), **2012**, p. 82790M.
- [13] V. S. R. Jampani, D. J. Mulder, K. R. De Sousa, A. H. Gélébart, J. P. F. Lagerwall, A. P. H. J. Schenning, *Adv. Funct. Mater.* **2018**, *28*, 1801209.
- [14] V. S. R. Jampani, R. H. Volpe, K. R. De Sousa, J. F. Machado, C. M. Yakacki, J. P. F. Lagerwall, *Sci. Adv.* **2019**, *5*, eaaw2476.
- [15] M. Vennes, S. Martin, T. Gisler, R. Zentel, *Macromolecules* **2006**, *39*, 8326–8333.
- [16] M. Vennes, R. Zentel, *Macromol. Chem. Phys.* **2004**, *205*, 2303–2311.
- [17] X. Liu, Y. Xu, J. P. A. Heuts, M. G. Debije, A. P. H. J. Schenning, *Macromolecules* **2019**, *52*, 8339–8345.
- [18] M. Okubo, T. Fujibayashi, M. Yamada, H. Minami, *Colloid Polym. Sci.* **2005**, *283*, 1041–1045.
- [19] R. K. Wang, H. R. Liu, F. W. Wang, *Langmuir* **2013**, *29*, 11440–11448.
- [20] E. Stefanis, C. Panayiotou, *Int. J. Thermophys.* **2008**, *29*, 568–585.
- [21] S. Haseloh, R. Zentel, *Macromol. Chem. Phys.* **2009**, *210*, 1394–1401.
- [22] J. S. Song, L. Chagal, M. A. Winnik, *Macromolecules* **2006**, *39*, 5729–5737.
- [23] Q. Zhang, X. Tan, W. Wang, Q. Yu, Q. Wang, C. Miao, Y. Guo, X. Zhuang, Z. Yuan, *ACS Sustain. Chem. Eng.* **2019**, *7*, 8678–8686.

## 6. Supporting information

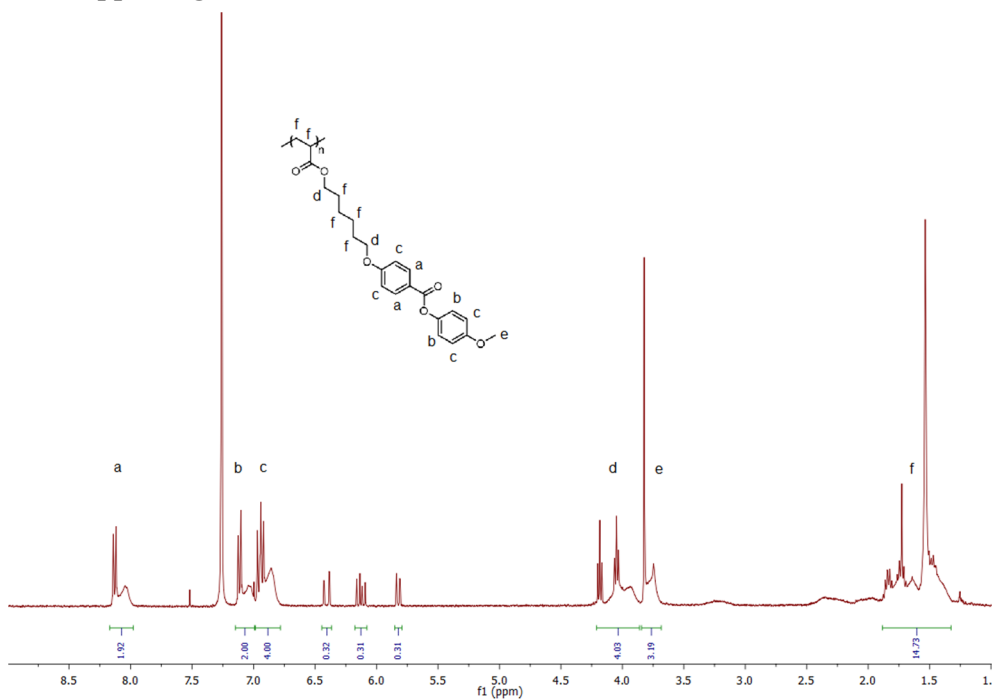


Figure S1.  $^1\text{H}$  NMR spectrum of linear LC seeds using monomer 1 after polymerizing for 2 hours. The three sets of peaks at 5.5 to 6.5 ppm correspond to the remaining acrylate groups.

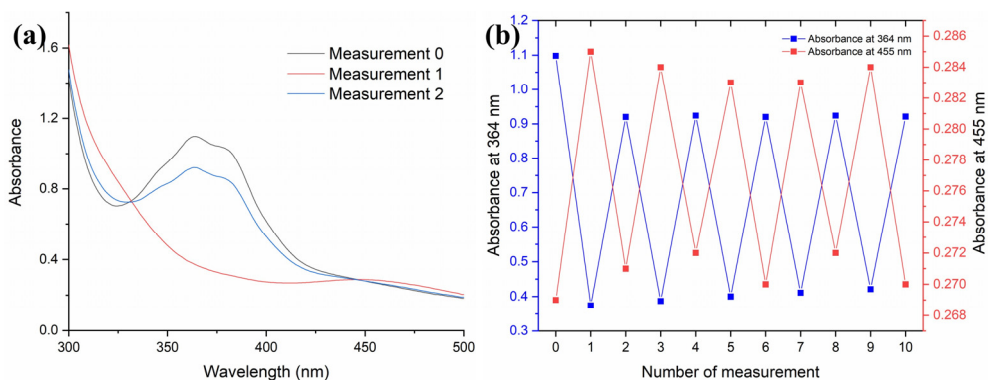


Figure S2. (a) UV-Vis spectra of LC polymer shells in entry 3 suspended in chlorobenzene. (b) Absorbance at 364 nm (*trans*-isomer of azobenzene) and 455 nm (*cis*-isomer of azobenzene) after alternative irradiations with 365 nm and 455 nm

lights. Prior to measurements 1, 3, 5, 7, and 9, the suspension was irradiated with 365 nm light. Prior to measurements 2, 4, 6, 8, and 10, the suspension was irradiated with 455 nm light.

Table S1. The HSP and counts of the functional groups in the LC monomers.

	$\delta_d$ (MPa) <sup>1/2</sup>	$\delta_p$ (MPa) <sup>1/2</sup>	$\delta_H$ (MPa) <sup>1/2</sup>	count in <b>1</b> <sup>a</sup>	count in <b>2</b> <sup>a</sup>	count in <b>3</b> <sup>a</sup>	count in <b>4</b> <sup>a</sup>
-CH<	0.6450	0.6491	-0.2018	1	2	2	1
-CH <sub>2</sub> -	-0.0269	-0.3045	-0.4119	6	12	12	6
-OCH <sub>2</sub> -	0.0310	0.8826	-0.1528	1	2	2	1
-OCH <sub>3</sub>	-0.5828	0.1764	0.1460	1	0	0	0
-COO-	0.2039	3.4637	1.1389	2	4	2	1
AC	0.8446	0.6187	0.0084	2	3	2	1
ACH	0.1105	-0.5303	-0.4305	8	11	8	4
ACCH <sub>3</sub>	0.2174	-0.5705	-1.1473	0	1	0	0
N	1.5438	2.5780	1.1189	0	0	2	0
COOH	-0.291	0.9042	3.7391	0	0	0	1

<sup>a</sup>The polymerized form of the monomers is used.

The HSP of the individual monomers in the polymerized form was then calculated according to the reference<sup>20</sup> (shown below).

Table S2. The HSP of the LC monomers.				
	<b>1</b>	<b>2</b>	<b>3</b>	<b>4</b>
$\delta_d$ (MPa) <sup>1/2</sup>	20.2	23.1	24.4	19.0
$\delta_p$ (MPa) <sup>1/2</sup>	11.2	16.1	15.8	9.92
$\delta_H$ (MPa) <sup>1/2</sup>	4.15	1.03	3.42	8.32

The HSP of the LC polymer shell was then estimated with the HSP and the weight fraction of the individual LC monomers. Finally, the solubility distance ( $R_a$ ) to ethanol and THF is calculated<sup>20,23</sup>.

Table S3. The HSP of the LC monomer mixtures and their respective $R_a$ to ethanol and THF.					
	<b>1/2/3</b>	<b>1/3</b>	<b>1/2/4</b>	Ethanol	THF
$\delta_d$ (MPa) <sup>1/2</sup>	20.6	20.4	20.4	15.8	16.8
$\delta_p$ (MPa) <sup>1/2</sup>	11.6	11.4	11.6	8.8	5.7
$\delta_H$ (MPa) <sup>1/2</sup>	3.96	4.11	4.51	19.4	8
$R_{a, \text{ethanol}}$	18.4	18.1	17.8		
$R_{a, \text{THF}}$	10.4	10.0	10.0		





## Chapter 3

# Programmable liquid crystalline polymer particles as microactuators prepared via thiol-ene dispersion polymerization

### Abstract

Narrowly dispersed, 10 micron-sized, LC polymer particles were first prepared via thiol-ene dispersion polymerization and then embedded and mechanically deformed in a polyvinyl alcohol film, followed by photopolymerization of the residual acrylate groups. Ellipsoidal microactuators in which the mesogens are aligned parallel to the long axis were obtained and showed reversible thermally driven actuation owing to the nematic to isotropic transition of the LC molecules. The LC polymer particles were also compressed to form disk-shaped microactuators in which the mesogens are aligned perpendicular to the short axis, demonstrating that the reported method is a versatile method to fabricate LC polymer particles as microactuators with programmable properties.

This chapter is partially reproduced from X. Liu, X. Pan, M. G. Debije, J. P. A. Heuts, D. J. Mulder, A. P. H. J. Schenning, *Soft Matter* **2020**, *16*, 4908–4911.

## 1. Introduction

LC microactuators have received considerable interest as they exhibit reversible changes in morphology in response to specific stimuli, and thus have potential applications in biomedicine and microfluidics.<sup>1-6</sup> Various stimuli have been used to trigger a transformation of the morphology of these LC polymer particles, including heat and light.<sup>7-10</sup> Changes in morphology are a result of phase changes of the LC mesogens, leading to changes in molecular order and conformation of polymer chains in the particles.<sup>11,12</sup> Most LC microactuators have been prepared via microfluidics by polymerizing spherical LC monomer droplets, and upon disrupting the LC order, the particles undergo a shape change to a non-spherical morphology.<sup>1-6,8,9</sup> An alternative method of producing shape changing particles was by deforming shape memory particles. Ho *et al.* developed a simple approach, in which polymer particles were immobilized in a poly(vinyl alcohol) (PVA) matrix and stretched.<sup>12,13</sup> The approach has been widely applied for its simplicity and versatility comparing to other techniques aiming to deform microscopic objects, such as nanoimprint lithography.<sup>14-20</sup> However, these non-LC particles only show “one-way” shape recovery; that is, from the temporary shape to the programmed permanent shape. Marshall *et al.* combined microfluidics and stretching and prepared LC microactuators by stretching spherical LC monomer droplets prior to polymerization; the resulting LC microactuators showed a “reverse” shape change, that is, from ellipsoidal (LC) to spherical (isotropic), although only ellipsoidal particles were prepared.<sup>21</sup> Microfluidics, however, face challenges in preparing small-sized particles (with diameters ( $D$ )  $\sim 10 \mu\text{m}$ ). Furthermore, programming microactuators into arbitrary shapes other than ellipsoidal has not been reported.

Recently, an advanced method has been reported for fabricating centimeter-size liquid crystal elastomer (LCE) actuators with programmable shapes through a two-step polymerization approach.<sup>13-20</sup> Briefly, in the first step, LC monomers are partially polymerized via a thiol-ene polymerization reaction and then mechanically

aligned. During the second step, a radical polymerization is carried out to polymerize the remaining acrylate end groups. In doing so, the LCE actuators consist of two competing polymer structures: the first thiol-ene structure that favors the initial shape before programming, and the second polyacrylate structure that favors the programmed shape.

To the best of our knowledge, the fabrication of LC microactuators in the 10  $\mu\text{m}$  range with reversible shape changes has not been reported. Bowman *et al.* described the preparation of micron-sized non-LC particles with a narrow particle size distribution based on thiol-ene dispersion polymerization.<sup>21,22</sup> By incorporating dynamic covalent functional groups in the network, the permanent shape of the particles can be tuned with specific stimuli.<sup>23</sup> However, these non-LC particles only show “one-way” shape recovery; that is, from the temporary shape to the programmed permanent shape. Nevertheless, this thiol-ene dispersion polymerization opens up a route towards the preparation of LC microactuators with reversible shape changes through the two-step polymerization approach (*vide supra*).

We now report the facile preparation of 10 micron-sized LC actuators with low dispersity and reversible shape changes based on this two-step approach. Making use of thiol-ene dispersion polymerization reported by Bowman *et al.*, narrowly dispersed, micron-sized LC polymer particles with excess acrylate groups were obtained.<sup>21,22</sup> The LC polymer particles were then immobilized in a polyvinyl alcohol (PVA) matrix and stretched. The deformed particles were then irradiated with UV light to photopolymerize the residual acrylate groups in the nematic phase. The LC mesogens were aligned mechanically during stretching, yielding ellipsoidal microactuators. Subsequent exposure to different temperatures yielded macroscopic, yet reversible shape changes between spheroids ( $T < T_{\text{NI}}$ ;  $T_{\text{NI}}$  = nematic to isotropic transition temperature) and spheres ( $T > T_{\text{NI}}$ ), due to the change of LC phase. Furthermore, by compressing the PVA/particle composite films, disk-shaped

microactuators can also be produced, indicating that this method can prepare LC microactuators of different director patterns.<sup>10</sup>

## **2. Experimental**

### **2.1. Materials**

2-methyl-1,4-phenylene bis(4-(3-(acryloyloxy)propoxy)benzoate) (**1**) was purchased from Merck Chemicals. 2-methoxy ethanol (99.8%), pentaerythritol tetrakis(3-mercaptopropionate) (**2**, 95%), 2,2'-(Ethylenedioxy)diethanethiol (**3**, 95%), triethylamine (**4**, TEA, 99.5%), PVP (**5**,  $M_n = 40,000$  g/mol), SDS (99%), urea (99.5%), formamide (99%) , and disperse red 1 acrylate (**7**, 95%) were purchased from Sigma-Aldrich. Irgacure 819 (**6**) was purchased from CIBA Inc. All solvents were purchased from Biosolve. 10 × 10 square Petri dishes and round Petri dishes with 4 compartments were purchased from VWR.

### **2.2. Thiol-ene dispersion polymerization**

100 mg of **1** (0.1699 mmol) and 30 mg PVP were added to a vial, and 3 mL 2-methoxy ethanol was added to dissolve the chemicals. 7.4  $\mu$ L **2** (0.0193 mmol), 18.8  $\mu$ L **3** (0.1158 mmol) and 2 mL ethanol were then added. Finally, 7.2  $\mu$ L TEA was added and the vial was agitated on a shaking platform overnight. After polymerization, the suspension was centrifuged and the particles were washed with ethanol twice. The particles were stored in ethanol prior to use.

### **2.3. Stretching of the PVA/particle film and photopolymerization**

1 mg **6** and 1 mg **7** were dissolved in 100  $\mu$ L chloroform ( $\text{CHCl}_3$ ) and sonicated in 5 mL 0.2% (w/v) SDS solution. The LC polymer particles were then centrifuged and redispersed in a minimal volume of ethanol and added to the emulsion and agitated on a shaking platform overnight.

10 g PVA, 1 g urea, and 1 g formamide were dissolved in 100 mL water. 1 mL of the previously described particle suspension with photoinitiator and dye was mixed with 10 mL of the PVA solution. Then the mixture was poured into a 10 × 10 cm square petri dish and dried in an oven at 60 °C overnight.

The dry PVA/particle film was cut into strips (approximately 0.5 × 2 cm) and stretched manually on a hot plate preheated to 60 °C. The draw ratio was approximately 3. The stretched strips were then cooled to room temperature and polymerized with a mercury lamp (EXFO Omnicure S2000,  $\lambda = 350\text{-}450$  nm) for 15 mins. After photopolymerization, the PVA host was dissolved in water and the solution was centrifuged. The recovered particles were repeatedly washed with water and ethanol. The particles were stored in ethanol before use.

#### **2.4. Compression of the PVA/particle film and photopolymerization**

The initiator and dye were introduced to the particles as described above. 0.5 mL of the particle suspension was mixed with 5 mL of 10 wt% PVA aqueous solution. The mixture was poured into a compartment of a round petri dish and dried in an oven at 60 °C overnight.

The dried PVA/particle film was cut into approximately 1 × 1 cm squares and stacked until the final thickness was approximately 1 mm. Then the film was compressed at 130 °C and 150 MPa for 20 mins. The final thickness of the film after compression was approximately 250  $\mu\text{m}$ . Then the film was cooled down to room temperature and polymerized with a mercury lamp (EXFO Omnicure S2000,  $\lambda = 350\text{-}450$  nm) for 30 mins. After photopolymerization, the PVA host was dissolved in water and centrifuged. The recovered particles were repeatedly washed with water and ethanol. The particles were stored in ethanol before use.

#### **2.5. Characterization**

POM images were taken with a Leica CTR6000 polarized optical microscope and a Leica DFC 420C camera. The temperature was controlled with a Linkam temperature control stage. Attenuated total reflection Fourier transfer infrared spectra (ATR-IR) were measured with a Varian 670-IR spectrometer. SEM images were taken with a JEOL TM 220 A.

### 3. Result and discussion

#### 3.1. Synthesis of the LC polymer particles by thiol-ene dispersion polymerization

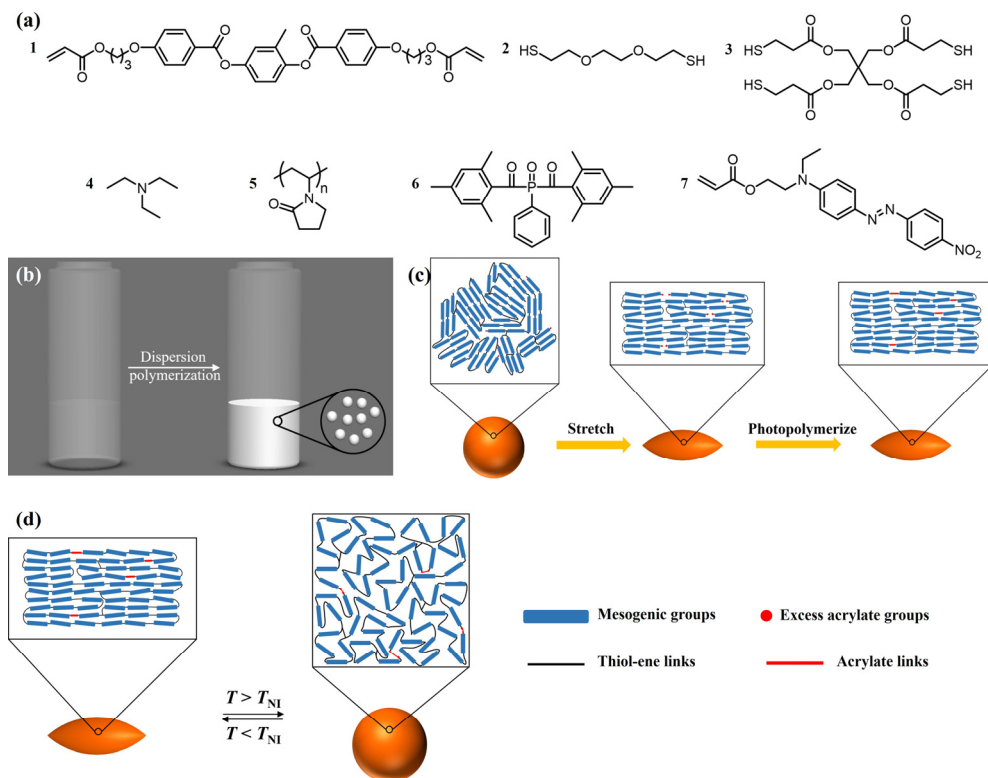


Figure 1. (a) Chemical structures of the particle components. Schematic representation of dispersion polymerization (b), stretching of the particles (c), and thermally driven actuation of the particles (d).

Previous literature suggests that establishing a delicate balance between the thiol-ene structure and the acrylate structure in the network is crucial to achieving reversible shape changes: the reported optimal molar ratio of thiol groups to acrylate groups is 1:1.1, and 25% of the total number of thiol groups should come from the tetrathiol cross-linker.<sup>17</sup> The monomer mixture used in the current study is based on these findings and consists of an LC monomer (**1**), a dithiol chain extender (**2**), and a tetrathiol cross-linker (**3**) (Figure 1a).<sup>17</sup>

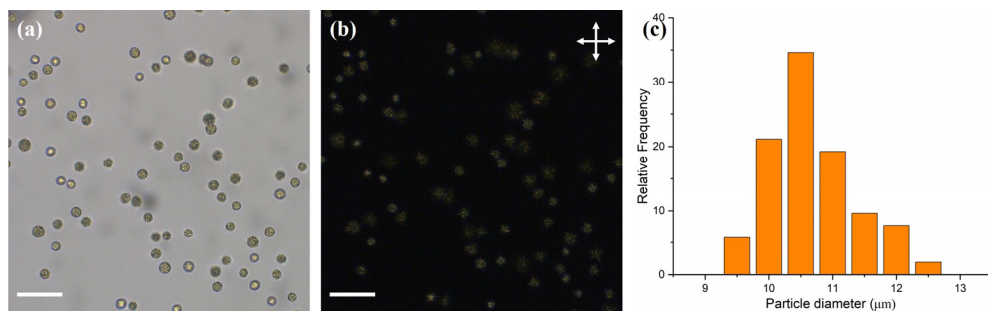


Figure 2. POM images of LC polymer particles prepared via thiol-ene dispersion polymerization without (a) and with (b) cross polarizers. Scale bar = 50 μm. (c) Particle diameter histogram of the LC polymer particles.

The first polymer structure in the LC polymer particles was prepared via thiol-ene dispersion polymerization. The monomer mixture and the steric stabilizer, PVP (**5**), were dissolved in the mixed solvent of 2-methoxy ethanol and ethanol. Upon addition of TEA (**4**), the catalyst, the solution quickly turned hazy, and the polymerization was carried out at room temperature overnight. By carefully controlling the composition of the solvent mixture, narrowly distributed particles with an average particle diameter of 10.5 μm and a coefficient of variation of 9% determined by POM (Figure 2) were prepared. The particles appeared to be polydomain based on the birefringence observed between cross polarizers (Figure 2b).

### 3.2. Programming LC microactuators by mechanical stretching



In order to photopolymerize the excess acrylate groups in the LC polymer particles, a photoinitiator, Irgacure 819 (6), and a polymerizable dye, disperse red 1 acrylate (7), used as an indicator to verify the photopolymerization, were dissolved in  $\text{CHCl}_3$  and emulsified in an aqueous SDS (0.2% w/v in water) solution. This emulsion was mixed with the LC polymer particles and agitated overnight. Upon complete absorption of the  $\text{CHCl}_3$  droplets, the suspension was added to the PVA solution (composition per 100 mL water: 10 g PVA, 1g urea, and 1g formamide as plasticizers) and dried to form the PVA/particle film. The film was then cut into strips and stretched (draw ratio = 3) at 60 °C to deform the spherical LC polymer particles. The stretched strips were cooled to room temperature, followed by photopolymerization of the remaining acrylate groups. After photopolymerization, the PVA strips were dissolved in water to yield the ellipsoidal LC polymer particles (Figure 3a and b). The lengths along the long and the short axes were determined as 15.5  $\mu\text{m}$  and 7.5  $\mu\text{m}$ , respectively. Most likely the LC moieties align along the long particle axis, as the LC polymer particles appeared dark if the cross polarizers were parallel or perpendicular to the long axis (Figure 3c and d). This indicates that ellipsoidal LC polymer particles are formed in which the LC mesogens are aligned in the stretching direction along the long axis. Since the number of acrylate groups in the particles is very low, the characteristic signals of acrylate groups were too weak for an accurate conversion measurement with infrared spectroscopy (Figure S1). Hence, to verify the success of photopolymerization, the particles were extracted with THF to determine whether the dispersed red 1 acrylate dye was incorporated into the network. The dye was extracted from the particles before photopolymerization but not from the particles after photopolymerization, indicating that the photopolymerization was indeed successful and the dye was grafted to the particles.

For the thermal actuation study, the ellipsoidal LC polymer particles were dispersed in glycerol, and a drop of the dispersion was added to a glass cell and

analyzed with POM. The dispersion was first equilibrated at 50 °C and then heated to 70 °C at 3 °C/min. The ellipsoidal LC polymer particles showed a shape change from ellipsoidal to spherical during heating, and upon cooling to 50 °C, the spheres became ellipsoidal again (Figure 3e). The heating-cooling cycle was repeated and the shape change was similar to the first cycle, which indicates that the process was reversible (Fig. S2). The birefringence of the particles was observed with POM at 50 °C and disappeared at 70 °C, suggesting that the actuation was a result of the LC-isotropic phase transition.

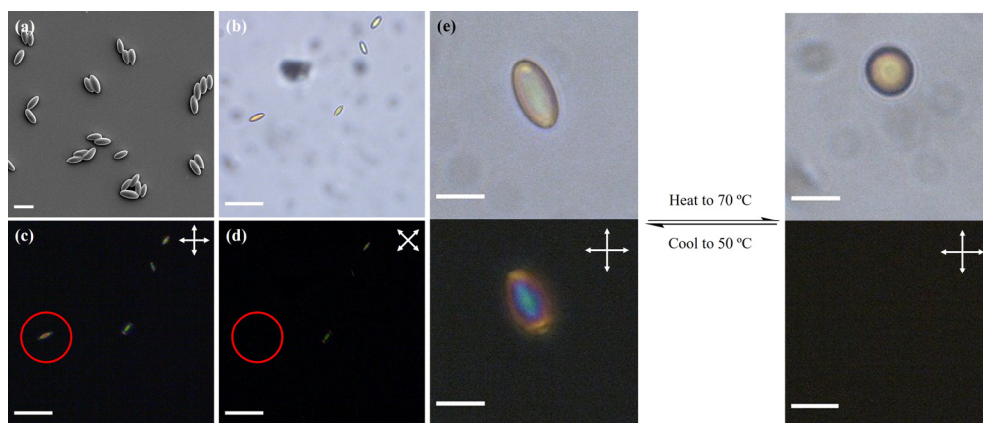


Figure 3. SEM image (a) and POM image without (b) and with (c) cross polarizers of the LC polymer particles after stretching and photopolymerization. (d) The cross polarizers were rotated such that the long axis of a particle (circled) was parallel to one of the polarizers. (e) Thermally driven actuation of the stretched particles without (top) and with (bottom) cross polarizers. Scale bar = 20  $\mu\text{m}$  for (a); scale bar = 50  $\mu\text{m}$  for (b), (c) and (d); scale bar = 50  $\mu\text{m}$  for (e).

### 3.3. Programming LC microactuators with mechanical compression

To demonstrate that the initial shape and director of the LC polymer particles can be programmed, the PVA/particles were also compressed to produce disk-shaped LC polymer particles in which the mesogens are aligned perpendicular to the short axis. The particles were slightly elongated because the PVA matrix flowed outwards during compression and created a shear field (Figure 4a). The average lengths along

the long and short axes were determined as 13  $\mu\text{m}$  and 11  $\mu\text{m}$ , respectively. By tracking a particle that rotated in glycerol, the shape was confirmed as a disk (Figure 4b). A thermal actuation study was performed on the disk-shaped LC polymer particles by first equilibrating at 60  $^{\circ}\text{C}$  and then heated to 75  $^{\circ}\text{C}$  at 3  $^{\circ}\text{C}/\text{min}$ . The shape of the particles changed from disk-shaped to spherical, corresponding to the appearance of birefringence under POM (Figure 4c), and upon cooling to 60  $^{\circ}\text{C}$ , the shape returns to disk-shaped again.

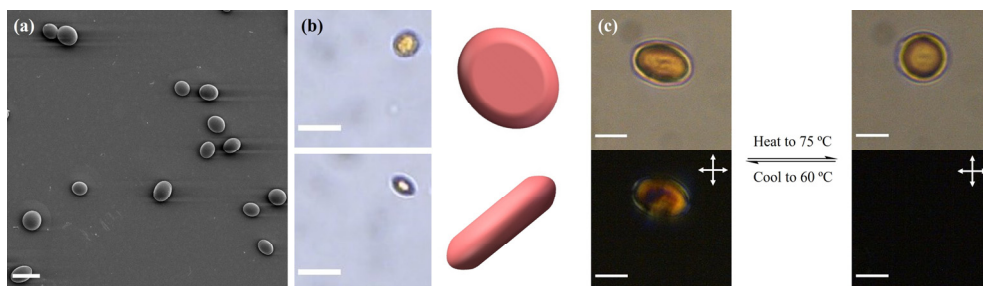


Figure 4. (a) SEM images of the particles after compression and photopolymerization (scale bar = 20  $\mu\text{m}$ ); (b) POM images and schematic representation of a particle when facing upwards (top) and to the side (bottom) (scale bar = 20  $\mu\text{m}$ ). (c) Thermally driven actuation of the particles without (top) and with (bottom) cross polarizers (scale bar = 10  $\mu\text{m}$ ).

#### 4. Conclusion

We report the preparation of thermally driven LC microactuators in the 10  $\mu\text{m}$  range with programmable reversible shape changes. The LC polymer particles were prepared by thiol-ene dispersion polymerization and the excess acrylate groups were photopolymerized after the particles were stretched or compressed in a PVA matrix. By changing the temperature of the environment, the LC phase of the LC polymer particles can be altered between the nematic and isotropic phases, and as a result, the shape of the microactuators can be tuned between spherical and ellipsoidal. By compressing the PVA/particle film, disk-shaped microactuators can also be produced. This work can lead to a new, versatile method for preparing micron-sized

actuators with programmable properties, making these soft actuators appealing for applications ranging from biomedical to microfluidic devices.

## 5. Reference

- [1] C. Ohm, N. Kapernaum, D. Nonnenmacher, F. Giesselmann, C. Serra, R. Zentel, *J. Am. Chem. Soc.* **2011**, *133*, 5305–5311.
- [2] E. K. Fleischmann, H. L. Liang, N. Kapernaum, F. Giesselmann, J. Lagerwall, R. Zentel, *Nat. Commun.* **2012**, *3*, 1178.
- [3] C. Ohm, E. K. Fleischmann, I. Kraus, C. Serra, R. Zentel, *Adv. Funct. Mater.* **2010**, *20*, 4314–4322.
- [4] C. Ohm, C. Serra, R. Zentel, *Adv. Mater.* **2009**, *21*, 4859–4862.
- [5] T. Hessberger, L. Braun, R. Zentel, *Polymers (Basel)*. **2016**, *8*, 410.
- [6] E. K. Fleischmann, F. R. Forst, K. Köder, N. Kapernaum, R. Zentel, *J. Mater. Chem. C* **2013**, *1*, 5885–5891.
- [7] H. Yu, H. Liu, T. Kobayashi, *ACS Appl. Mater. Interfaces* **2011**, *3*, 1333–1340.
- [8] L. B. Braun, T. Hessberger, R. Zentel, *J. Mater. Chem. C* **2016**, *4*, 8670–8678.
- [9] V. S. R. Jampani, D. J. Mulder, K. R. De Sousa, A. H. Gélébart, J. P. F. Lagerwall, A. P. H. J. Schenning, *Adv. Funct. Mater.* **2018**, *28*, 1801209.
- [10] V. S. R. Jampani, R. H. Volpe, K. R. De Sousa, J. F. Machado, C. M. Yakacki, J. P. F. Lagerwall, *Sci. Adv.* **2019**, *5*, eaaw2476.
- [11] R. Article, E. M. Terentjev, *J. Phys. Condens. Matter* **1999**, *11*, R239–R257.
- [12] C. Ohm, M. Brehmer, R. Zentel, *Adv. Mater.* **2010**, *22*, 3366–3387.
- [13] C. M. Yakacki, M. Saed, D. P. Nair, T. Gong, S. M. Reed, C. N. Bowman, *RSC Adv.* **2015**, *5*, 18997–19001.
- [14] M. K. McBride, A. M. Martinez, L. Cox, M. Alim, K. Childress, M. Beiswinger, M. Podgorski, B. T. Worrell, J. Killgore, C. N. Bowman, *Sci. Adv.* **2018**, *4*, eaat4634.
- [15] L. Yu, H. Shahsavan, G. Rivers, C. Zhang, P. Si, B. Zhao, *Adv. Funct. Mater.* **2018**, *28*, 1–8.

- [16] D. R. Merkel, N. A. Traugutt, R. Visvanathan, C. M. Yakacki, C. P. Frick, *Soft Matter* **2018**, *14*, 6024–6036.
- [17] M. Barnes, R. Verduzco, *Soft Matter* **2019**, *15*, 870–879.
- [18] L. Wang, W. Liu, L. X. Guo, B. P. Lin, X. Q. Zhang, Y. Sun, H. Yang, *Polym. Chem.* **2017**, *8*, 1364–1370.
- [19] E. C. Davidson, A. Kotikian, S. Li, J. Aizenberg, J. A. Lewis, *Adv. Mater.* **2019**, *1905682*, 1–6.
- [20] N. Torras, K. E. Zinoviev, J. Esteve, A. Sánchez-Ferrer, *J. Mater. Chem. C* **2013**, *1*, 5183–5190.
- [21] C. Wang, M. Podgórski, C. N. Bowman, *Mater. Horizons* **2014**, *1*, 535–539.
- [22] C. Wang, X. Zhang, M. Podgórski, W. Xi, P. Shah, J. Stansbury, C. N. Bowman, *Macromolecules* **2015**, *48*, 8461–8470.
- [23] L. M. Cox, X. Sun, C. Wang, N. Sowan, J. P. Killgore, R. Long, H. A. Wu, C. N. Bowman, Y. Ding, *ACS Appl. Mater. Interfaces* **2017**, *9*, 14422–14428.

## 6. Supporting information

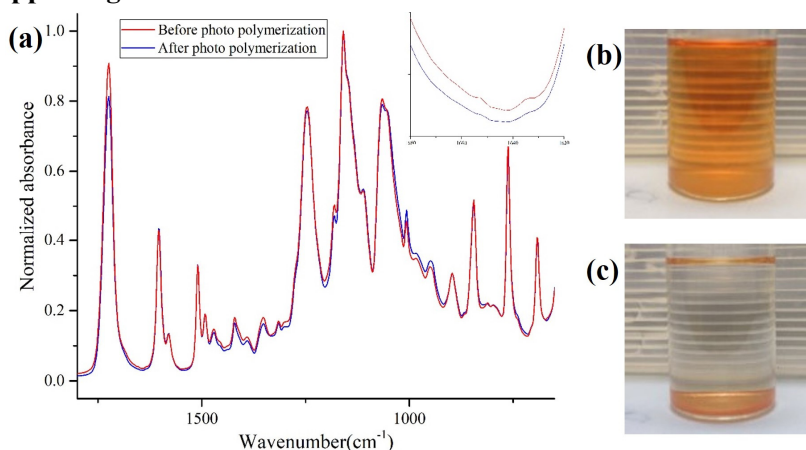


Figure S1. (a) IR spectrum of LC polymer particles before (red) and after (blue) photopolymerization. LC polymer particles extracted with THF before (b) and after (c) photopolymerization.

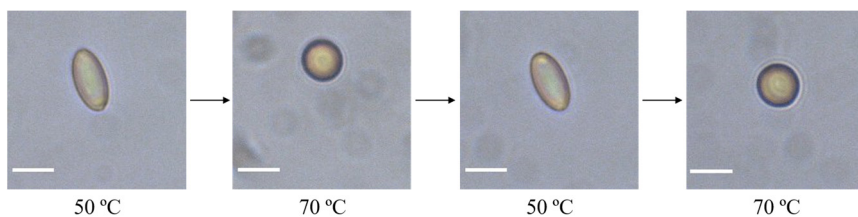


Figure S2. Thermally driven actuation of the stretched particles in two heating-cooling cycles. The shape change of the particle was fully reversible. (Scale bar = 10  $\mu\text{m}$ )

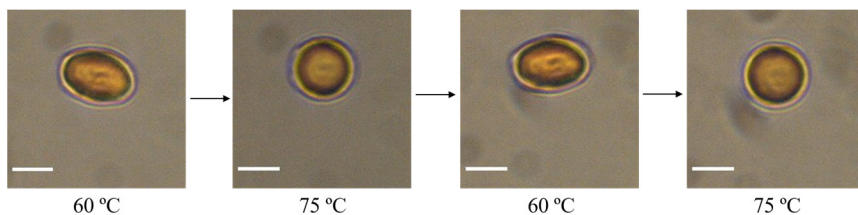


Figure S3. Thermally driven actuation of the compressed particles in two heating-cooling cycles. The shape change of the particle was fully reversible. (Scale bar = 10  $\mu\text{m}$ )



## Chapter 4

# Monodisperse liquid crystalline polymer particles synthesized via precipitation polymerization

### Abstract

In this chapter, the preparation of monodisperse, crosslinked LC particles via precipitation polymerization is reported. This versatile and scalable method yields LC polymer particles with a smectic liquid crystal order. Although the LC monomers are randomly dissolved in solution, the oligomers self-align and LC order is induced. For the polymerization, a smectic LC monomer mixture consisting of crosslinkers and benzoic acid hydrogen-bonded dimers is used. The average diameter of the particles increases at higher polymerization temperatures and in better solvents, whereas the monomer and initiator concentration have only a minor impact on the particle size. After deprotonating of the benzoic acid groups, the particles show rapid absorption of a common cationic dye, methylene blue. The methylene blue in the particles can be subsequently released with the addition of  $\text{Ca}^{2+}$ , while monovalent ions fail to trigger the release. These results reveal that precipitation polymerization is an attractive method to prepare functional LC polymer particles of a narrow size distribution and on a large scale.

This chapter is partially reproduced from X. Liu, Y. Xu, J. P. A. Heuts, M. G. Debije, A. P. H. J. Schenning, *Macromolecules* **2019**, 52, 8339–8345.



## 1. Introduction

LC polymer particles prepared by dispersion polymerization had a low dispersity and the technique is scalable.<sup>1-4</sup> Nevertheless, previous studies have shown that the introduction of crosslinkers and functional groups tend to destabilize the dispersion and lead to coagulum, poor morphology, and high polydispersity.<sup>5,6</sup> This drawback severely limits the applicability of dispersion polymerization.

Precipitation polymerization is an attractive method to prepare polymer particles with narrow size distributions on a relatively large scale. In precipitation polymerization, radicals first grow in the solution until the solubility limit is reached, and the oligomers precipitate and form preliminary particles, which further grow primarily by capturing propagating radicals from the solution.<sup>7</sup> Monodisperse, highly crosslinked, and functional polymer particles have been prepared by this method.<sup>8,9</sup> The polymerization method does not require specific equipment or surfactants. Moreover, particles with complex structures can also be prepared, including core-shell and hollow particles.<sup>10-14</sup> To date, however, precipitation polymerization has never been used to prepare LC polymer particles.

We now describe the preparation of LC polymer particles by precipitation polymerization. This versatile and scalable method yields polymer particles with a low dispersity of diameters between 0.7 and 1.4  $\mu\text{m}$ . Although the LC monomers are randomly dissolved in solution, well-defined particles with a smectic LC order are obtained. The average diameter of the particles increases at higher polymerization temperatures and in better solvents, whereas the monomer and initiator concentration have only a minor impact on the particle size. The LC polymer particles can be used to rapidly absorb and selectively release molecules in the presence of divalent cations. Hence precipitation polymerization is an attractive new method to prepare functional LC polymer particles of a narrow size distribution on a large scale.

## 2. Experimental

## 2.1. Materials

4-(6-acryloxy-hexyl-1-oxy) benzoic acid (**1**) and 4-((4-(6-(acryloyloxy)hexyloxy)phenoxy)carbonyl)phenyl 4-(6-(acryloyloxy)hexyloxy) benzoate (**2**) were purchased from Synthron Chemicals, Germany. Phenyl acetate (>98%) was purchased from TCI Europe. Other solvents were purchased from Biosolve. Luperox 331 P80 (1,1-Bis(*tert*-butylperoxy)cyclohexane, 80 wt.% in benzyl butyl phthalate, technical grade), AIBN (98%), potassium hydroxide (KOH, 85%), calcium chloride (CaCl<sub>2</sub>), lithium chloride (LiCl), potassium chloride (KCl), and sodium chloride (NaCl) were purchased from Sigma-Aldrich. Methylene blue (MB) was purchased from Acros Organics.

## 2.2. Synthesis of the liquid crystalline particles

50 mg of **1** and 50 mg of **2** were added to a 50 mL round bottom flask; the flask was then pumped and backfilled with argon 3 times. The initiator (AIBN for polymerization at 65 °C, Luperox 331 P80 for polymerization at 95 °C) was dissolved in ethyl acetate or phenyl acetate and added to the flask (see Table 1 for details). The flask was put into an oil bath preheated to the polymerization temperature for 24 hrs. After polymerization, the suspension was centrifuged and washed with ethanol to obtain the particles.

## 2.3. Fabrication of nanoporous particles

The pristine particles were sonicated in 10 mM KOH solution at room temperature until completely dispersed to deprotonate the convert the benzoic acid groups into potassium benzoate salts. Then the particles were centrifuged and washed with deionized water twice.

## 2.4. Absorption and release of methylene blue.

For the absorption kinetics, 10  $\mu\text{L}$  of MB solution ( $\text{MB}/\text{COO}^- = 1$ ) was added to 2.95 mL 0.01 M KOH solution in a 3 mL cuvette and the absorption of the solution was measured. Then 36.7  $\mu\text{L}$  0.5 mg/mL particle suspension was added to the solution and the absorption spectrum of the solution was measured every minute.

To monitor the release kinetics, 10  $\mu\text{L}$  of MB solution and 36.7  $\mu\text{L}$  0.5 mg/mL particle suspension ( $\text{MB}/\text{COO}^- = 1$ ) were added to 2.95 mL 0.01 M KOH solution and equilibrated for an hour. Then 2.7 mL of the solution was transferred to a 3 mL cuvette and the absorption of the solution was measured. Then 300  $\mu\text{L}$  of 10 mM salt solution was added and the absorption spectrum of the solution was measured every minute to monitor the release of MB.

## 2.5. Characterization

POM images were taken with a Leica CTR6000 polarized optical microscope and a Leica DFC 420C camera. The temperature was controlled with a Linkam temperature control stage. DSC curves were measured with a DSC Q2000 from TA Instruments, with 3  $^{\circ}\text{C}/\text{min}$  temperature ramp from  $-20$  to  $130^{\circ}\text{C}$  and 5 minutes isotherm. The second heating and cooling cycles were used for characterization. XRD was performed on a Ganesha lab instrument with a GeniX-Cu ultra-low divergence source producing X-ray photons with a wavelength of 1.54  $\text{\AA}$  and a flux of  $1 \times 10^8$  ph/s. Scattering patterns were collected with a Pilatus 300 K silicon pixel detector with  $478 \times 619$  pixels each  $172 \mu\text{m}^2$  in size. Dynamic light scattering (DLS) was measured with Anton Paar Litesizer 500 in 1 mM KCl solution in backscattering mode at  $25^{\circ}\text{C}$ . UV-Vis spectra were measured with a Shimadzu UV-3102 PC. SEM images were taken with a JEOL TM 220 A. The average size and coefficient of variation of the particle size distribution ( $C_v = \frac{\bar{d}}{SD}$ ) were measured and calculated over 100 particles per sample.

### 3. Result and discussion

#### 3.1. LC monomer mixture

The LC monomer mixture consists of a hydrogen-bonded benzoic acid monomer (**1**) that attracts cations when deprotonated, and an LC cross-linker (**2**) to maintain the network, in a 1/1 w/w ratio (Figure 1a). The phase behavior of the mixtures was determined via POM. An isotropic-nematic transition was observed at around 115 °C, and the mixture further converts into a smectic A phase at around 105 °C (Figure S1).

#### 3.2. Synthesis of the liquid crystalline particles by precipitation polymerization

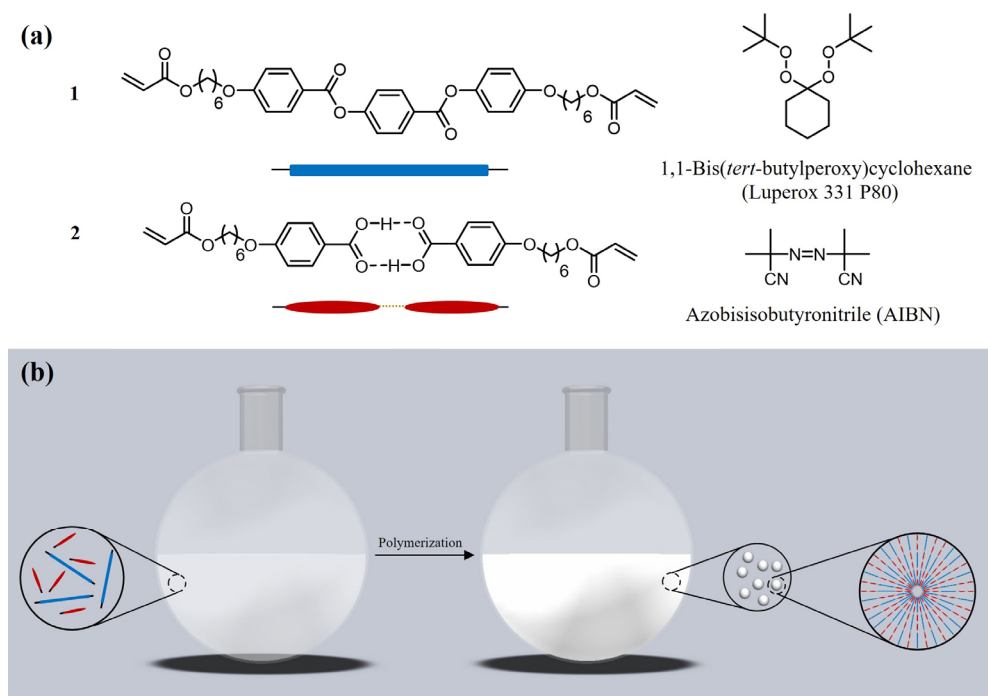


Figure 1. (a) The chemical structure of the monomers and initiators. (b) Schematic representation of precipitation polymerization method to synthesize liquid crystalline polymer particles.

The LC polymer particles were synthesized by precipitation polymerization. The solvent is a vital factor for precipitation polymerization, as it needs to dissolve both the monomers and free radical initiator, but also allow oligomers reaching a critical chain length to precipitate and form the preliminary particles.<sup>7</sup> Upon screening of multiple solvents (including acetonitrile, toluene, dioxane, isopropanol, and dimethylformamide), phenyl acetate and ethyl acetate were found to produce monodisperse particles. Monomers, initiator, and solvent were added to an oxygen-free flask and polymerized at different temperatures for 24 hours to yield the particles. We first investigated the effect of monomer concentration, initiator concentration, solvent, and temperature on the average particle size and size distribution with SEM and DLS (Table 1 and Figure 2).

Table 1. Polymerization condition at each run and the corresponding results.

Entry	[Initiator] J <sup>a</sup>	[Monomer] J <sup>b</sup>	Solvent	Temperature (°C)	D <sub>n</sub> (μm)	C <sub>v</sub> (%)	D <sub>z</sub> (μm)	Yield (%)
1	1%	2%	Phenyl acetate	95	0.62	7.5	0.79	12
2	2%	2%	Phenyl acetate	95	1.05	6.5	1.13	75
3	3%	2%	Phenyl acetate	95	0.92	5.0	1.06	71
4	4%	2%	Phenyl acetate	95	0.97	3.7	1.08	73

5	2%	1%	Phenyl acetate	95	0.82	5.4	0.84	31
6	2%	3%	Phenyl acetate	95	0.95	6.7	1.02	67
7	2%	4%	Phenyl acetate	95	1.03	6.8	1.07	70
8	2%	2%	Phenyl acetate	65	0.70	5.2	0.88	89
9	2%	2%	Ethyl acetate	65	1.44	5.4	1.79	57

<sup>a</sup> w/w ratio to monomer; <sup>b</sup> w/v ratio to solvent;  $D_n$  = number average diameter determined via SEM (min. 100 particles);  $C_v = D_n / SD$ ;  $D_z$  = Z-average diameter determined via DLS; Yield = weight of particles / weight of monomers.

The effect of initiator and monomer concentrations on the final particle size and distribution was performed in phenyl acetate at 95 °C using Luperox 331 P80 as initiator. Initiator and monomer concentrations were varied from 1% to 4% (entries 1 to 7). With increasing initiator and decreasing monomer concentrations, the coefficient of variation decreases slightly. The diameter of the particles was around 1  $\mu\text{m}$  regardless of the initiator and monomer concentrations if they were both  $\geq 2\%$ . However, smaller particles and lower yields were observed when either the initiator or monomer concentration was low ( $<2\%$ ), probably because the initiator efficiency was decreased, the oligomer chains had difficulty in forming preliminary particles, and the conversion of the monomers was limited under dilute conditions, also

indicated by the low yield. When the polymerization was carried out at 65 °C and with AIBN as initiator (entry 8), smaller particles were obtained compared to polymerization performed at 95 °C. The decreased particle size can be attributed to the decreased solubility of the oligomer chains at lower temperatures, which meant the nucleation occurs faster, resulting in the formation of smaller particles. Particles synthesized in ethyl acetate were larger than particles synthesized in phenyl acetate (entry 8 versus entry 9), as ethyl acetate is a better solvent for the polymers, resulting

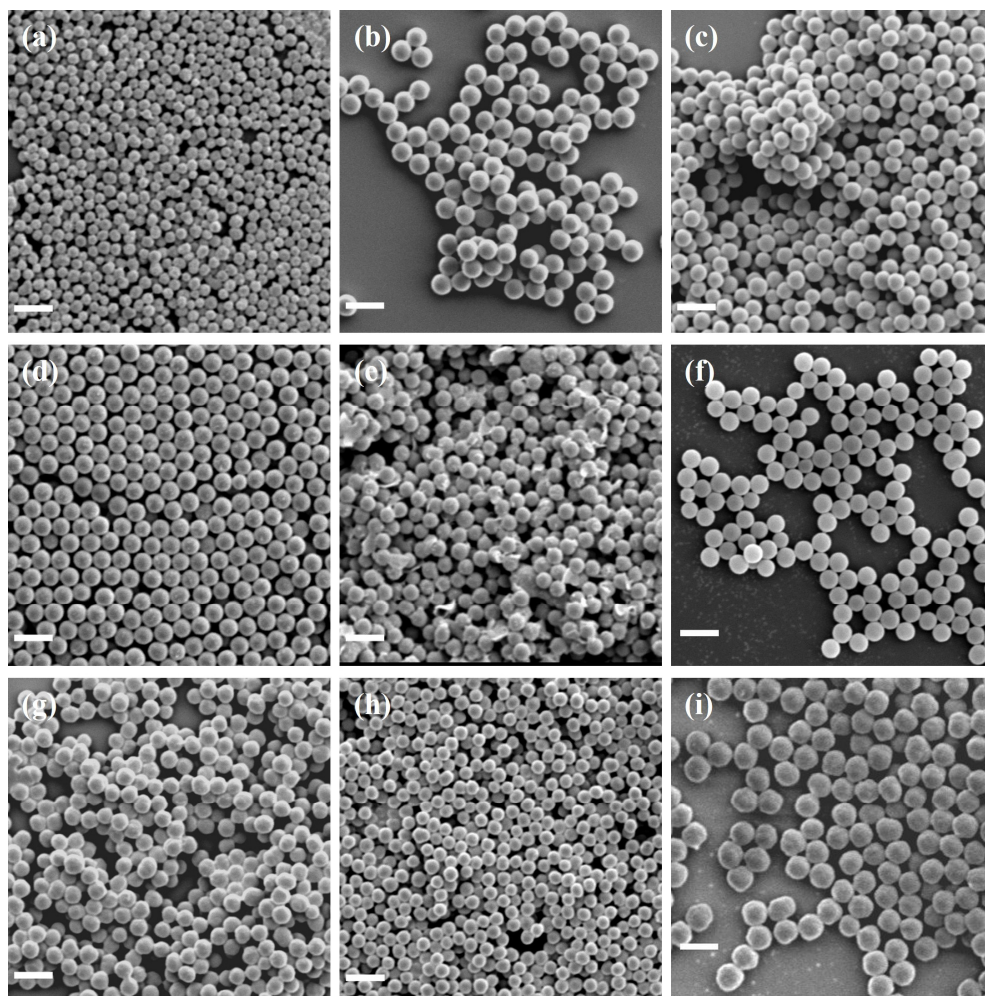


Figure 2. SEM images of particles synthesized in entry 1 to 9 (table 1). Scale bar = 2  $\mu\text{m}$ .

in slower nucleation and larger particles. As suggested in the literature, solvent and temperature affect the size and morphology of the particles through changing the Flory parameter,  $\chi$ .<sup>15</sup> With low  $\chi$ , the interaction between solvent and polymer is favorable and leads to an extended growth of oligomer chains in the solution, and as a result, gives larger particles. Particles prepared in entry 4 were characterized in more detail and used in adsorption and release studies.

### 3.3. Characterization of the particles

POM analysis using cross polarizers was used to investigate the internal structure and molecular alignment in the polymer particles. The particles were first suspended in water and then dried between two glass slides to be nicely dispersed and to eliminate Brownian motion. As shown in Figure 3a and b, so-called Maltese crosses were observed in the same direction as the crossed polarizers. This indicates that the LC molecules align homeotropically, that is, perpendicular to the particle surface (Figure 3c).<sup>16</sup> Interestingly, although the LC monomers are randomly dissolved, the oligomers apparently self-align inducing liquid crystalline order. The polymer particles were further characterized by XRD, revealing a peak at 0.4 nm, which can be attributed to the intermolecular spacing of the molecules (Figure 3d). However, no layer spacing was observed which might be due to the low contrast in the particles (*vide infra*).

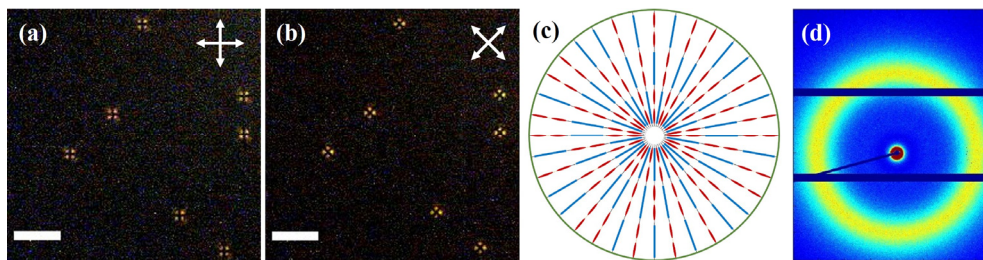


Figure 3. (a) and (b) POM images of the particles with cross polarizers. Scale bar = 5  $\mu\text{m}$ . (c) Radial alignment of the liquid crystal molecules in the particles. (d) XRD of the particles. The particles used were entry 4.



### 3.4. Formation of nanoporous particles

To show that the LC particles can be used to absorb and release molecules, nanoporous particles were prepared. The particles were treated with 0.01 M KOH solution to break the hydrogen bonding between COOH groups and transform them into  $\text{COO}^-\text{K}^+$  salts. IR spectra confirmed complete deprotonation, as the peaks corresponding to hydrogen bonds at 2500 to 2700  $\text{cm}^{-1}$  and 1677  $\text{cm}^{-1}$  disappeared completely and the peaks corresponding to asymmetric and symmetric stretching of carboxylate salt at 1545  $\text{cm}^{-1}$  and 1392  $\text{cm}^{-1}$  appeared (Figure S2). The average size and size distribution of the particles remained unchanged during the KOH treatment (Figure 4a), most likely due to the high crosslinking density that prevented the polymer particles from swelling. A new signal at 3.4 nm and the corresponding second-order peak at 1.7 nm were observed in XRD, which were assigned to the layer spacing in the LC particles (Figure 4b and c). This layer spacing might be originating from the thermotropic smectic LC mixture used for the precipitation polymerization. The appearance of the layer spacing signal is probably due to the introduction of potassium into the particles. The “pristine” particles only consist of carbon, oxygen, and hydrogen, elements with low electron density, resulting in low contrast in XRD measurements. After replacing hydrogen in the benzoic acid groups with potassium with higher electron density, the contrast is improved and the layer spacing becomes visible.

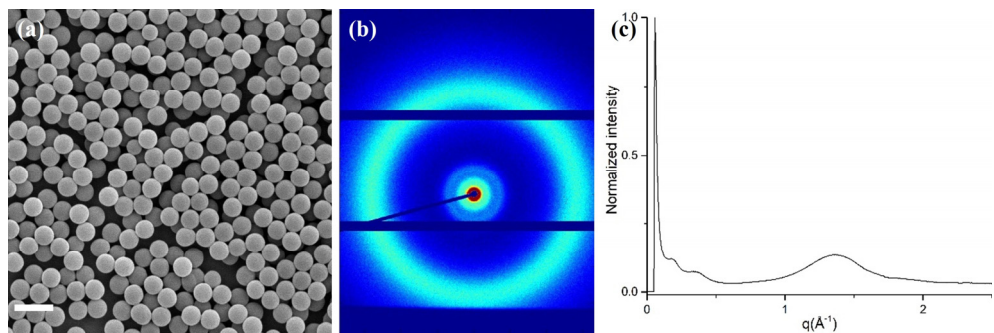


Figure 4. SEM (a), XRD (b), and XRD 1D profile (c) of the polymer particles after KOH treatment. Scale bar = 2  $\mu\text{m}$ .

### 3.5. Absorption and release characteristics

The loading and release properties of the particles were investigated by using methylene blue as a probe. To an aqueous solution of MB, nanoporous particles were added and the absorption process was monitored by UV-Vis measurement. The spectra of MB in solution and in particles were significantly different (shown in Figure 5b inset). The absorption of MB results in a decrease in the absorbance at 665 nm, which is most likely due to MB aggregation within the particles, as the local concentration is high.<sup>17–19</sup> By plotting the absorbance at 665 nm versus time, the absorption was found to be completed within a few minutes, indicating fast absorption kinetics. The MB-loaded particles were collected for SEM and XRD analysis. The particle diameter increased slightly to 1  $\mu\text{m}$  (Figure 5d), while the layer spacing remained as 3.4 nm, although the intensity of peaks in XRD was lower, a result of the lower electron density and decreased contrast of MB (Figure 5e and f).

Different chloride salt solutions were added to the loaded particles to study the release of MB triggered by cations. Monovalent salts, including sodium chloride, lithium chloride, and potassium chloride did not trigger the release of MB, as the absorbance at 665 nm only changed slightly. However, when the bivalent salt calcium chloride was added, the absorbance increased, indicating that MB was released from the particles, which was the result of the higher affinity of  $\text{Ca}^{2+}$  to

benzoate groups.<sup>20</sup> The release kinetics were monitored in the same way as for the absorption process, and MB release was found to be completed within a few minutes, increasing with higher calcium chloride concentration. The minimum concentration required to trigger MB release was 0.01 mM (Figure 5c). The concentration of  $\text{Ca}^{2+}$  needed to release MB was much lower and the release was faster than reported earlier,<sup>21,22</sup> which might be the result of the high affinity of the well-defined porous structure within the particles.

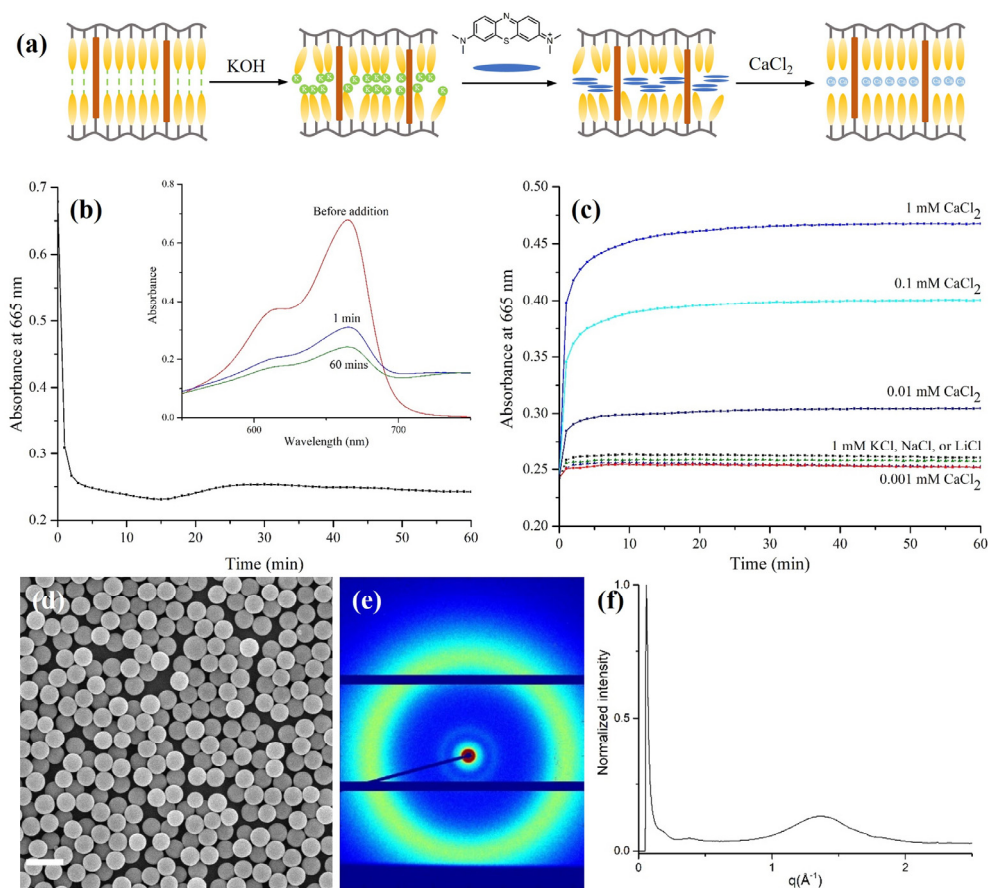


Figure 5. (a) Schematic representation of the MB absorption and release by the nanoporous polymer particles. (b) UV-Vis measurement of the absorption process. UV-Vis spectra of MB in solution and MB absorbed by the particles are shown in the inset. (c) Time-resolved UV-Vis measurement of the release process monitoring the

peak absorbance of the MB. (d) to (f) SEM, XRD, and XRD 1D profile of the polymer particles containing MB (MB/COO<sup>-</sup> = 1). Scale bar = 2 μm.

#### 4. Conclusion

We report the preparation of monodisperse, micron-sized, highly crosslinked, and functionalized LC particles by versatile and scalable precipitation polymerization. Although the LC monomers are randomly dissolved in solution, the oligomers self-align, and liquid crystalline order is induced. The LC molecules align radially within the particles. The size of the particles can be tuned by both temperature and solvent, while the monomer and initiator concentration (>2%) have only minor impacts. The particles could be used to absorb and release molecules in water which makes them attractive for water purification, drug delivery, and selective recovery of valuable chemicals. These results reveal that precipitation polymerization is an attractive method to prepare functional liquid crystalline polymer particles of a narrow size distribution and on a large scale. Preliminary experiments show that our precipitation polymerization method can also be applied to other LC mixtures to prepare monodisperse well-defined LC polymers particles (Figure S3).

#### 5. Reference

- [1] M. Vennes, S. Martin, T. Gisler, R. Zentel, *Macromolecules* **2006**, *39*, 8326–8333.
- [2] S. Haseloh, R. Zentel, *Macromol. Chem. Phys.* **2009**, *210*, 1394–1401.
- [3] M. Vennes, R. Zentel, *Macromol. Chem. Phys.* **2004**, *205*, 2303–2311.
- [4] S. Haseloh, P. Van Der Schoot, R. Zentel, *Soft Matter* **2010**, *6*, 4112–4119.
- [5] J. S. Song, M. A. Winnik, *Macromolecules* **2005**, *38*, 8300–8307.
- [6] J. S. Song, L. Chagal, M. A. Winnik, *Macromolecules* **2006**, *39*, 5729–5737.
- [7] J. S. Downey, R. S. Frank, W. H. Li, H. D. H. Stöver, *Macromolecules* **1999**, *32*, 2838–2844.

- [8] R. S. Frank, J. S. Downey, K. Yu, H. D. H. Stöver, *Macromolecules* **2002**, *35*, 2728–2735.
- [9] G. Zheng, H. D. H. Stöver, *Macromolecules* **2002**, *35*, 7612–7619.
- [10] D. Qi, X. Yang, W. Huang, *Polym. Int.* **2007**, *56*, 208–213.
- [11] W. H. Li, H. D. H. Stöver, *Macromolecules* **2000**, *33*, 4354–4360.
- [12] G. Li, X. Yang, F. Bai, *Polymer (Guildf)*. **2007**, *48*, 3074–3081.
- [13] G. Li, X. Yang, B. Wang, J. Wang, X. Yang, *Polymer (Guildf)*. **2008**, *49*, 3436–3443.
- [14] X. Yang, L. Chen, B. Huang, F. Bai, X. Yang, *Polymer (Guildf)*. **2009**, *50*, 3556–3563.
- [15] A. L. Medina-Castillo, J. F. Fernandez-Sanchez, A. Segura-Carretero, A. Fernandez-Gutierrez, *Macromolecules* **2010**, *43*, 5804–5813.
- [16] H. P. C. Van Kuringen, D. J. Mulder, E. Beltran, D. J. Broer, A. P. H. J. Schenning, *Polym. Chem.* **2016**, *7*, 4712–4716.
- [17] W. Spencer, J. R. Sutter, *J. Phys. Chem.* **1979**, *83*, 1573–1576.
- [18] E. Braswell, *J. Phys. Chem.* **1968**, *72*, 2477–2483.
- [19] E. K. Golz, D. A. Vander Griend, *Anal. Chem.* **2013**, *85*, 1240–1246.
- [20] M. Moirangthem, R. Arts, M. Merckx, A. P. H. J. Schenning, *Adv. Funct. Mater.* **2016**, *26*, 1154–1160.
- [21] C. Ding, S. Xu, J. Wang, Y. Liu, X. Hu, P. Chen, S. Feng, *Polym. Adv. Technol.* **2012**, *23*, 1283–1286.
- [22] M. Deleers, J. P. Servais, E. Wülfert, *BBA - Biomembr.* **1985**, *813*, 195–200.

## 6. Supporting information

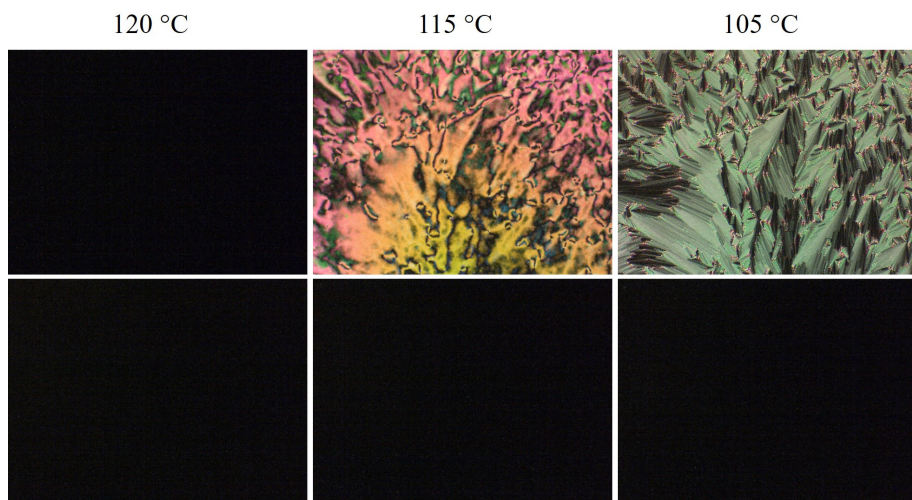


Figure S1. POM images of the LC monomer mixture under planar (top row) or homeotropic (bottom row) boundary conditions at 120, 115, and 105 °C.

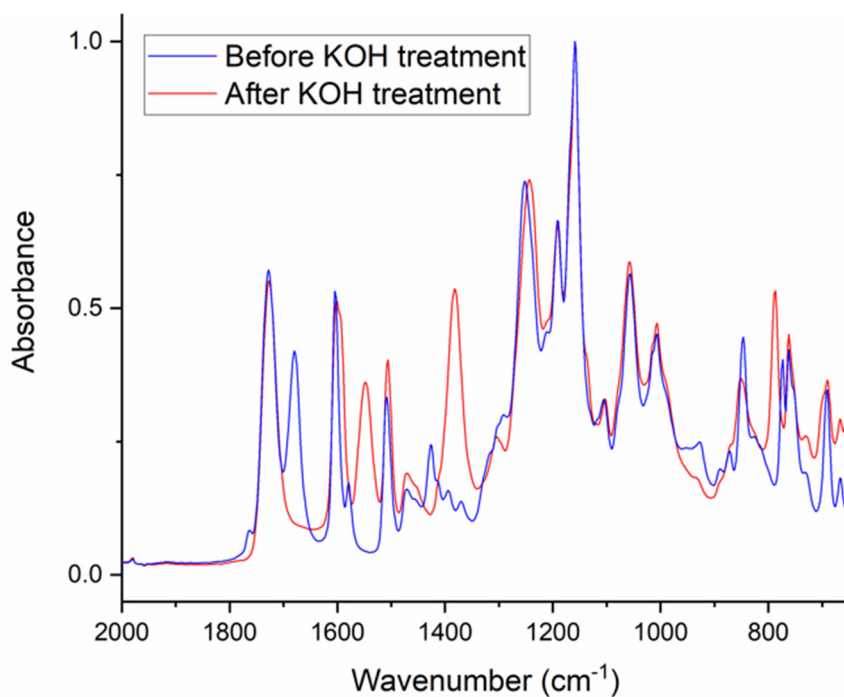


Figure S2. IR spectra of the LC polymer particles before (blue curve) and after (red curve) KOH treatment.

(a)

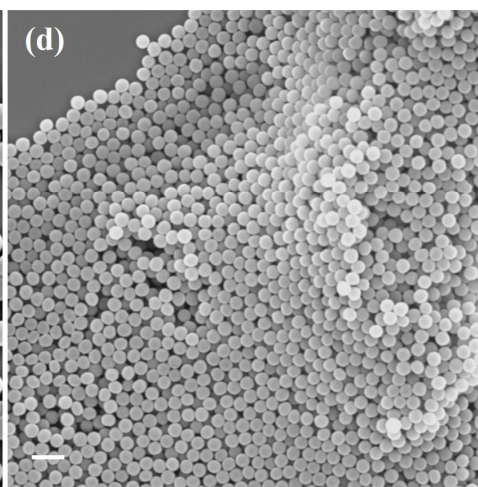
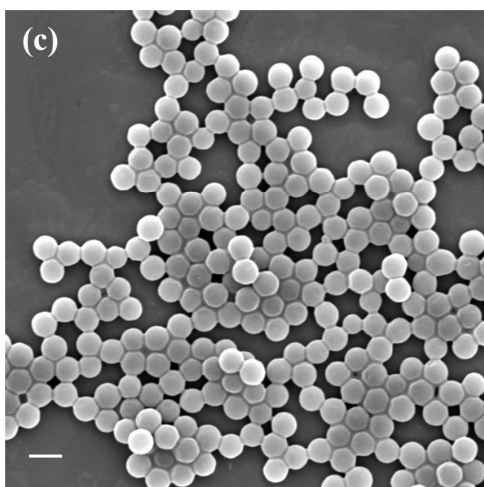
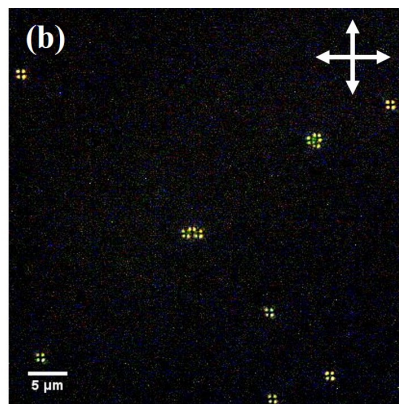
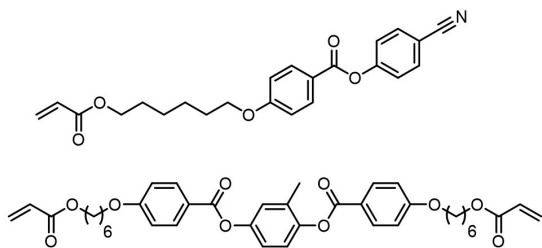


Figure S3. (a) The chemical structure of monomers of the nematic LC mixture. (b) and (c) POM and SEM image of particles synthesized by precipitation polymerization using the mixture shown in (a) in a 1/1 w/w ratio. The polymerization conditions are the same as entry 9 in Table 1. Scale bar = 2 μm. (d) SEM image of particles synthesized by precipitation polymerization using the mixture shown in Figure 1a in a 9/1 w/w ratio. Scale bar = 2 μm.





## Chapter 5

# Flower-like colloidal particles through precipitation polymerization of redox responsive liquid crystals

### Abstract

Despite the plethora of available anisotropic inorganic particles, it remains challenging to fabricate non-spherical polymer particles, especially with angular features. Here we report on the synthesis of monodisperse, flower-like, liquid crystalline (LC) polymer particles by precipitation polymerization of an LC monomer mixture consisting of benzoic acid-functionalized acrylates and redox responsive disulfide-functionalized diacrylates. Introduction of a minor amount of disulfide-functionalized diacrylates ( $\leq 10$  wt%) induced the formation of flower-like shapes. The shape of the particles can be tuned from flower- to disk-like to spherical by simply elevating the polymerization temperature which affects both the LC phase and chain mobility. The solvent environment also has a pronounced effect on the particle size. Time-resolved TEM reveals that the final particle morphology was formed in the early stages of the polymerization and that subsequent polymerization resulted in continued particle growth without affecting the morphology. Finally, the degradation of the particles under reducing conditions was much faster for flower-like particles than for spherical particles, a result of their higher surface-to-volume ratio. This work introduces a facile and scalable preparation of non-spherical anisotropic organic particles which may lead to potential applications ranging from superhydrophobic coatings to redox responsive carrier systems.

## 1. Introduction

Shape-anisotropic colloids are of great interest across a wide range of scientific disciplines and application areas. When we look at particles dispersed in a liquid, their geometry may impact individual motional behavior<sup>1-4</sup> and interaction with other objects,<sup>5</sup> with shape entropy influencing assembly behavior in crowded environments.<sup>6,7</sup> Surface roughness alters the hydrodynamics and rheological behavior of particle dispersions.<sup>8</sup> Shape-anisotropy affects particle interaction with light,<sup>9</sup> leading to advances in plasmonic nanosensors,<sup>10</sup> opacifiers,<sup>11</sup> and switchable, full-color reflective dispersions.<sup>12</sup> The shape and surface roughness<sup>13</sup> of colloidal particles alters their wetting characteristics, with applications in fluid repellent coatings,<sup>14-16</sup> and Pickering emulsions.<sup>17,18</sup> Particle geometry is also emerging as an important factor in biological cell interactions and uptake.<sup>19,20</sup>

Despite the plethora of available anisotropic colloids, it remains challenging to fabricate non-spherical polymer particle colloids. One approach is to physically deform spherical thermoplastic polymer particles by stretching above their glass transition temperature,<sup>21-23</sup> or via template-guided 2D<sup>24,25</sup> and 3D<sup>26</sup> partial film formation. Templated or confined geometric synthetic routes, such as photolithography,<sup>27,28</sup> particle replication in non-wetting templates (PRINT),<sup>29</sup> and droplet-based microfluidic routes,<sup>30,31</sup> can also bring results. Although these methods offer direct control of morphology, they face difficulties as the dimension of the particles decreases to sub-micron range; in addition, the low productivity and stringent preparation conditions remain challenging.

Bottom-up, template-free synthetic routes, though impressive, still commonly result in rounded morphologies, such as dumbbells,<sup>32,33</sup> patchy<sup>34</sup> and raspberry-type armored particles,<sup>35</sup> or more exotic “octopus ocellatus” particles.<sup>36</sup> Even polymerization-induced self-assembly (PISA) techniques usually lead to rounded spherical, cylindrical, or vesicular shapes.<sup>37</sup> To obtain suprastructures with angular shapes, crystallization is often employed. Indeed living-crystallization-

driven self-assembly<sup>38</sup> allows for this angular complexity in particle geometry. Alternatively, by using a liquid crystalline monomer, colloidal suprastructures obtained through PISA by radical polymerization showed a more angular appearance, characteristic of crystallinity.<sup>39</sup>

In the 1960s, highly crystalline polyimide powders of intricate morphology were prepared through imidization of polyamic acids.<sup>40,41</sup> An illustrative example of this was 1-5  $\mu\text{m}$  average diameter polyimide particles with a sheaf or coral-like morphology.<sup>42</sup> Synthesis of conjugated polymers under heterophase conditions produce crystalline cylindrical-shaped particles, also with sharp edges.<sup>43</sup> This concept of preparing polymers which phase separate from and precipitate out of solution into a particle which then crystallizes is intriguing, especially when providing a route to angular shapes, especially if control of the particle size distribution can be achieved. Whereas precipitation polymerization often shows a lack of control over particle formation and growth, when the conditions are right it is possible to prepare monodisperse particles, as for example in the free radical precipitation polymerization of divinylbenzene in acetonitrile.<sup>44</sup>

Previously we reported on the preparation of spherical polymer particles via precipitation polymerization of a smectic LC monomer mixture consisting of a crosslinker and benzoic acid hydrogen-bonded dimers.<sup>45</sup> In this paper, we report the preparation of monodisperse, ‘flower-like’ particles via precipitation polymerization of a liquid crystalline (LC) monomer mixture. The monomer mixture consists of the same benzoic acid-functionalized acrylates as used before but the crosslinker is replaced by a redox responsive disulfide-functionalized diacrylate. It is found that the introduction of a minor fraction of the disulfide-functionalized diacrylates ( $\leq 10$  wt%) induces the formation of a flower-like morphology. The shape of these particles can be tuned from flower-like to spherical simply by elevating the polymerization temperature, while the solvent itself mainly influences the particle size. The flower-like morphology already forms during the early stages of the

polymerization, after which particle growth occurs. Degradation of the particles by breaking the disulfide groups under reducing conditions is dramatically accelerated in the flower-like particles, attributed to their high surface-to-volume ratio.

## **2. Experimental**

### **2.1. Materials**

4-(3-acryloxy-propyl-1-oxy)benzoic acid, and 4-(6-acryloxy-hexyl-1-oxy)benzoic acid (**2**) were purchased from Synthron Chemicals, Germany, and recrystallized in ethanol and water before use. 2-Mercaptoethanol (99%), 4-dimethylaminopyridine (DMAP, 99%), pyridine (99%), phenyl acetate (99%), 2,2'-azobis(2-methylpropionitrile) (AIBN,98%), Luperox A75 (benzyl peroxide, BPO, 75%, remainder water), 1,1'-Azobis(cyclohexanecarbonitrile) (ACCN, 98%), Luperox P80 (1,1-bis(tert-butylperoxy)cyclohexane, 80 wt % in benzyl butyl phthalate, technical grade), and tert-butyl peroxybenzoate (98%) were purchased from Sigma-Aldrich. 4-hydroxybenzenethiol was purchased from TCI Europe. 1-Ethyl-3-(3-dimethylaminopropyl)carbodiimide hydrochloride (EDC) was purchased from Fluorochem. All solvents were purchase from Biosolve.

### **2.2. Synthesis of disulfanediylbis(4,1-phenylene) bis(4-(3-(acryloyloxy)propoxy)benzoate) (1)**

4-[(4-Hydroxyphenyl)disulfanyl]phenol was synthesized via a published procedure.<sup>1</sup> Briefly, 2 g of 4-hydroxybenzenethiol was added to 8 mL DMSO and the solution was heated to 60 °C for 2 hours. After the reaction, ice water was added to the solution and the mixture was filtered. The pale yellow solid was collected and dried in a vacuum oven overnight (3.91 g, 15.6 mmol, 99%).

4-[(4-Hydroxyphenyl)disulfanyl]phenol (2 g, 8 mmol), 4-(3-acryloxy-propyl-1-oxy)benzoic acid (4.4 g, 17.6 mmol), DMAP (0.391 g, 3.2 mmol), and 30 mL dry dichloromethane (DCM) were added to a round bottom flask equipped with

a magnetic stir bar. The mixture was cooled to 0 °C and EDC (3.8 g, 20 mmol) dissolved in 10 mL DCM was added dropwise. Then the mixture was stirred at room temperature overnight. After the reaction, the solution was washed with 1 M HCl, saturated NaHCO<sub>3</sub>, and deionized water. DCM was removed under reduced pressure and the solid was recrystallized in ethanol twice to yield the product as an off-white powder. (2.92 g, 4.08 mmol, 51%)

<sup>1</sup>H NMR (399 MHz, CDCl<sub>3</sub>): δ 8.13 (d, *J* = 8.5 Hz, 4H), 7.55 (d, *J* = 8.4 Hz, 4H), 7.17 (d, *J* = 8.4 Hz, 4H), 6.97 (d, *J* = 8.6 Hz, 4H), 6.47 – 6.37 (m, 2H), 6.14 (dd, *J* = 17.3, 10.4 Hz, 2H), 5.89 – 5.81 (m, 2H), 4.38 (t, *J* = 6.3 Hz, 4H), 4.16 (t, *J* = 6.1 Hz, 4H), 2.21 (p, *J* = 6.2 Hz, 4H).

<sup>13</sup>C NMR (101 MHz, CDCl<sub>3</sub>): δ 166.12, 164.62, 163.19, 150.64, 134.00, 132.36, 131.02, 129.55, 128.27, 122.61, 121.67, 114.34, 64.70, 61.16, 28.53.

MS (MALDI-TOF): [M + H]<sup>+</sup> calculated for C<sub>38</sub>H<sub>35</sub>O<sub>10</sub>S<sub>2</sub>: 715.17; found [M + Na]<sup>+</sup> 737.18, [M + DMAP]<sup>+</sup> 837.30. (Figure S3)

It should be noted that monomer **1** can also be synthesized with pyridine instead of DMAP as the catalyst using the same procedure as described above. The H and C NMR spectra of **1** are the same but in the MS spectrum the DMAP adduct is not present anymore:

MS (MALDI-TOF): [M + H]<sup>+</sup> calculated for C<sub>38</sub>H<sub>35</sub>O<sub>10</sub>S<sub>2</sub>: 715.17; found [M + Na]<sup>+</sup> 737.17. (Figure S4)

### 2.3. Synthesis of the LC particles

90 mg of **1** and 10 mg of **2** were added to a 50 mL round-bottom flask; the flask was pumped and backfilled with N<sub>2</sub> 3 times. The initiator (AIBN (65 °C), BPO (75 °C), ACCN (85 °C and 90 °C), Luperox P80 (95 °C), or tert-butyl peroxybenzoate (105 °C), 4 wt% vs. monomers) was dissolved in 5 mL solvent and added to the flask. The flask was put into an oil bath preheated to the polymerization

temperature for 24 hours. After polymerization, the suspension was washed with ethanol 3 times and centrifuged to yield the particles.

#### **2.4. Degradation of the LC particles**

0.1 mg LC particles were dispersed in 1 mL 10 mM KOH solution. A DLS measurement was performed at 25 °C ( $t = 0$  min). Then, 10  $\mu$ L 0.1 M 2-mercaptoethanol aqueous solution was added to the suspension. A series of time-resolved DLS measurements were performed at 25 °C with a time interval of 2 mins.

#### **2.5. Characterization**

Nuclear magnetic resonance (NMR) spectra were recorded on a 400 MHz Bruker Avance III HD spectrometer with tetramethyl silane used as an internal standard. Differential scanning calorimetry (DSC) curves were measured with a DSC Q2000 from TA Instruments. Scanning electron microscopy (SEM) images were taken with a JEOL TM 220 A. Transmission electron microscopy (TEM) images were taken with a Tecnai 20 (type Sphera) by FEI operating with a LaB 6 filament at 200 kV. Tomographic tilt series are manually collected from minimum  $-65^\circ$  to maximum  $+65^\circ$  at  $5^\circ$  steps with Inspect3D software (Thermo Fisher Scientific). Alignment and reconstruction of the series were performed using IMOD. X-ray diffraction (XRD) was performed on a Ganesha lab instrument with a GeniX-Cu ultralow divergence source producing X-ray photons with a wavelength of 1.54 Å and a flux of  $1 \times 10^8$  ph/s. Scattering patterns were collected with a Pilatus 300 K silicon pixel detector with  $478 \times 619$  pixels, each  $172 \mu\text{m}^2$  in size. Dynamic light scattering (DLS) was measured with Anton Paar Litesizer 500 in backscattering mode at 25 °C. Matrix-assisted laser desorption/ionization time-of-flight (MALDI-TOF) measurements were carried out on a Perspective Biosystem Voyager-DE PRO spectrometer by using  $\alpha$ -Cyano-4-hydroxycinnamic acid as matrix material.

### 3. Results and Discussion

Monomer **1** (Figure 1a) was synthesized by esterification of the disulfide core and benzoic acid-functionalized acrylates (see the supporting information (SI) for details).<sup>46</sup> The LC monomer mixture was then prepared by mixing monomers **1** and **2** (Figure 1a) in a 10/90 weight ratio. Differential scanning calorimetry (DSC) shows an exothermal peak at around 92 °C, corresponding to the LC to isotropic transition, with a peak at approximately 50 °C, corresponding to the LC to crystalline transition (Figure S5). The monomers and thermal initiator were dissolved in a solvent, polymerized overnight, and washed with ethanol to yield the final particles (for experimental details see the SI). Initial studies were conducted in phenyl acetate at 65 °C based on our earlier results using a similar LC monomer mixture containing a different cross-linker, *vide supra*.<sup>45</sup> The resulting polymer particles were flower-like, with flaky moieties on the surfaces and an average diameter of ~750 nm (Figure 1b and 1c). 3D Tomography was used to investigate the particle morphology in more detail (Figure 1d) and confirmed the flaky moieties throughout the particles. The glass transition temperature ( $T_g$ ) of the LC polymer particles was determined by DSC and found to be around 82 °C (Figure S6). The flower-like polymer particles do not change their shape when heated above  $T_g$  at 105 °C overnight (Figure S7), confirming the permanent shape of the particles.

The concentration of cross-linking monomer **1** was varied to investigate its impact on the final shape of the particles. As shown in Figure 2a, without monomer **1**, fairly spherical particles with rough surfaces were obtained. Flower-like particles were obtained when 5% or 10% of monomer **1** was used (Figures 2b and 2c). Further increasing the weight ratio of monomer **1** to above 20% resulted in particles with nearly spherical shapes, and no particles were formed at all when pure monomer **1** was used. Meanwhile, the diameter of the particles increased from 500 nm to 1.3  $\mu\text{m}$  with increasing monomer **1**. It is concluded that the introduction of a minor amount of monomer **1** ( $\leq 10$  wt%) can induce the flower-like shape, while further increasing

the amount of monomer **1** led to spherical particles, probably because higher cross-linking leads to kinetically trapped structures. The monomer composition of 10/90 resulted in the most pronounced flower-like morphologies and was used for the investigations in the remainder of this research.

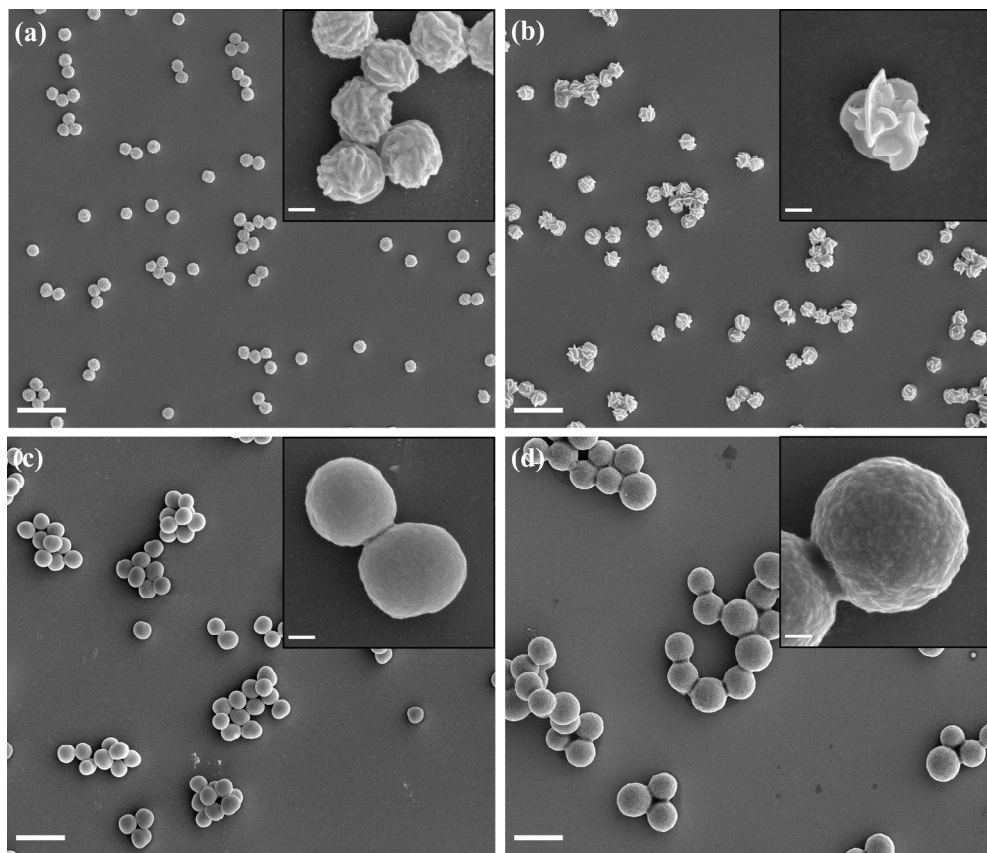


Figure 2. SEM images of particles prepared with monomer **1** and **2** in weight ratios (a) 0/100, (b) 5/95, (c) 20/80, and (d) 50/50 in phenyl acetate at 65 °C. Scale bar = 2  $\mu$ m in all large images and 200 nm in all insets.

Since previous publications indicated that the polymerization conditions, including the solvent and polymerization temperature, may have a profound influence on particle morphologies, LC polymer particles were prepared using a



series of solvent mixtures and polymerization temperatures to reveal the impact of these conditions.<sup>45,47</sup>

Precipitation polymerization was carried out in solvent mixtures of ethyl acetate and phenyl acetate at different volume ratios at 65 °C to investigate the impact of the solvent on the particles since in a previous publication, monodisperse LC polymer particles were prepared in these two solvents.<sup>45</sup> As shown in Figure 3, particles prepared from all solvent mixtures are flower-like. Particles prepared in phenyl acetate-rich solvent mixtures all have a similar average diameter of 750 nm, while particles prepared in ethyl acetate-rich solvent mixtures show increasing diameters from 1.2  $\mu\text{m}$  to 1.8  $\mu\text{m}$ , with apparently smoother, less flaky surfaces. The increase in diameter is likely due to the higher solubility of the polymer in ethyl acetate, which results in slower and less nucleation and thus larger particles.<sup>45</sup> These results suggest that the particle size and morphology are both affected by the solvent-polymer interaction.

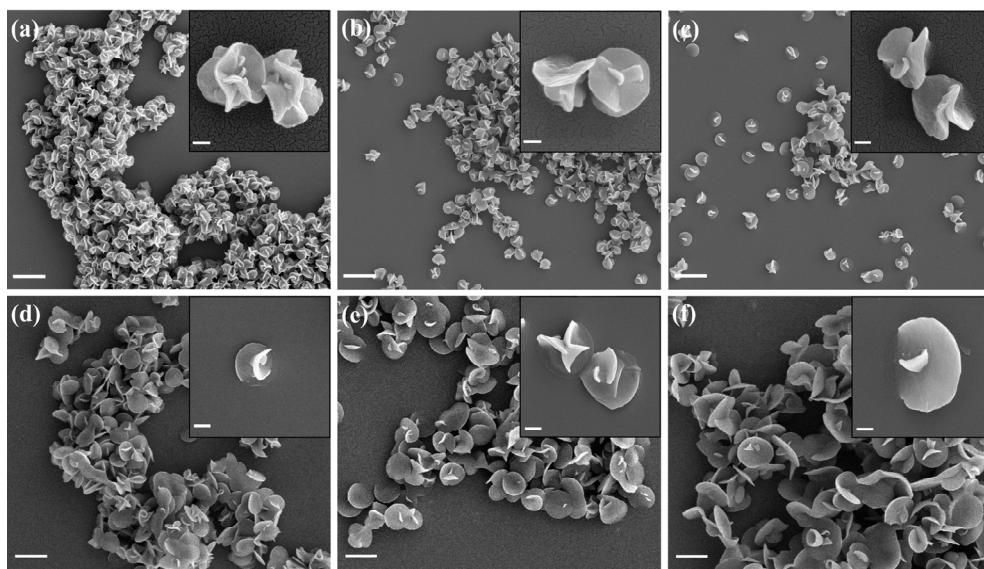


Figure 3. Particles prepared at 65 °C in mixtures of phenyl acetate and ethyl acetate. The volume ratios of phenyl acetate and ethyl acetate are (a) 100/0, (b) 80/20, (c) 60/40, (d) 40/60, (e) 20/80, and (f) 0/100, respectively. Scale bar = 2  $\mu\text{m}$  in the large

images; scale bar = 200 nm (inset of (a), (b), and (c)) and 1  $\mu\text{m}$  (inset of (d), (e), and (f)).

Another critical parameter in precipitation polymerization is the polymerization temperature, which not only affects the solvent-polymer interaction, but also the liquid crystal phase and chain mobility in the polymerizing particles. Polymerization was performed in pure phenyl acetate at a series of temperatures from 65  $^{\circ}\text{C}$  to 105  $^{\circ}\text{C}$ . As shown in Figure 4, the average diameters lie between 400 nm (90  $^{\circ}\text{C}$ ) and 750 nm (65  $^{\circ}\text{C}$ ). The morphology of the particles prepared at 65  $^{\circ}\text{C}$  and 75  $^{\circ}\text{C}$  were flower-like, while the particles prepared at 85  $^{\circ}\text{C}$  and 90  $^{\circ}\text{C}$  were disk-shaped, and particles prepared at 95  $^{\circ}\text{C}$  and 105  $^{\circ}\text{C}$  were spherical. This result indicates that the polymerization temperature has a profound influence on the final morphology and the flower-like morphology is stable due to cross-linking.

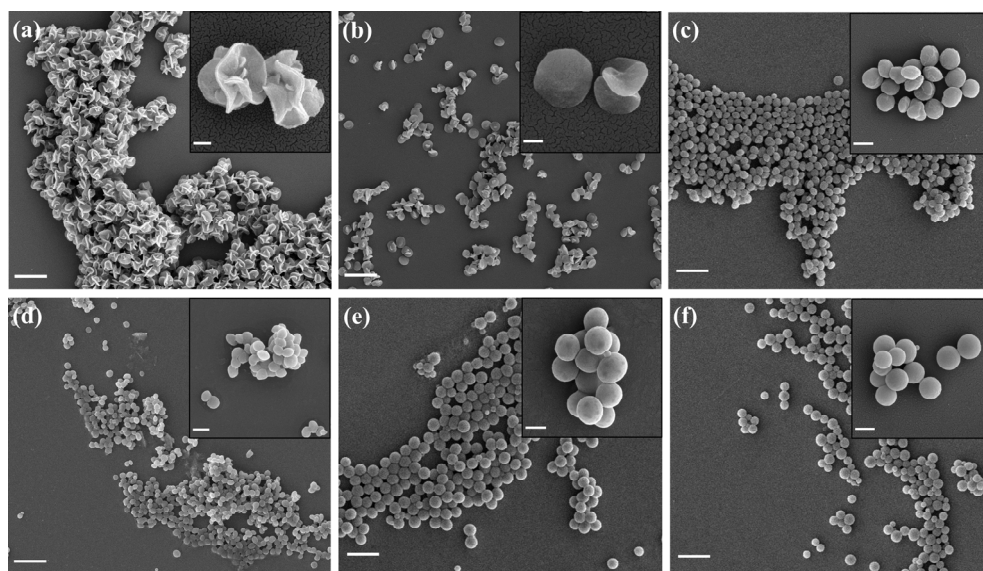


Figure 4. Particles prepared in phenyl acetate at 65  $^{\circ}\text{C}$  (a), 75  $^{\circ}\text{C}$  (b), 85  $^{\circ}\text{C}$  (c), 90  $^{\circ}\text{C}$  (d), 95  $^{\circ}\text{C}$  (e), and 105  $^{\circ}\text{C}$  (f). Scale bar = 2  $\mu\text{m}$  (larger image) and 200 nm (inset) in (a) and (b); Scale bar = 5  $\mu\text{m}$  (larger image) and 500 nm (inset) in (c), (d), (e), and (f).

To investigate the LC order in the particles, flower-like (65 °C), disk-shaped (90 °C), and spherical (105 °C) particles were treated with 10 mM KOH to introduce potassium ions and increase contrast prior to medium-angle X-ray scattering (MAXS) measurements.<sup>45</sup> The first and second-order peaks correspond to a layer spacing of 3.2 nm which can be attributed to the lamellar order of the molecules as found earlier.<sup>48</sup> The intensity of the peaks was found to decrease with increasing polymerization temperature, indicating that the order was decreased at elevated temperatures (Figure 5). Although the thermotropic LC mixture is in the isotropic state the polymer chains might align resulting in the layered structure in the differently shaped particles.

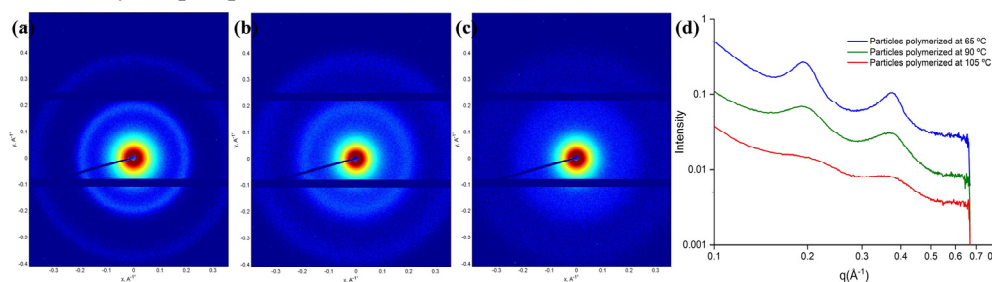


Figure 5. MAXS patterns of particles prepared at 65 °C (a), 90 °C (b), and 105 °C (c). (d) MAXS 1D profile derived from (a) to (c). The first-order and second-order peaks corresponding to a layer spacing of 3.2 nm.

The evolutions of the morphologies of the above particles were investigated by time-resolved TEM. A small volume of the polymerization mixture was withdrawn from the flask every hour and washed with ethanol to remove the unreacted monomers for time-resolved TEM. As shown in Figure 6a to 6e, the particles prepared at 65 °C showed flower-like morphologies from the outset (1-hour polymerization) which continued to grow in size as the polymerization progressed. The initial diameter was approximately 300 nm, increasing to 750 nm overnight. Both spherical and ellipsoidal shapes were initially observed in the 90 °C polymerization, eventually leading to the formation of disk-shaped particles (Figure

6f to 6j). For polymerizations carried out at 105 °C, only spherical particles were observed throughout the entire polymerization process (Figure 6k to 6o). In summary, the shape of the LC particles is already formed at the initial stage of the polymerization, and subsequent polymerization only results in the growth of the particles with no change in morphology.

Based on these results, we postulate the formation of the flower-like morphology was the combined result of liquid crystalline molecular order and limited chain mobility. The liquid crystalline molecular order is reduced and the chain mobility is increased at elevated temperatures, and thus resulted in the rounded morphology of the particles.

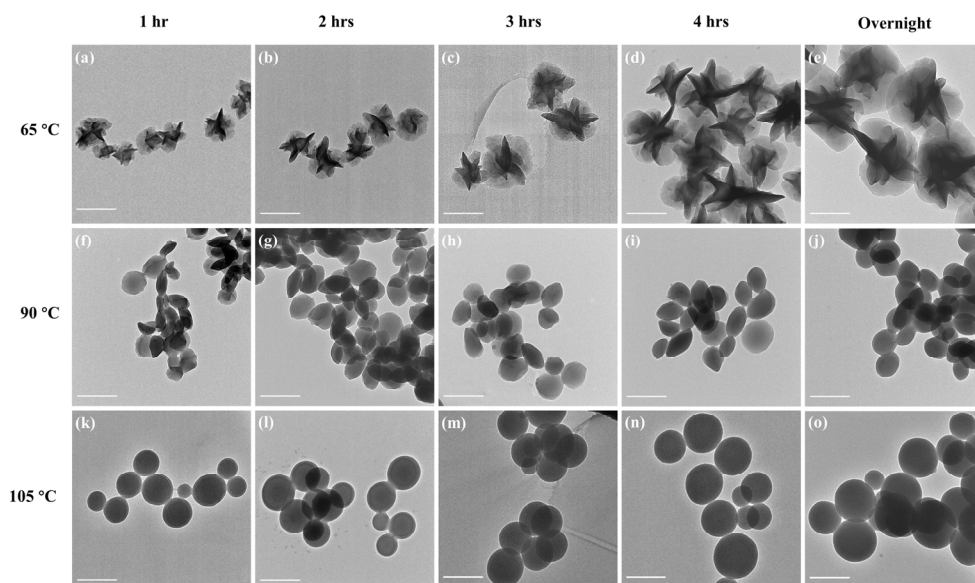


Figure 6. Time-resolved TEM images of the particles prepared in phenyl acetate at different polymerization temperatures and times (scale bar = 500 nm).

As the disulfide bonds in the cross-linker are sensitive to a reductive environment, particles prepared in phenyl acetate at 65 °C and 105 °C were subjected to degradation experiments. LC particles were first dispersed in 10 mM KOH solution to prepare a 0.1 mg/mL particle suspension, and then 2-mercaptoethanol

was added so that its concentration was 1 mM. A rapid decrease in hydrodynamic diameter from 1.59  $\mu\text{m}$  to 0.1  $\mu\text{m}$  indicated the rapid degradation of the flower-like particles into soluble linear polymers, whereas no apparent change in hydrodynamic diameter was observed for the spherical particles (Figure 7). Such a discrepancy can be attributed to the difference in surface-to-volume ratio, even that these particle samples have the same chemical composition and comparable size.

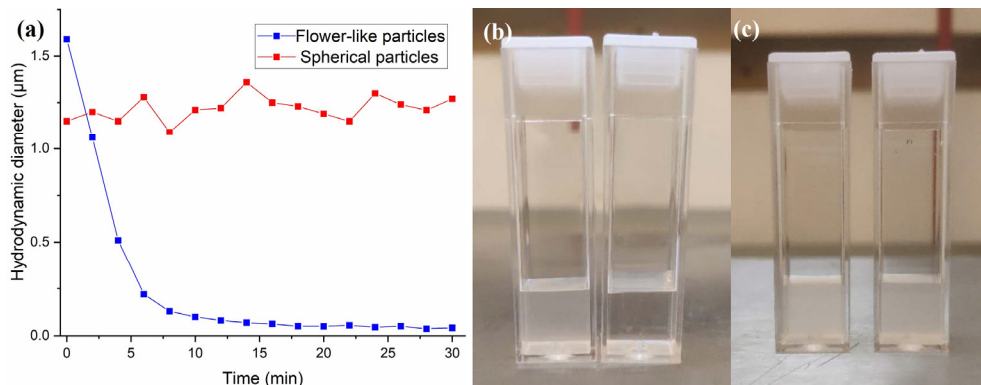


Figure 7. Time-resolved hydrodynamic diameter of the degradation process monitored with DLS (a). Images of the particle suspension before (left) and after (right) degradation of flower-like particles (b, polymerized in phenyl acetate at 65  $^{\circ}\text{C}$ ) and spherical particles (c, polymerized in phenyl acetate at 105  $^{\circ}\text{C}$ ).

#### 4. Conclusions

In this paper, we report the facile synthesis of monodisperse flower-like particles via one-step precipitation polymerization of liquid crystalline monomers. By adding  $\leq 10$  wt% of cross-linker **1** in the monomer mixture, a flower-like morphology was induced. Particle sizes and the number of "petals" in the "flower" were found to mainly depend on the solvent used as reaction medium, whereas the morphology of the particles can be tuned from flower-like to disk-shaped and further to spherical by elevating the polymerization temperature. A gradual decrease in the molecular order in particles prepared at higher polymerization temperature, which may contribute to the formation of rounded particles. It was found that the

morphology of the particles was formed at the early stage of polymerization, while the following polymerization resulted in the growth of particle size without significantly changing the morphology. Finally, the flower-like particles were degraded much more rapidly than their spherical counterparts in reductive environments, attributed to their significantly higher surface-to-volume ratio.

Our work introduces a facile and scalable preparation of non-spherical organic particles of a narrow size distribution and may lead to potential applications ranging from superhydrophobic coatings to redox responsive carrier systems.

## 5. References

- [1] F. Perrin, *J. Phys. Radium* **1934**, *5*, 497–511.
- [2] F. Perrin, *J. Phys. Radium* **1936**, *7*, 1–11.
- [3] Y. Han, A. M. Alsayed, M. Nobili, J. Zhang, T. C. Lubensky, A. G. Yodh, *Science (80-. )*. **2006**, *314*, 626–630.
- [4] Y. C. Saraswat, F. Ibis, L. Rossi, L. Sasso, H. B. Eral, P. Fanzio, *J. Colloid Interface Sci.* **2020**, *564*, 43–51.
- [5] L. Onsager, *Ann. N. Y. Acad. Sci.* **1949**, *51*, 627–659.
- [6] M. Adams, Z. Dogic, S. L. Keller, S. Fraden, *Nature* **1998**, *393*, 349–352.
- [7] G. van Anders, D. Klotsa, N. K. Ahmed, M. Engel, S. C. Glotzer, *Proc. Natl. Acad. Sci.* **2014**, *111*, E4812–E4821.
- [8] L. C. Hsiao, S. Pradeep, *Curr. Opin. Colloid Interface Sci.* **2019**, *43*, 94–112.
- [9] G. Mie, *Ann. Phys.* **1908**, *330*, 377–445.
- [10] L. Rodríguez-Lorenzo, R. de la Rica, R. A. Álvarez-Puebla, L. M. Liz-Marzán, M. M. Stevens, *Nat. Mater.* **2012**, *11*, 604–607.
- [11] G. Jacucci, B. W. Longbottom, C. C. Parkins, S. A. F. Bon, S. Vignolini, *J. Mater. Chem. C* **2021**, *9*, 2695–2700.
- [12] Q. He, K. H. Ku, H. Vijayamohan, B. J. Kim, T. M. Swager, *J. Am. Chem. Soc.* **2020**, *142*, 10424–10430.
- [13] M. Hu, C.-P. Hsu, L. Isa, *Langmuir* **2020**, *36*, 11171–11182.
- [14] W. Jiang, C. M. Grozea, Z. Shi, G. Liu, *ACS Appl. Mater. Interfaces* **2014**, *6*, 2629–2638.

- [15] D. Xu, M. Wang, X. Ge, M. Hon-Wah Lam, X. Ge, *J. Mater. Chem.* **2012**, *22*, 5784–5791.
- [16] A. M. Telford, B. S. Hawkett, C. Such, C. Neto, *Chem. Mater.* **2013**, *25*, 3472–3479.
- [17] M. Zanini, C. Marschelke, S. E. Anachkov, E. Marini, A. Synytska, L. Isa, *Nat. Commun.* **2017**, *8*, 15701.
- [18] T. M. Ruhland, A. H. Gröschel, N. Ballard, T. S. Skelhon, A. Walther, A. H. E. Müller, S. A. F. Bon, *Langmuir* **2013**, *29*, 1388–1394.
- [19] A. E. Nel, L. Mädler, D. Velegol, T. Xia, E. M. V Hoek, P. Somasundaran, F. Klaessig, V. Castranova, M. Thompson, *Nat. Mater.* **2009**, *8*, 543–557.
- [20] K. Zhang, H. Fang, Z. Chen, J. S. A. Taylor, K. L. Wooley, *Bioconjug. Chem.* **2008**, *19*, 1880–1887.
- [21] M. Nagy, A. Keller, *Polym. Commun.* **1989**, *30*, 130–132.
- [22] J. A. Champion, Y. K. Katare, S. Mitragotri, *Proc. Natl. Acad. Sci. U. S. A.* **2007**, *104*, 11901–11904.
- [23] C. C. Ho, A. Keller, J. A. Odell, R. H. Ottewill, *Colloid Polym. Sci.* **1993**, *271*, 469–479.
- [24] L. Zheng, P. Huang, L. Zhang, D. Guo, Q. Yan, *Part. Part. Syst. Character.* **2016**, *33*, 842–850.
- [25] L. M. Ramírez, S. T. Milner, C. E. Snyder, R. H. Colby, D. Velegol, *Langmuir* **2010**, *26*, 7644–7649.
- [26] B. W. Longbottom, B. Somuncuoğlu, J. J. Punter, S. Longbottom, S. A. F. Bon, *Soft Matter* **2017**, *13*, 4285–4293.
- [27] D. C. Pregibon, M. Toner, P. S. Doyle, *Science (80-. )*. **2007**, *315*, 1393–1396.
- [28] S. Badaire, C. Cottin-Bizonne, A. D. Stroock, *Langmuir* **2008**, *24*, 11451–11463.
- [29] T. J. Merkel, K. P. Herlihy, J. Nunes, R. M. Orgel, J. P. Rolland, J. M. DeSimone, *Langmuir* **2010**, *26*, 13086–13096.
- [30] S. Xu, Z. Nie, M. Seo, P. Lewis, E. Kumacheva, H. A. Stone, P. Garstecki, D. B. Weibel, I. Gitlin, G. M. Whitesides, *Angew. Chemie Int. Ed.* **2005**, *44*, 724–728.
- [31] Z. Nie, S. Xu, M. Seo, P. C. Lewis, E. Kumacheva, *J. Am. Chem. Soc.* **2005**, *127*, 8058–8063.

- [32] H. R. Sheu, M. S. El-Aasser, J. W. Vanderhoff, *J. Polym. Sci. Part A Polym. Chem.* **1990**, *28*, 629–651.
- [33] J.-G. Park, J. D. Forster, E. R. Dufresne, *J. Am. Chem. Soc.* **2010**, *132*, 5960–5961.
- [34] A. Lotierzo, B. W. Longbottom, W. H. Lee, S. A. F. Bon, *ACS Nano* **2019**, *13*, 399–407.
- [35] C. Barthet, A. J. Hickey, D. B. Cairns, S. P. Armes, *Adv. Mater.* **1999**, *11*, 408–410.
- [36] M. Okubo, K. Kanaida, T. Matsumoto, *Colloid Polym. Sci.* **1987**, *265*, 876–881.
- [37] F. D’Agosto, J. Rieger, M. Lansalot, *Angew. Chemie Int. Ed.* **2020**, *59*, 8368–8392.
- [38] L. MacFarlane, C. Zhao, J. Cai, H. Qiu, I. Manners, *Chem. Sci.* **2021**, *12*, 4661–4682.
- [39] S. Guan, C. Zhang, W. Wen, T. Qu, X. Zheng, Y. Zhao, A. Chen, *ACS Macro Lett.* **2018**, *7*, 358–363.
- [40] E. A. Laszlo, *Aromatic Polyimide Particles from Polycyclic Diamines*, **1965**, U.S. Patent No. 3,179,631.
- [41] E. A. Laszlo, *Aromatic Polyimides from Meta-Phenylene Diamine and Para-Phenylene Diamine*, **1965**, U.S. Patent No. 3,179,633.
- [42] Y. Nagata, Y. Ohnishi, T. Kajiyama, *Polym. J.* **1996**, *28*, 980–985.
- [43] J. D. Ruiz Perez, S. Mecking, *Angew. Chemie - Int. Ed.* **2017**, *56*, 6147–6151.
- [44] K. Li, H. D. H. Stöver, *J. Polym. Sci. Part A Polym. Chem.* **1993**, *31*, 3257–3263.
- [45] X. Liu, Y. Xu, J. P. A. Heuts, M. G. Debije, A. P. H. J. Schenning, *Macromolecules* **2019**, *52*, 8339–8345.
- [46] F. Vibert, S. R. A. Marque, E. Bloch, S. Queyroy, M. P. Bertrand, S. Gastaldi, E. Besson, *Chem. Sci.* **2014**, *5*, 4716–4723.
- [47] A. L. Medina-Castillo, J. F. Fernandez-Sanchez, A. Segura-Carretero, A. Fernandez-Gutierrez, *Macromolecules* **2010**, *43*, 5804–5813.
- [48] H. P. C. Van Kuringen, G. M. Eikelboom, I. K. Shishmanova, D. J. Broer, A. P. H. J. Schenning, *Adv. Funct. Mater.* **2014**, *24*, 5045–5051.



## 6. Support information

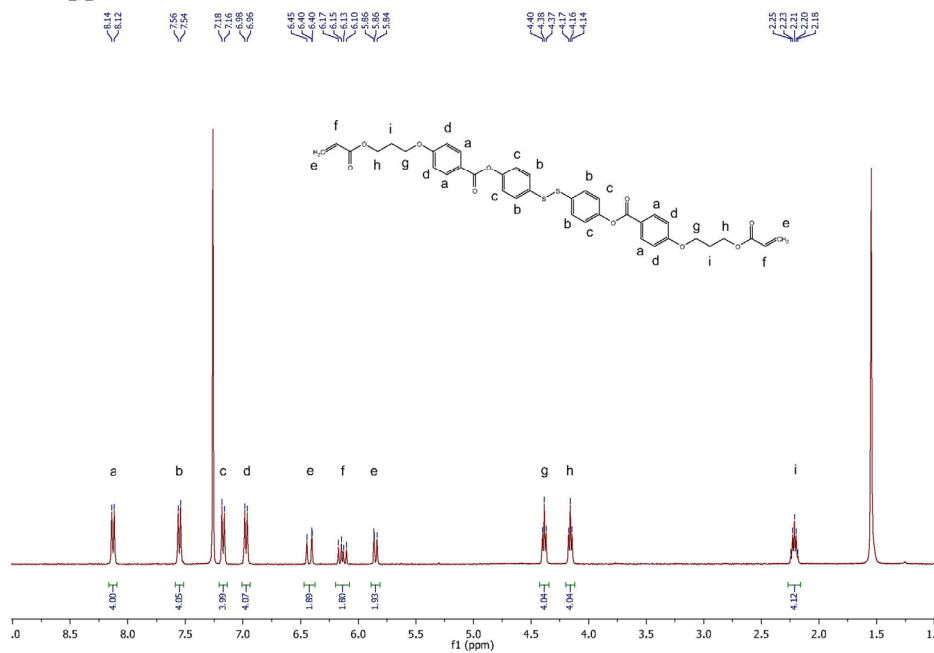


Figure S1. <sup>1</sup>H NMR spectrum of monomer 1.

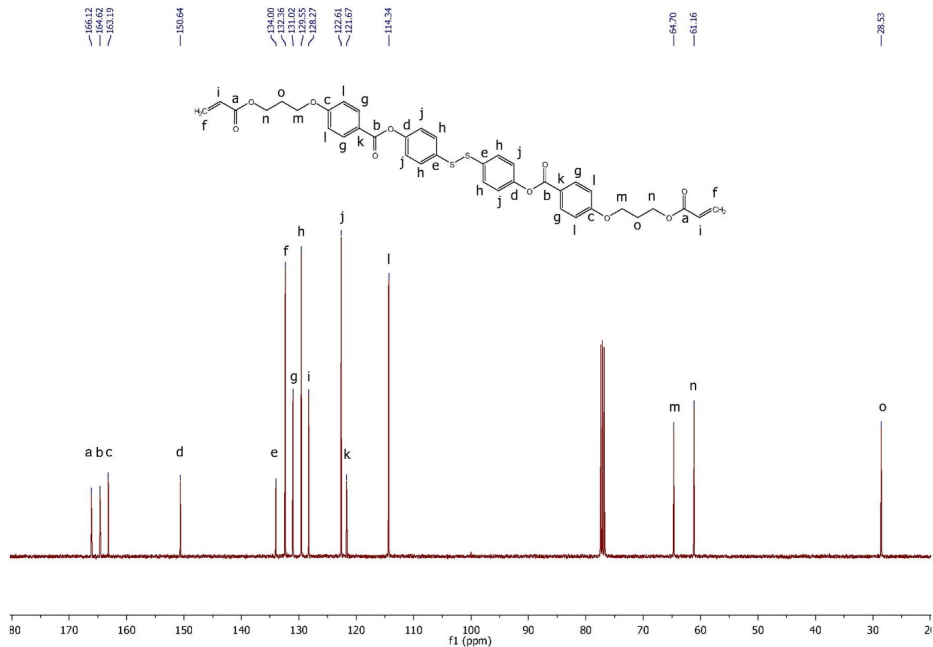


Figure S2. <sup>13</sup>C NMR spectrum of monomer 1.

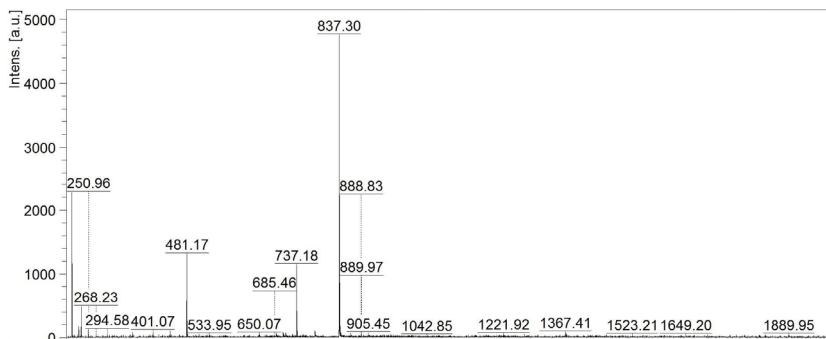


Figure S3. MALDI-TOF spectrum of monomer **1** prepared with DMAP as the catalyst.

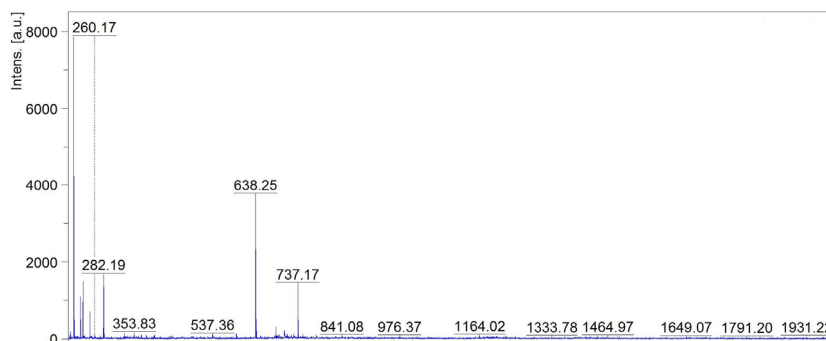


Figure S4. MALDI-TOF spectrum of monomer **1** prepared with pyridine as the catalyst.

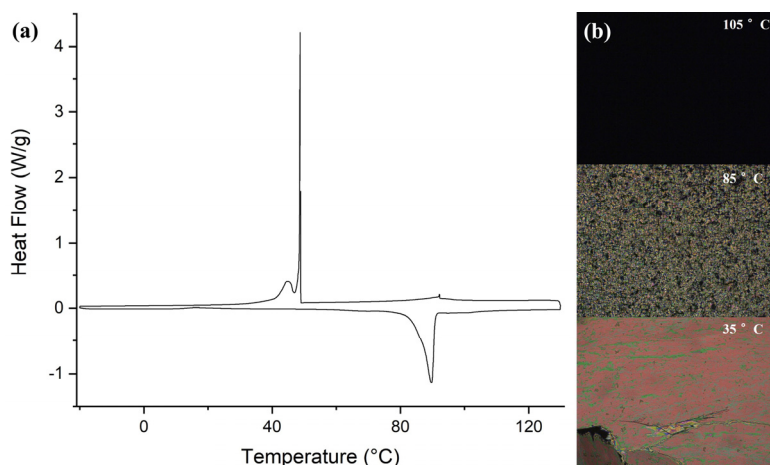


Figure S5. (a) DSC curve of the LC monomer mixture (weight ratio of **1** and **2** = 1:9). The isotropic to LC transition temperature was found around 92 °C, and the LC to

crystalline temperature was around 50 °C (exothermal up). (b) POM images of the monomer mixture at 105 °C (isotropic), 85 °C (LC), and 35 °C (crystalline) (planar alignment).

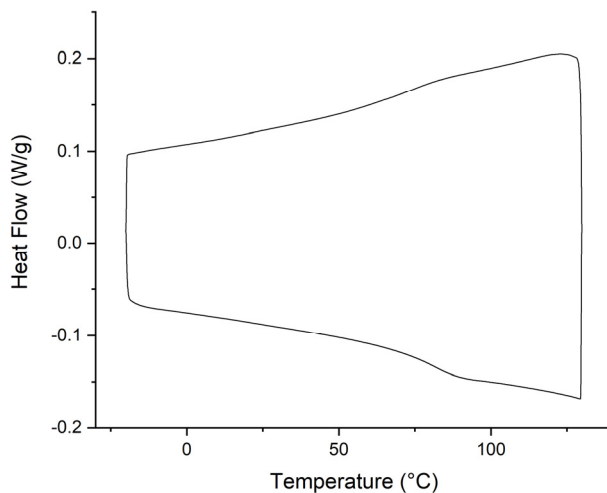


Figure S6. DSC curve of the polymer particles (weight ratio of **1** and **2** = 1:9). The glass transition temperature was found around 82 °C.

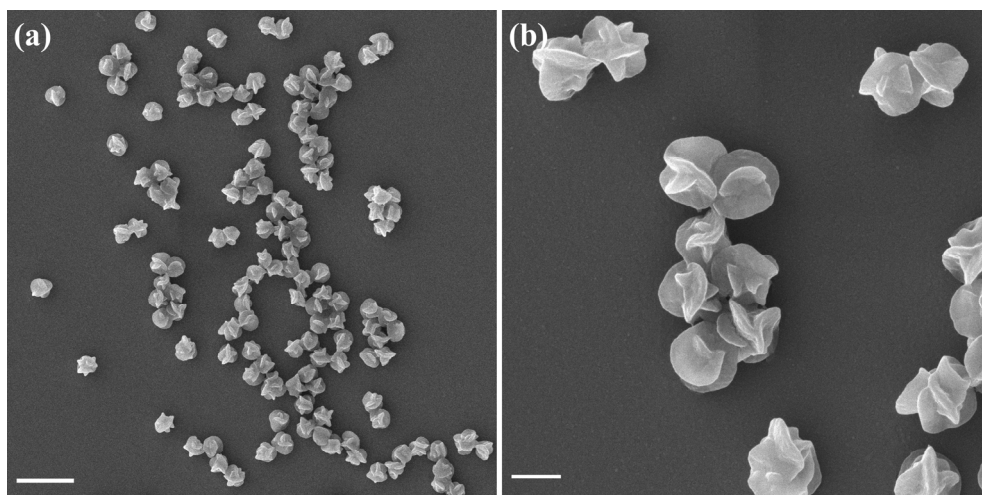


Figure S7. SEM images of LC particles polymerized in phenyl acetate at 65 °C and heated to 105 °C overnight: scale bar = 2  $\mu\text{m}$  (in (a)) and 500 nm (in (b)).



## **Chapter 6**

# **Technology assessment**

## **1. Introduction**

This thesis demonstrates that LC polymer particles with tunable alignment, shape, chemical structure, controlled particle size, and narrow polydispersity can be easily prepared via dispersion and precipitation polymerizations. The LC polymer particles have well-defined LC alignment and uniform structure and responsivity. In chapter 2, seeded dispersion polymerization was explored based on established one-step dispersion polymerization, aiming to prepare LC polymer shells with programmable alignment and morphology. Then, the dispersion polymerization was combined with thiol-ene reaction to produce dual-network LC polymer particles as programmable microactuators in chapter 3. In chapter 4, as a supplement to dispersion polymerization, precipitation polymerization was introduced to prepare carboxylic acid-functionalized LC polymer particles as responsive absorbents that are challenging to produce by dispersion polymerization. In chapter 5, a disulfide-functionalized LC diacrylate was synthesized and incorporated in the LC monomer mixture to prepare redox-responsive flower-like LC polymer particles. In this last chapter, we reflect on the results obtained throughout this thesis. The classical polymerization techniques will be compared with the microfluidic route to prepare LC polymer particles. Synthetic routes to prepare new Janus-type LC polymer particles will also be presented. Finally, the possible applications of these LC polymer particles as micro-actuators and as absorption and release systems will be discussed.

## **2. Preparation of LC polymer particles, microfluidic versus classical polymerization methods**

Microfluidics is an appealing technique for preparing polymer particles, offering an alternative to the classical polymerization techniques (Figure 1). In microfluidics, instead of generating droplets with mechanical agitation or sonication, they are produced by the drag forces of the continuous phase detaching monomers

from the tubing outlet of the monomer phase.<sup>1</sup> With optimization of the preparation conditions, monodisperse monomer droplets are generated and polymerized to yield monodisperse polymer particles.<sup>2</sup>

Zentel *et al.* explored the preparation of LC polymer particles with microfluidics.<sup>3</sup> They first heated the LC monomers to the isotropic phase, generating LC monomer droplets, and followed by cooling the droplets to the LC state and photopolymerizing. The resulting LC polymer particles were initially spherical, converting into a cigar-like shape when heated to the isotropic state. A more detailed study confirmed that flow rates were critical in microfluidics preparation, as it affected both the particle size and the LC alignment within the final particles. With increased flow rate of the continuous phase and flow rate ratio between the continuous and monomer phases, the diameter of the particles decreased to a minimum value of 220  $\mu\text{m}$ . The relative elongation deformation of the LC polymer particles when thermally actuated increased with a higher flow rate of the continuous phase during initial production, which suggested the LC molecules were more ordered.<sup>4</sup> Moreover, the flow also determines the alignment of the LC molecules (concentric at low shear force and parallel to the flow at high shear forces).<sup>5</sup> To date, LC polymer particles with various shapes,<sup>5</sup> LC phases,<sup>6,7</sup> multi-domains,<sup>8</sup> magnetic field-responsivities,<sup>9</sup> and core-shell structures<sup>10,11</sup> have been successfully prepared with microfluidics.

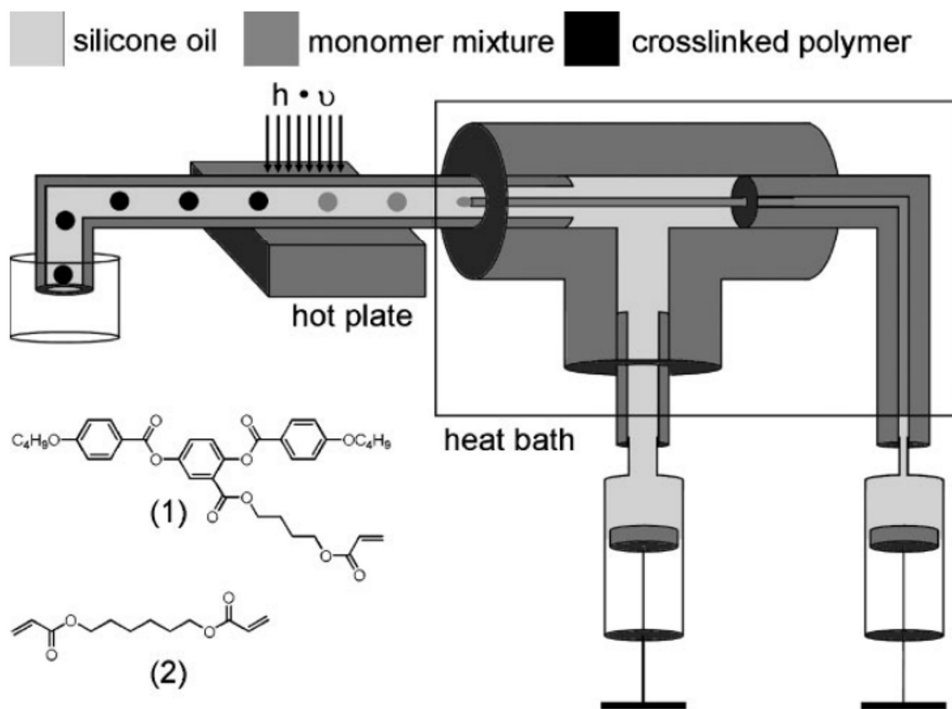


Figure 1. Schematic representation of a microfluidics setup to prepare LC polymer particles. Reprinted (adapted) with permission from Ref. 3.

Microfluidics and classical polymerization techniques have their own scope of applications (Table 1). Microfluidics can be applied to prepare LC polymer particles with a typical diameter of a few hundred micrometers. The flow in the micro-channels affects the particle size and aligns the LC molecules, which is difficult to achieve by surface anchoring (e.g. solvent-LC interaction) because of the large diameter of the LC monomer droplets.<sup>4</sup> It is difficult to decrease the dimension of the LC polymer particles to  $< 10 \mu\text{m}$ , as the control of flow rates only offers limited room for decreasing particle sizes,<sup>4</sup> and narrower micro-channels can be easily clogged by polymer debris.<sup>12</sup> To prepare LC polymer particles smaller than  $10 \mu\text{m}$ , classical polymerization techniques are more suitable. Therefore, the choice of



classical polymerization or microfluidic methods depends on the eventual application and set of requirements for the eventual LC polymer particles.

Table 1. Comparison of microfluidics and classical polymerization techniques

	Microfluidics	Classical polymerization techniques
Component	Solvent (immiscible), LC monomers, initiators	Solvent (immiscible or miscible), LC monomers, initiators, stabilizers (optional)
Particle size/ distribution	$d > 100 \mu\text{m}$ / monodisperse	$d < 10 \mu\text{m}$ / monodisperse or polydisperse
LC phase	Nematic, cholesteric	Nematic, smectic, cholesteric
Alignment	Concentric, parallel to the flow	Bipolar, radial, cholesteric, etc.
Alignment force	The flow of the continuous phase	Solvent-LC interfacial properties

### 3. Janus LC polymer particles

Janus particles refer to particles with two or more domains with distinctive morphology or surface chemistry, and in the case of LC polymer particles, different LC phases or the same LC phase but different alignment can also make LC polymer particles “Janus”.<sup>13</sup> By constructing Janus LC polymer particles, the functionalities of different LC alignments and phases, non-LC conventional polymer, and even inorganic materials can be incorporated in one LC polymer particle and significantly extend the scope of application. A possible preparation route is microcontact printing, in which an “ink” is first absorbed on a stamp (typically poly(dimethyl siloxane), PDMS), and then transferred to a substrate (the particles) only in the area of contact

via either physisorption or chemical reactions.<sup>14</sup> In a previous publication, particles were compressed on polyethylenimine (PEI) functionalized with biotin or avidin (Figure 2a and b).<sup>15</sup> The strong binding force between biotin and avidin directed the self-assembly of biotin- and avidin-functionalized particles and formed heterodimers (Figure 2c). This strategy can be applied to prepare paired LC polymer particles with distinctive internal alignments, LC phases, or functional groups tailored for specific

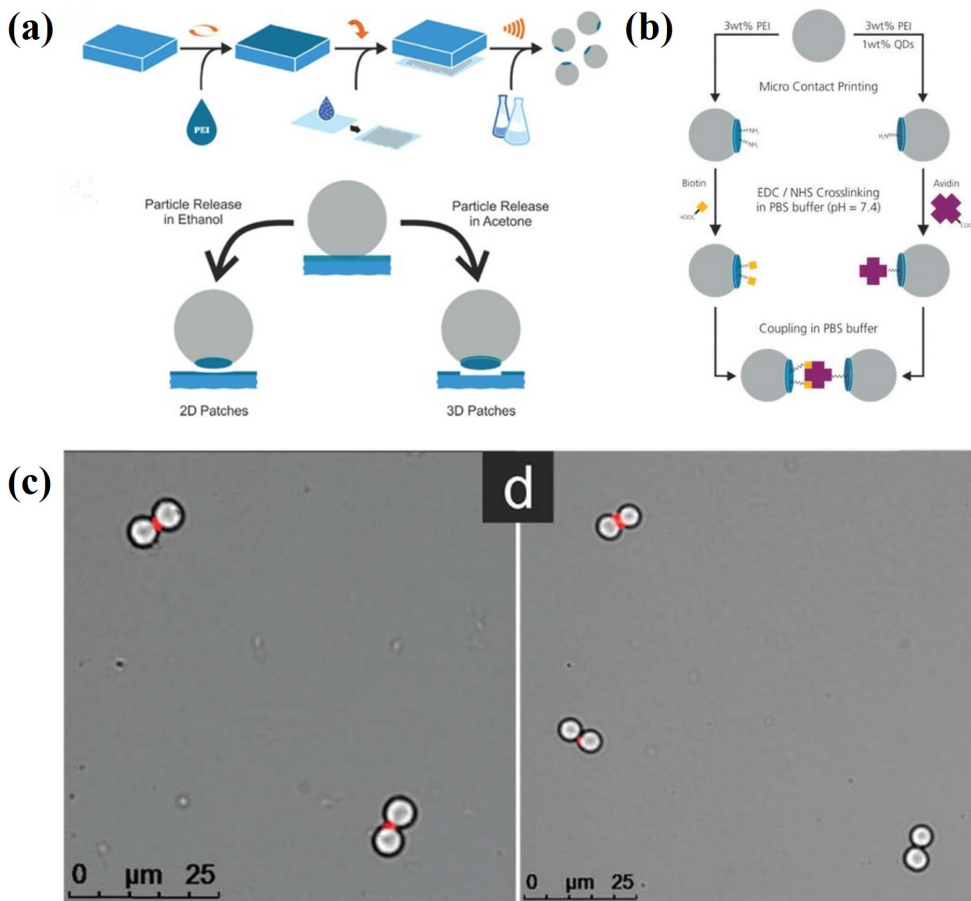


Figure 2. (a) Schematic representation of the microcontact procedure. (b) Schematic representation of the biotin and avidin functionalized particles and the coupling. (c) The self-assembled particles. The red dots are the quantum dots added to label the avidin-functionalized particles. Reprinted (adapted) with permission from Ref. 14.

applications, such as multi-stimuli-responsive micromotors,<sup>16</sup> or logic gate particles that show response when multiple stimuli are applied simultaneously.<sup>17</sup>

#### **4. LC polymer particles as micro-actuators**

Light responsive microactuators are currently receiving much attention in novel application fields such as optofluidics and micro-robotics.<sup>18</sup> Azobenzene has been intensively studied as a photo-active functional group in LC-based soft actuators, as it can undergo *cis-trans* isomerization upon alternative UV and blue light irradiation.<sup>19</sup> Such isomerization results in network contraction parallel to the LC molecular director and elongation perpendicular, which results in macroscopic dimensional and geometrical changes in the resulting polymer material.<sup>20</sup> In chapter 2, the preparation of hollow LC polymer shells functionalized with azobenzene as photo-active groups was reported, and *cis-trans* isomerization of the azobenzene groups was preserved. In the case of a bipolar LC shell, the director is parallel to the line joining the two defects, so upon UV irradiation, it is expected that the thickness of the LC shells will increase, while the perimeter and surface areas will decrease, resulting in a change in size or shape (Figure 3),<sup>21</sup> making these particles promising candidates for photo-driven micro-actuators, UV sensors, and micro-carriers that can absorb or release the cargo in response to UV irradiation. Because of the small dimensions of the LC shells, DLS or atomic force microscopy (AFM) may provide insight into the actuation process.

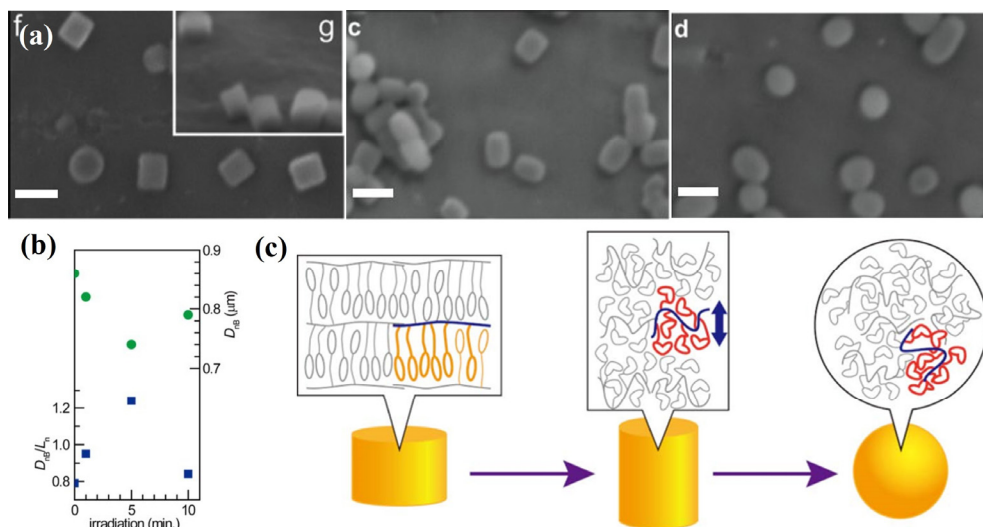


Figure 3. (a) SEM images of LC polymer particles before (left, the inset image is the same sample taken at 45° tilt) and after irradiation with UV light for 5 (middle) and 40 minutes (right). Scale bar = 1 μm. (b) Time evolution of aspect ratio (squares) and bottom diameter (circles) for the cylindrical particles. (c) Schematic representation of azobenzene-functionalized LC polymer particles showing a shape change with UV irradiation. Reprinted (adapted) with permission from Ref. 20.

Among non-spherical particles, bowl shape particles, which are particles with holes on the surface, have drawn much attention.<sup>22</sup> The particles are usually prepared by swelling solid PS particles with toluene followed by freeze-drying (Figure 4a and b).<sup>23</sup> The holes on the surface allow precisely controlled loading of other materials (Figure 4c).<sup>24</sup> Because of the appealing shape, these bowl shape PS particles are potentially interesting as micro-grippers that can release loads on demand.

In chapter 3, LC polymer particles that actuate between spherical and programmed shapes are reported. The LC polymer particles were first prepared by thiol-ene dispersion polymerization, followed by mechanical deformation into the desired shape and photopolymerization for fixation. By replacing mechanical deformation with the preparation in Figure 4a, the thiol-ene LC polymer particles

may be programmed into the bowl shape. After photopolymerization, the bowl shape LC polymer particles can actuate from bowl ( $T < T_{NI}$ ) to spherical shape ( $T > T_{NI}$ ). The actuation might result in the loading and unloading of other objects, making these particles interesting candidates as responsive micro-grippers and size-exclusive separation material for micron- or nano-sized objects.

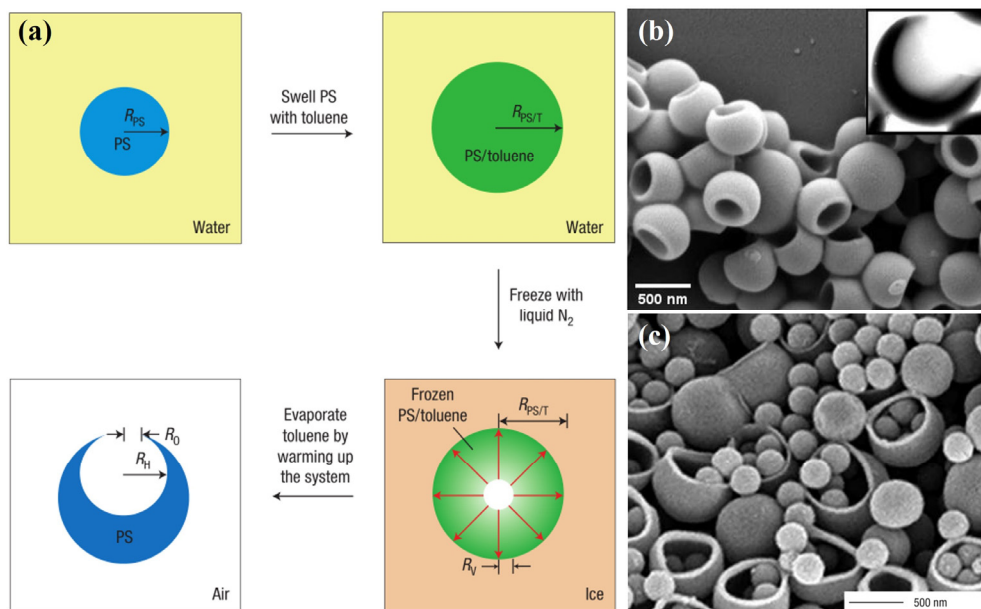


Figure 4. (a) Schematic representation of the preparation of bowl shape PS particles. (b) SEM images of the bowl shape PS particles. (c) SEM images of the bowl shape PS particles after loading with PS nanoparticles. Reprinted (adapted) with permission from Ref. 22.

## 5. LC polymer particles for absorption and release systems

pH-responsive nanoparticles that can release chemicals on demand have attracted much attention in the field of biomedicine since the pH in tumour tissues is more acidic than healthy tissue.<sup>25,26</sup> In chapter 4, carboxylic acid-functionalized LC polymer particles that can rapidly absorb methylene blue (MB) at a high capacity in a basic environment are reported. When added to an acidic environment, the

carboxylic groups are protonated, and this leads to the release of the MB. LC polymer particles prepared from a similar carboxylic acid-functionalized LC monomer mixture (Figure 5a) have been used to prepare LC polymer particles with an average diameter of 200 nm (Figure 5b) via dispersion polymerization in ethanol. These particles showed absorption of MB at high capacity (approximately 1 g MB/ 1 g LC polymer particles, Figure 5c), and the release of MB was pH-dependent, with more MB released at lower pH (Figure 5d). Furthermore, these particles show low cytotoxicity in MTS cell viability assay (Figure 5e). These preliminary results obtained together with the University of Utrecht (dr. R. van Nostrum) indicated that the LC polymer particles are promising candidates for pH-responsive drug carriers. Furthermore, by incorporating a disulfide-functionalized cross-linker, redox responsive LC polymer particles that can undergo intracellular degradation and release absorbate can be prepared, since the higher concentration of reducing agents like glutathione in the intracellular matrix can trigger the degradation.<sup>27</sup>

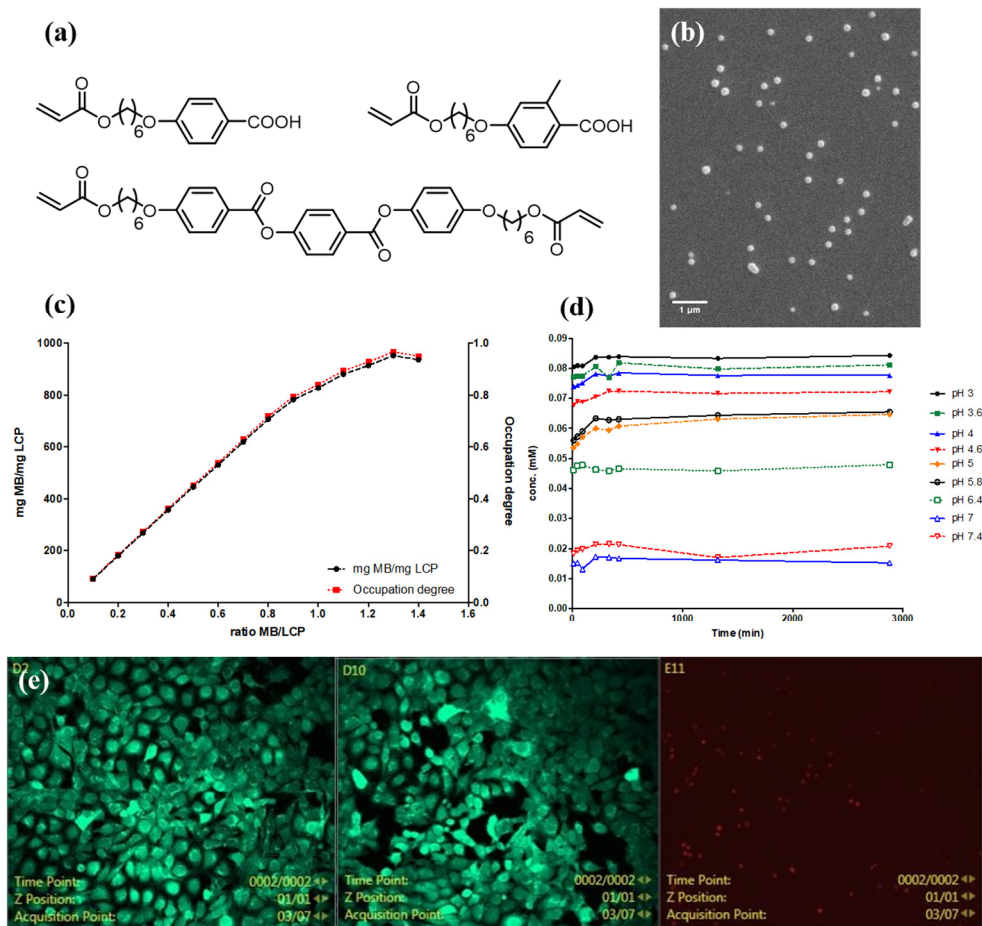


Figure 5. (a) The chemical structure of the LC monomer mixture (weight ratio = 0.45:0.45:0.1). (b) SEM image of the LC polymer particles ( $d \sim 200$  nm). Absorption capacity (c) and pH-dependent release profile (d) of the LC polymer particles. (e) MTS cell viability test of the LC polymer particles. Left image: Cells with LC polymer particles; middle image: positive control (live cells); right image: negative control (dead cells).

## 6. Conclusion

LC polymer particles combine the liquid crystallinity of bulk LC polymers with the micron-scale dimensions of conventional polymer particles. These micron- or nano-objects with anisotropy and responsivity provide exciting possibilities in

both future research and industrial applications, including responsive reflective coatings, water purification, and drug delivery. With careful selection of the preparation techniques as well as the design of the properties of the particles, including particle size, architecture, LC phase, molecular alignment, and chemistry, LC polymer particles can provide unique solutions to challenges like microactuators and controlled release systems.

## 7. Reference

- [1] P. B. Umbanhowar, V. Prasad, D. A. Weitz, *Langmuir* **2000**, *16*, 347–351.
- [2] M. Bouquey, C. Serra, N. Berton, L. Prat, G. Hadziioannou, *Chem. Eng. J.* **2008**, *135*, 93–98.
- [3] C. Ohm, C. Serra, R. Zentel, *Adv. Mater.* **2009**, *21*, 4859–4862.
- [4] C. Ohm, E. K. Fleischmann, I. Kraus, C. Serra, R. Zentel, *Adv. Funct. Mater.* **2010**, *20*, 4314–4322.
- [5] C. Ohm, N. Kapernaum, D. Nonnenmacher, F. Giesselmann, C. Serra, R. Zentel, *J. Am. Chem. Soc.* **2011**, *133*, 5305–5311.
- [6] S. S. Lee, B. Kim, S. K. Kim, J. C. Won, Y. H. Kim, S. H. Kim, *Adv. Mater.* **2015**, *27*, 627–633.
- [7] S. S. Lee, H. J. Seo, Y. H. Kim, S. H. Kim, *Adv. Mater.* **2017**, *29*, 1–8.
- [8] T. Hessberger, L. B. Braun, F. Henrich, C. Müller, F. Gießelmann, C. Serra, R. Zentel, *J. Mater. Chem. C* **2016**, *4*, 8778–8786.
- [9] D. Ditter, P. Blümler, B. Klöckner, J. Hilgert, R. Zentel, *Adv. Funct. Mater.* **2019**, *29*, 1–12.
- [10] E. K. Fleischmann, H. L. Liang, N. Kapernaum, F. Giesselmann, J. Lagerwall, R. Zentel, *Nat. Commun.* **2012**, *3*, 1178.
- [11] V. S. R. Jampani, D. J. Mulder, K. R. De Sousa, A. H. Gélébart, J. P. F. Lagerwall, A. P. H. J. Schenning, *Adv. Funct. Mater.* **2018**, *28*, 1801209.
- [12] X. Wang, E. Bukusoglu, N. L. Abbott, *Chem. Mater.* **2017**, *29*, 53–61.
- [13] J. Hu, S. Zhou, Y. Sun, X. Fang, L. Wu, *Chem. Soc. Rev.* **2012**, *41*, 4356–4378.



- [14] T. Kaufmann, M. T. Gokmen, C. Wendeln, M. Schneiders, S. Rinnen, H. F. Arlinghaus, S. A. F. Bon, F. E. Du Prez, B. J. Ravoo, *Adv. Mater.* **2011**, *23*, 79–83.
- [15] M. Zimmermann, D. John, D. Grigoriev, N. Pureskiy, A. Böker, *Soft Matter* **2018**, *14*, 2301–2309.
- [16] L. Zhang, H. Zhang, M. Liu, B. Dong, *ACS Appl. Mater. Interfaces* **2016**, *8*, 15654–15660.
- [17] E. A. Mahmoud, J. Sankaranarayanan, J. M. Morachis, G. Kim, A. Almutairi, *Bioconjug. Chem.* **2011**, *22*, 1416–1421.
- [18] A. Belmonte, Y. Y. Ussembayev, T. Bus, I. Nys, K. Neyts, A. P. H. J. Schenning, *Small* **2020**, *16*, 1905219.
- [19] S. Xie, A. Natansohn, P. Rochon, *Chem. Mater.* **1993**, *5*, 403–411.
- [20] A. H. Gelebart, D. Jan Mulder, M. Varga, A. Konya, G. Vantomme, E. W. Meijer, R. L. B. Selinger, D. J. Broer, *Nature* **2017**, *546*, 632–636.
- [21] T. Itoh, T. Tamamitsu, T. Aki, K. Tsutsui, Y. Mori, H. Kudo, M. Tokita, H. Shimomoto, E. Ihara, *ACS Appl. Polym. Mater.* **2020**, *2*, 2485–2494.
- [22] G. Guan, Z. Zhang, Z. Wang, B. Liu, D. Gao, C. Xie, *Adv. Mater.* **2007**, *19*, 2370–2374.
- [23] S. H. Im, U. Jeong, Y. Xia, *Nat. Mater.* **2005**, *4*, 671–675.
- [24] S. J. Hwang, J. H. Park, J. H. Son, J. H. Choi, H. Seo, M. Park, J. Kim, G. D. Moon, D. C. Hyun, *Polymer (Guildf)*. **2018**, *135*, 338–347.
- [25] W. Gao, J. M. Chan, O. C. Farokhzad, *Mol. Pharm.* **2010**, *7*, 1913–1920.
- [26] M. Kanamala, W. R. Wilson, M. Yang, B. D. Palmer, Z. Wu, *Biomaterials* **2016**, *85*, 152–167.
- [27] Q. N. Bui, Y. Li, M. S. Jang, D. P. Huynh, J. H. Lee, D. S. Lee, *Macromolecules* **2015**, *48*, 4046–4054.

## **Curriculum Vitae**

Xiaohong Liu was born on July 20<sup>th</sup>, 1994 in Guangzhou, China. He graduated from South China University of Technology (SCUT) with a bachelor's degree in material science and technology (material chemistry) in 2016. After obtaining a master's degree from the University of Akron in polymer science under the supervision of Dr. Abraham Joy in 2017, he started his PhD in the SFD group under the supervision of Prof. Albert Schenning. His research topic is liquid crystalline polymer particles prepared from dispersion and precipitation polymerization, and the most important results are presented in this thesis.

## List of publications

- (1) Liu, X.; Xu, Y.; Heuts, J. P. A.; Debije, M. G.; Schenning, A. P. H. J. Monodisperse Liquid Crystal Network Particles Synthesized via Precipitation Polymerization. *Macromolecules* **2019**, *52* (21), 8339–8345. <https://doi.org/10.1021/acs.macromol.9b01852>.
- (2) Liu, X.; Pan, X.; Debije, M. G.; Heuts, J. P. A.; Mulder, D. J.; Schenning, A. P. H. J. Programmable Liquid Crystal Elastomer Microactuators Prepared via Thiol-Ene Dispersion Polymerization. *Soft Matter* **2020**, *16* (21), 4908–4911. <https://doi.org/10.1039/d0sm00817f>.
- (3) Liu, X.; Moradi, M.-A.; Bus, T.; Heuts, J. P. A.; Debije, M. G.; Schenning, A. P. H. J. Monodisperse Liquid Crystalline Polymer Shells with Programmable Alignment and Shape Prepared by Seeded Dispersion Polymerization. *Macromolecules* **2021**, *54* (13), 6052–6060. <https://doi.org/10.1021/acs.macromol.1c00884>.
- (4) Liu, X.; Debije, M. G.; Heuts, J. P. A.; Schenning, A. P. H. J. Liquid crystalline polymer particles prepared by classical polymerization techniques. (Accepted)

## Acknowledgement

How time flies! Attending the SFD meeting for the first time feels like just yesterday, and now I am wrapping up my PhD thesis with this acknowledgment. It has been a long journey, but fortunately, it has also been a lovely journey with all the support and kindness I received along the way.

My first thank you surely goes to Albert, my first promotor. Thanks for offering me this position in SFD 4 years ago, and let me work freely and live in luxury. Also, I need to thank you for all your input in my research and all those discussions we had that make my work more structured. Your enthusiasm and upbeat personality are truly supportive and motivating. I know we don't always think the same way, but I must admit that your suggestions do always turn out to be better than mine. I wish you every good fortune and success in your research as well as your life. Hans, an impeccable chemist, thanks for all your help in my PhD. You not only provided ideas to make things work but reminded me of things that I overlooked. I surely won't be able to make my way to being a polymer chemist without you. Michael, I wish that I were a quarter as imaginative as you. You always have countless ideas to offer and encourage me when I was not happy with my work. I will definitely miss the cheerful but also robust meetings. Dirk, your knowledge and enthusiasm for liquid crystals have been not only helpful but also encouraging, and thank you for all your input for me and the SFD group. Prof. Stefan Bon and Dr. Rene van Nostrum, it is a pleasure to collaborate with you, and thanks for being my committee members and your input in this thesis. Prof. Katja Loos, thanks for being my committee member even though we work in different fields. It is an honor to have you on board, and I hope you enjoy this thesis.

There are also some names in the SFD group that I need to mention in this acknowledgement. Marjolijn, you are the first person who welcomed me to SFD, and your help over the years has been more than tremendous. Tom, thanks for all the

ordering of chemicals, SEM, and TEM images, you have made life much easier for everyone in the SFD. Dirk-Jan, Alberto, and Sterre, thanks for all the discussions and support in the particle meetings. Sebastian, Pei, and Mert, you are excellent office mates and it is always pleasant to have discussions with you on both science and non-scientific matter. Danqing, Stijn, Jeroen (2x), Marc, Sean, Yari, Roel, Simon, Gilles, Ellen, Bruno, Roberta, Henk, Marina, Rob, Cees, Johan, Arne, Davey, Fabian, and all those I haven't mentioned here, thank you for your help over the years and making SFD such a nice and welcoming group. I wish you all the best, and I look forward to catching up with you one day.

And finally, my dear friend Yun, I enjoy every moment with you, and I wish you think the same of me. If by any chance we reunite one day, I look forward to hearing your story like we did before. Good luck with your career and your life, and I wish you happiness every single day.

我真是一个幸运的人，没有吃太多的苦，就走了很远的路。回想六年前的夏天，出国留学是我做过的最正确的选择。在这六年里，我欣赏过不一样的风景，体验过异国他乡的烟火，认识了各色各样的人。在这本论文的结尾，我想深深地感谢那些让我如此幸运的人。

首先要感谢的是我的父母。父母之爱子，则为之计深远，感谢你们为我和这个家付出的几十年的努力，你们的勤劳、勇敢和乐观是你们给我最宝贵的财富。在操劳了大半辈子以后，我希望你们能好好享受接下来的时光，领略陌生而美丽的风景，体验不一样的生活。还有我的爷爷、奶奶、外公，我会永远铭记你们的音容笑貌和谆谆教诲。外婆，欣闻您近来身体好转了，祝您有一个健康、幸福的晚年。

我还要感谢我的所有亲人。在这个流行吐槽奇葩亲戚的年代里，你们给我的始终都是支持和鼓励。在出国的这几年里，我一直怀念着你们带来的美味佳肴和欢声笑语，希望我们将来能有更多的团聚时光。

接下来是我的同学和朋友。吕老师，我总是惊叹于你苦中作乐的精神，愿你心想事成，一切顺利。益妈妈，生活不易，希望你情感上和事业上都能一帆风顺。潘兴龙，我们一起买菜一起加班的样子是我博士生涯的点点注解。有空多上线，打不了职业，难道还打不了白银吗？冯伟，媛媛，东钰，婉姝，蔚信，岸萍，刘杰，你们既是学术上的良师又是生活上的益友，感谢你们的一路陪伴和提点，希望我们有朝一日能重逢。我的智障师弟子轩，我们的聊天记录可以写成相声——科研篇，不知何时能出续集？刘巍，盼你盼了两年，到我落笔的时候你还是没来，你托我的东西再不拿走就要长蘑菇了。凌轩，儒宝，涛涛，以及各位凌晨三点还在奋战的召唤师们，希望我们还能有机会继续开黑。

最后，感谢看到这里的读者，希望我的工作对你有所帮助，也祝你研究顺利，硕果累累。

刘晓泓

2021-8-30 于 Eindhoven, the Netherlands